UNIVERSITY OF SOUTHAMPTON

FACULTY OF ENGINEERING, SCIENCE & MATHEMATICS

School of Engineering Sciences

A Mechanism to Accelerate the Late Ablation in

Pulsed Plasma Thrusters

by

Rodrigo Intini Marques

Thesis for the degree of Doctor of Philosophy

February 2009

UNIVERSITY OF SOUTHAMPTON

ABSTRACT

FACULTY OF ENGINEERING, SCIENCE & MATHEMATICS

SCHOOL OF ENGINEERING SCIENCES

Doctor of Philosophy

A Mechanism to Accelerate the Late Ablation in Pulsed Plasma Thrusters

by Rodrigo Intini Marques

Pulsed Plasma Thrusters (PPTs) are long standing electric propulsion thrusters that are reliable, relatively simple and low cost. One of the main issues with the PPT is its poor utilization of the propellant and low efficiency. Typically only 40-60% of the propellant contributes to the production significant impulse and the efficiency is around 8%. The cause of the PPT's poor propellant utilization is the late time ablation (LTA), which has a major impact on the efficiency. LTA is the sublimation of propellant that takes place after the main discharge, due to the propellant, usually Polytetrafluoroethylene (Teflon®), being at a temperature above its sublimation point. The LTA produces a low speed gas and macro particles that do not contribute significantly to the thrust. This work presents a way of accelerating the late time ablation by employing an additional discharge after the main discharge, in a separate pair of electrodes. A new thruster, called the two-stage pulsed plasma thruster (TS-PPT) was built and tested. This thruster has two pair of electrodes: primary and secondary. The primary is placed in contact with the propellant surface, as in a regular PPT. The secondary is placed downstream, relatively far from the propellant. A new approach, dividing the PPT thrust generation in two phases, was envisioned. The first phase is responsible for the ablation process and takes place in the first pair of electrodes. The second phase takes place in the second pair of electrodes and is responsible for the acceleration process. The phase division

allowed for propellant metering and better propellant utilization. Evidence was found that a pair of electrodes placed downstream, further from the propellant surface is able to discharge in the late ablation portion of the propellant and can impart extra energy into the exhaust and improve propellant utilization. A simple analytical model was developed to predict trends. A prototype of a TS-PPT was designed and built. A vacuum facility was modified, adapted, partially designed and built. An average mass bit consumption test was carried out. A simple time-of-flight experiment revealed that the fastest portions of the plasma from the primary electrodes discharge were travelling at around 33 km/s. Several current measurements were performed and calculations of the total electrical resistance, total inductance, electromagnetic impulse bit, specific impulse, efficiency, and other parameters were calculated based on experimental data. Experimental results indicated that significant improvements in the specific impulse and efficiency are possible by utilising a two-stage PPT. Specific impulses as high as 4000s were calculated based on experimental results, indicating a better propellant utilization.

Ao Povo do Brasil, dedico.

Dedicated to the people of Brazil.

"Space: The Final Frontier".

- Eugene Wesley "Gene" Rodenberry (1921-1991)

Acknowledgements

Firstly, I would like to thank my supervisor, Prof. Stephen Gabriel. He was more than a supervisor. He was and is a great friend.

I thank Prof. Demétrio Bastos Netto, that made it possible for me to come to the UK to do my PhD when he was the head of the Combustion and Propulsion Laboratory (LCP) at INPE – Brazilian National Space Research Centre.

I thank Dr. Fernando de Souza Costa, current head of the LCP/INPE, for the inspiration to work with electric propulsion. Dr. Costa also provided equipments for my PhD and made it possible to manufacture a prototype of the TS-PPT and also the UniSat-5 PPT at LCP/INPE.

Thanks to all the technicians at SEMA – Manufacture Centre – of INPE that helped to build the UniSat-5 PPT and to everybody at LCP workshop that helped to build the first TS-PPT prototype.

I thank to the Brazilian National Council for Scientific and Technological Development – CNPQ – Conselho Nacional de Desenvolvimento Científico e Tecnológico -, from the Brazilian Ministry of Science and Technology, for granting a PhD scholarship. Also, thanks to the Brazilian São Paulo State Research Funding Aid Agency - FAPESP – Fundação de Amparo à Pesquisa do Estado de São Paulo – for funding a research that leaded to this PhD.

I thank my mother, Eunice Beatris Intini, my father Valter José Marques and my brother, Leandro Intini Marques for their support and trust.

I thank Yang Yang for his support and understanding over the years.

In no particular order I would like to thank my friends Paolo Gessini, Michele Coletti, Sam Roberts, David Webb, Cheryl Collingwood, Gabriel Bianchi, Angelo Grubišič and Sabrina Pottinger for the friendship during these years.

Thanks to the people at the University of Southampton that made it possible for me to do my research, including Dawn Attree, Alessia Plutino, Julia Zimbler and Maureen Hanney. A special thanks to my friend Sonya Manton.

Thanks to the technician Mike Street for his help with CAD drawings and mechanical design. Also thanks to James Chitty for the help with obtaining materials for the thrusters and to the technician Simon Klitz for helping with the assembly of various components of the vacuum facility.

Contents

List of Figures

xviii

Chapter 1

1. Introduction

Chemical propulsion thrusters rely on the internal energy stored in the molecular bonds of its propellant. The propellant, therefore, is both the energy source and the working fluid. Differently, electric propulsion devices obtain its energy from external power sources and the working fluid, also called propellant, is normally - but not always - inert. The energy imparted to the propellant is used to eject it at high speeds. One advantage of having an external power source is that the amount of energy that can be imparted to the working fluid is not limited by the propellant, but only limited by the external power source. It is then possible to impart an arbitrary amount of energy to the propellant. Due to the limitation on the internal energy, chemical thrusters have a maximum specific impulse[1] around 450s. Electric propulsion devices can achieve specific impulses of over 17,000s[2] (1)(2). Arcjets, Pulsed Plasma Thrusters, Hall thrusters and Gridded Ion Thrusters are electric thrusters that can achieve specific impulses of 500s, 1400s, 1600s and 3000s, respectively (3).

Electric propulsion devices are used in satellites and space vehicles for orbit correction (4)(5), orbit transfer (6), drag make up and formation flying (7)(8) and attitude control (9). Successful near Earth space missions employing electric propulsion (EP) devices have encouraged the use

---

[1] Specific impulse is defined as $I_s = \frac{\int F dt}{g_0 \int \dot{m} dt}$, where F is the thrust force in **N**, $g_0 \equiv 9.80665 \frac{m}{s^2}$, is the acceleration of gravity at sea level and $\dot{m}$ is the mass flow rate of propellant, in **kg/s**.

[2] Dual-Stage Four Grid Ion Thrusters (DS4G) can achieve such high specific impulses as well as some experimental gridded ion engines, amongst other electric thrusters.

of EP thrusters for interplanetary missions and long range space exploration, including beyond Solar System missions (10) (11).

Besides offering higher propellant ejection speed, electric thrusters also offer other advantages over chemical thrusters, such as: longer lifetime and, depending on the choice of propellants, less toxic propellants. The reduction in propellant mass allows missions of longer duration, and/or longer range missions, and/or more mass for the payload.

It should be noted that due to spacecraft power limitations and other current material limitations, the thrust produced by electric propulsion devices are very low, compared to chemical thruster.

1.1 Definition and Classification of Electric Propulsion Systems

Electric propulsion consists in the acceleration of a propellant - which can be initially a gas, liquid, solid or plasma - to produce thrust by electrically produced heat, electrostatic forces or electromagnetic forces.

To achieve exhausts speeds above 10,000 m/s, desirable for the majority of the interplanetary missions [3], different methods of propellant acceleration must be employed other than the propellant heating by chemical reactions(12). In order to increase the propellant acceleration by thermal expansion, the energy must come from an external source, with higher energy capacity than that available from chemical propellants. To achieve such high exhaust velocities, acceleration forces must be applied directly to the propellant, i.e., electrostatic and/or electromagnetic forces. Both the heating of the propellant at high temperatures and the direct application of forces to the propellant can be achieved by electric processes(12).

Based on Robert Jahn's classic book on Electric Propulsion (EP) (12) it is possible to classify EP devices in three types, even if some EP devices do not rely exclusively on a particular method of propellant acceleration:

1. Electrothermal: the propellant is heated by an electrical heater and expanded in a convergent/divergent nozzle. Examples: resistojets and arcjets.

---

[3] The specific impulse, I_{sp}, is related to the total velocity change, ΔV, of the spacecraft, $\Delta V = I_{sp} g_0 ln \frac{m_0}{m_f}$, therefore to maintain a certain mass fraction, $\frac{m_0}{m_f}$, for a given velocity change, it is necessary to increase the specific impulse.

2. Electrostatic or Ionic: the propellant is accelerated by direct application of electric fields to ionized particles. Examples: gridded ion thrusters, colloid thrusters, and field emission electric propulsion (FEEP).

3. Electromagnetic or Magneto Plasma Dynamic: the propellant is ionized and accelerated by the interaction of internal and external magnetic fields with electric currents on the propellant flow. Examples: Hall thrusters, Pulsed Plasma Thrusters, Pulsed Inductive Thrusters, and magneto-plasma-dynamic thrusters.

For the sake of comparison, Table 1 lists typical performance parameters of various types of electrical propulsion systems.

<div align="center">

Table 1: Typical performance parameters for various types of electric propulsion systems[a](3).(Adapted)

</div>

Type	Thrust Range (mN)	Specific Impulse (s)	Thruster Efficiency[b](%)	Thrust Duration	Typical Propellants	Specific Power (W/mN)
Resistojet	200-300	200-350	65-90	Months	NH_3, N_2H_4, H_2	0.5-6
Arcjet	200-1000	400-1000	30-50	Months	H_2, N_2, N_2H_4, NH_3	2-3
Ion engine	0.01-200	1500-5000	60-80	Months	Xe, Ar, Kr	10-70
Solid Pulsed Plasma Thruster – PPT	0.05-10	600-2000	5-16	Years	Teflon	10-50
MPD arcjet	0.001-2000	2000-5000	30-50	Weeks	Ar, Xe, H_2,Li	100
Hall Thruster	0.01-2000	1500-2000	30-50	Months	Ar, Xe	100
Monopropellant rocket[c]	30-100000	200-250	87-97	Minutes-Hours	N_2,H_4	___

[a] Values are references for comparison only.

[b] In this table, $Efficiency = \frac{thruster's\ kinetic\ output\ power}{electrical\ power\ input}$

[c]This is not an electric thruster and is listed here for comparison only.

1.2 Introduction to Pulsed Plasma Thrusters

Pulsed Plasma Thrusters – or PPTs – are electric propulsion devices that can be categorized as electromagnetic electric thrusters, although thermal expansion is also responsible for part of the thrust produced. One of the types of PPTs, developed in the early and middle 1960s, called gas-fed PPT (GF-PPT) employs an electric discharge through a flowing gas, e.g., xenon or argon. When the GF-PPT operates in a predominately electromagnetic mode, the accelerating mechanism is a current sheet driven by its self-induced Lorentz force. When the GF-PPT was developed, the main focus of EP was to develop primary propulsion systems, i.e., main propulsion systems responsible for orbit raising, orbit changing and manoeuvres or orbit transfer. However, the GF-PPT research and development receded by the end of the 60s, mainly due to the need for massive capacitors and the energy and lifetime requirements of the fast-acting valves required to ensure high propellant mass utilization efficiency (13). However, one derivative of this concept survived: the ablative pulsed plasma thruster (APPT or simply PPT)[4]. The PPT was aimed at solving the propellant mass utilisation problem without the use of valves, tanks and their respective control systems. A diagram of the PPT can be seen on Figure 1.

---

[4] For simplicity, in this text the acronym PPT will be used to refer to the APPT.
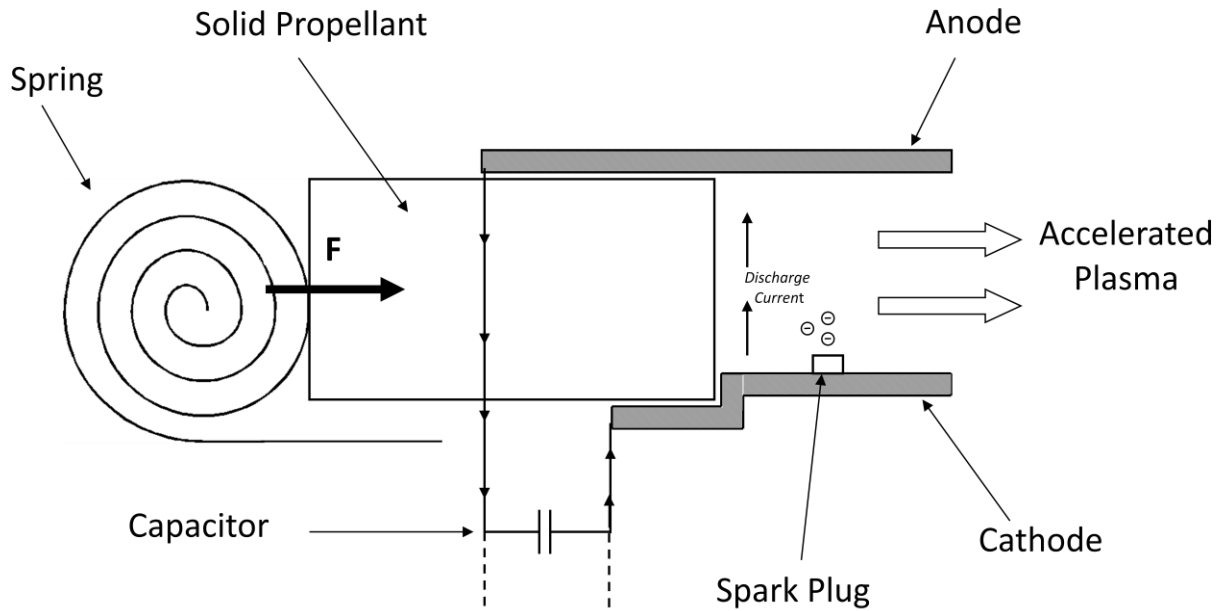
Figure 1: PPT diagram.

The PPT utilises a solid propellant, most commonly PTFE − Polytetrafluoroethylene − also known as Teflon®[5], a synthetic fluoropolymer. Tests with alternative propellants, such as Kynar, Viton, Fluorel, Kel-F, Genetron, Halon, Delrin , CTFE-2300, polyproplylene, polyethylene were performed, but no other propellant has shown better performance than PTFE in terms of both specific impulse and surface char. Also attempts of seeded plastics with metals were made as well as alternating layers of PTFE and other plastics, but again it did not improve the performance of the PPT (14).

A typical PPT operation cycle comprises a capacitive electric discharge initiated by electrons emitted by a spark plug mounted on the cathode, close to the propellant surface. During the

[5]Teflon® is a registered trademark of DuPont Company. Referring to Polytetrafluoroethylene simply as Teflon can cause confusion, as Teflon is a brand name and is used for a family of different fluoropolymers. In this text, all mentions to Teflon are referring uniquely to Polytetrafluoroethylene (PTFE) and these terms are used conversely.

discharge the propellant is heated and sublimated. The electric discharge then takes place in the generated gas that becomes ionised, forming the plasma. The plasma is subsequently accelerated by a combination of a self induced magnetic field (**B**), generated by the discharge current, and the current density (**J**). This resulting force, known as the Lorentz force, produces the thrust, jointly with gas dynamic forces, also known as pressure forces.

Differently from most electric thrusters, the Pulsed Plasma Thrusters can exist in several different configurations. Figures 2-6 depicts diagrams for several different PPTs' discharge chambers, showing schematically their respective magnetic field (**B**)[6], current density (**J**) and Lorentz force (**J×B**) vectors.

Figure 2 shows the rectangular configuration, the most common PPT configuration, where a spring feeds the PTFE bar.
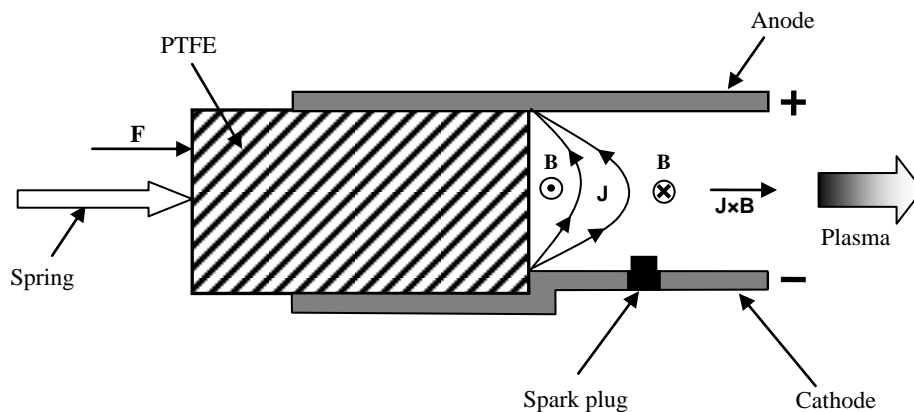
Figure 2: A schematic of a spring fed rectangular PPT configuration.

---

[6] The magnetic field, **B** - induced by the time varying current density, **J**, - shown in the pictures represent the field when it crosses the plane of the paper. The magnetic field surrounds the current density following the right hand rule.

Figure 3 shows a second rectangular PPT configuration without a propellant feeding mechanism. In this configuration the PTFE is attached to an insulator and, as it recedes, the discharge takes place increasingly upstream. This configuration intrinsically introduces variations of the impulse produced by the PPT as the location of the discharge with relation to the exit plane and the distance between the propellant discharge surface and the spark plug change as the propellant recedes. A possible advantage of this configuration is that the current in the plasma discharge and the backstrap repel[7], accelerating the plasma electromagnetically and producing a reaction force on the conductor (14).
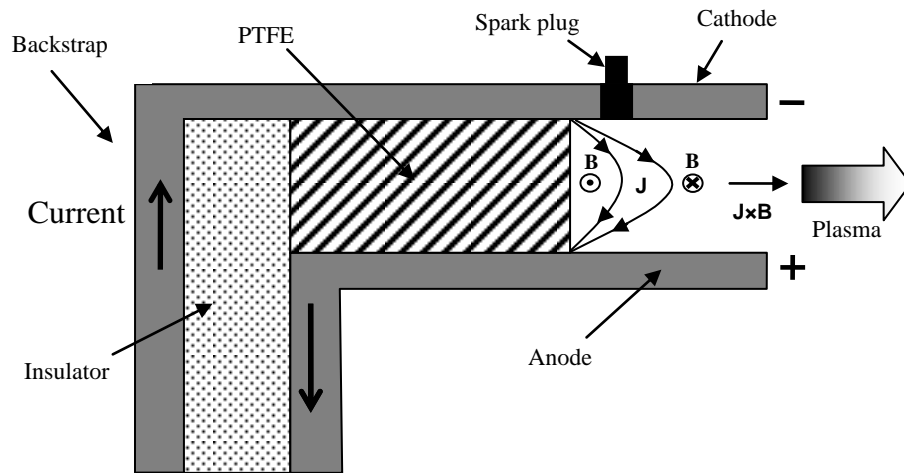
Figure 3: A schematic of a PPT rectangular configuration with no propellant feeding mechanism.

---

[7] The repelling occurs due to the currents having opposite directions.

Figure 4 shows a PPT in its coaxial configuration. In this configuration there is no spark plug and the discharge is initiated by directly applying an electric field to the main electrodes that is higher than the dielectric strength of the PTFE[8] to initiate a discharge. These thrusters are normally very small. Some of these PPTs, operating at energies of discharge between 1 J – 15J, are known as micro-PPTs. In some laboratory tests, an external spark plug can be used to initiate the discharge when this configuration is being tested (15).
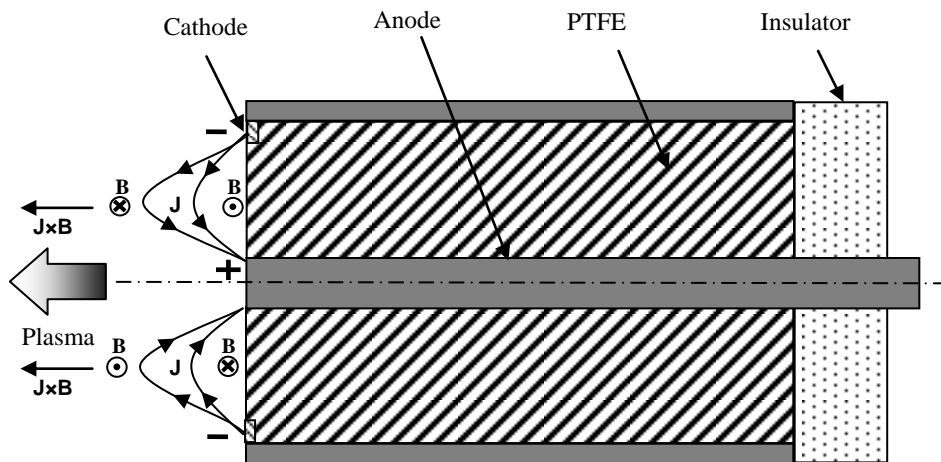
Figure 4: A schematic of a PPT coaxial configuration.

Figure 5 shows a PPT in another coaxial configuration with a conical shaped propellant bar and a spark plug. It is interesting to note that the propellant practically maintains it shape as it is

---

[8] The dielectric strength of PTFE is around 60×10^6 V/m (60 kV/mm).

ablated, with the exception that it tends to be slightly concave between the electrodes, as it is also the case with the other geometries[9].

---

[9] The concavity of the propellant between the electrodes is probably related to the fact that the electrodes dissipate the heat that would otherwise contribute to the sublimation of the propellant. As the PTFE is not a good heat conductor, further from the electrodes the heat of the discharge ablates the propellant more pronouncedly.

Figure 6 shows a Z-Pinch PPT, a configuration initially used for GF-PPT, adapted for the PPT (16). In this configuration the spark plug is placed close to the anode.
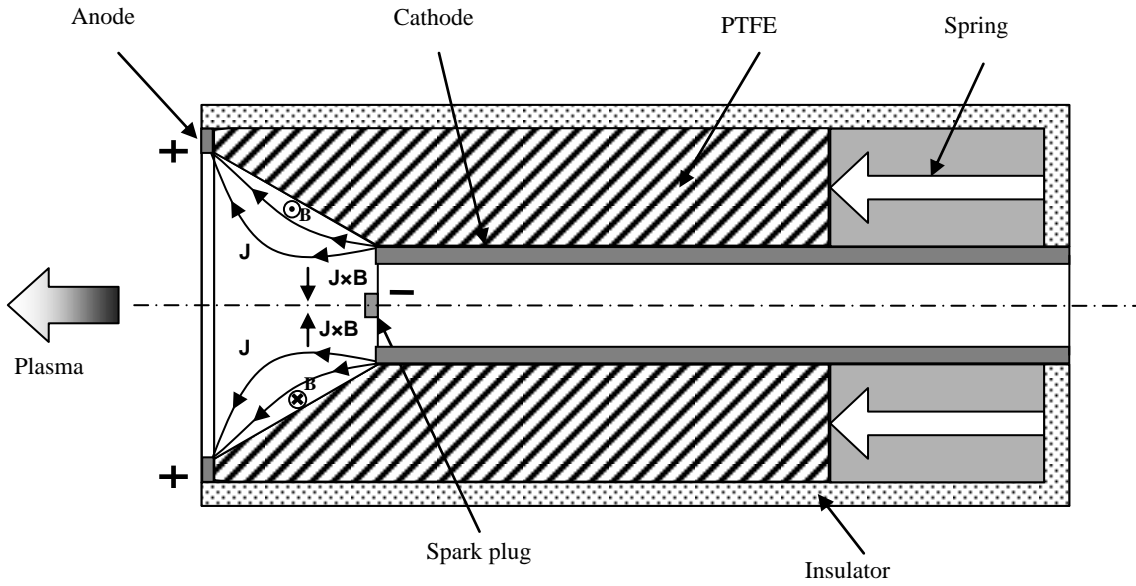
Figure 5: A schematic of a coaxial PPT with conical shaped propellant.
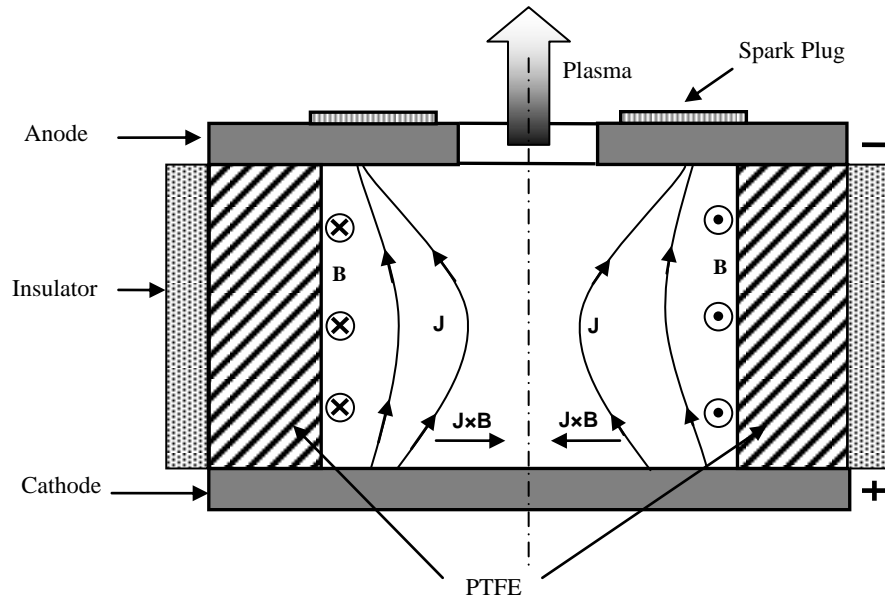
Figure 6: A schematic of a Z-Pinch configuration PPT.

11

1.3 Definition of PPT Performance Parameters

When studying a PPT it is convenient to define some performance parameters that will make it possible to compare different thrusters and also to refine the performance of a particular thruster. As many other electric propulsion devices, the PPT does not have a single exhaust velocity. Instead, it has different constituents of the exhaust being ejected at different speeds at different times. Therefore the definitions found in this section will be taking this into account.

1.3.1 Impulse Bit

It is convenient to define the *impulse bit* imparted by the PPT into a spacecraft. This is defined as the thrust force, T, integrated over the period in which this force is applied.

$$I_{bit} = \int_{t_0}^{t_1} |T|\, dt \tag{1.1}$$

Where t_0 and t_1 are the times where the force has been applied and removed, respectively[10].

1.3.2 Specific Impulse

Another important parameter used to measure the performance of spacecraft thrusters and useful for the PPT is the *specific impulse*, which is the ratio of the integral of the thrust to the integral of the rate of use of propellant by sea-level weight:

$$I_s = \frac{\int F dt}{g_0 \int \dot{m} dt} \tag{1.2}$$

Where g_0 is the sea-level gravitational acceleration ($g_0 \equiv 9.80665 \frac{m}{s^2}$).

---

[10] In this work, t_0 and t_1 may be omitted, but all apparently indefinite time integrals actually refer to the times t_0 and t_1 and are referring to the interval of time of a pulse of a single PPT discharge cycle.

A dimensional analysis of equation (2) will show that the *specific impulse* is measured in seconds.

If the PPT is operating at a fixed frequency f[11], meaning that a discharge cycle of a certain number of pulses (also known as a burst) occurs at this frequency, it is possible to obtain an equivalent of an average thrust, measured in Newtons:

$$F = f I_{bit} \tag{1.3}$$

1.4 Motivation and objective of this research

One of the main problems with PPTs is its low efficiency[12], typically less than 15%(17). Experiments (18) have shown that, in a single pulse, about 40% of the ejected mass from a PPT is not accelerated electromagnetically and leaves at relatively low-speed, therefore not contributing significantly to the impulse bit.

After the main discharge is finished the temperature of the propellant is still above its sublimation point (~260 ^{o}C) and a significant portion of propellant sublimates without being electromagnetically accelerated. This portion of mass that ablates after the main discharge is known as *late ablation* (14) or late time ablation (LTA). The objective of this work is to investigate a mechanism to accelerate the late ablation in order to increase the portion of propellant that is accelerated electromagnetically, increasing the PPT efficiency.

---

[11] PPTs typically operate at frequencies between 0.5Hz to 2Hz. But in theory it is possible to operate at any frequency, limited in practice mainly for the available power and thermal constraints.

[12] In this research, the PPT efficiency is defined as: $Efficiency = \frac{directed\ exhaust\ kinetic\ energy}{capacitor\ stored\ energy}$

Chapter 2

2. Background and Literature Review

As the PPT is the starting point of this research, this chapter describes it in more detail and presents a literature review on PPT research and development. An excellent review of the development and application of the PPT from 1963 to 1998 was done by Burton and Turchi (14), however it is convenient to revise the research and development with a focus on the late ablation acceleration and therefore with a new view.

2.1 Advantages of the PPT

The PPT presents several advantages with respect to some other thrusters. Beginning in 1968, Palumbo and Guman (19) studied the LES-6[13] PPT during 10 years in a flight experiment of almost 9000h of PPT operation (14). They pointed out the following characteristics of PPTs[14]:

1) Zero heating time. No energy spent in standby.

2) Inert and low failure propensity – no forces or torques when out of operation.

3) Scalable - it can be developed to attend several performance specifications, taking into account power source and mass limitations.

4) It can be used in spin stabilized or three-axis stabilized satellites.

5) Using a solid propellant, like PTFE, it has the following advantages: no tanks, feed lines, seals, mechanical valves; it is easy to calculate propellant consumption; zero-g operation

---

[13] The acronym LES refers to the Lincoln Experimental Satellite series from the Massachusetts Institute of Technology Lincoln Laboratories.

[14] The characteristics listed were adapted from the original and contain extra information.

compatibility; compatibility with cryogenic temperatures[15] and vacuum; presents no corrosion; non-toxic (considering only the solid state); storable for long periods; not affected by rapid changes of temperature or by large accelerations; the most common fuel - PTFE - is non-hygroscopic and non-oleoscopic.

6) Discrete impulse compatible with digital logic (good repeatability, possibility of thruster operation through a pulse using TTL – transistor-transistor-logic - digital).

7) Variable thrust (through variations in frequency and discharge energy).

8) Performance compatible with attitude control and orbit maintenance.

9) Operation in a large range of ambient temperatures (approximately between -240°C to +260°C)

10) Large capacity of thrust vector control by the varying the thrust in a very precise way with changes in the discharge frequency.

Additionally, the PPT can yield very low impulses, on the micro-Ns range, allowing an accurate adjustment of attitude and positioning, which is particularly important for the implementation of satellite constellations (20).

2.2 Review of the development

The PPT was the first electrical thruster to be used in space, in 1964, with the Soviet space probe Zond 2, launched towards Mars, and followed by the USA, with the LES-6 satellite, launched in

---

[15] Teflon can withstand temperatures as low as -240°C without chemical degradation.

1968. The augmented hydrazine thrusters, arcjets, ion and Hall thrusters were developed later (14).

The first known pulsed thruster was developed in Russia in 1934 (14). It worked by applying a capacitor discharge into a chamber with plastic. The gases generated passed through a converging-diverging metallic nozzle to be expanded and accelerated. It is unknown if the thrust was measured but the acceleration mechanism was predominantly electrothermal. Other early devices used a gas-feed system or were fed with soft-wax.

The following sections will analyse some investigations on PPTs that are relevant for this work. The literature review is divided into four categories: General Studies, Flight Qualification and Testing, Plume Studies and Propellant and Ablation Studies.

2.2.1 General Studies

Guman and Peko (21) reported in 1968 the use of solid PTFE as a propellant for a plasma accelerator. They studied more than 100 different PPT thrusters in a period of approximately two years. Analysing the propellant, they concluded that PTFE was apparently the only known subliming , ablating, non-reacting, and non-charring, solid that converts directly from a solid to a gas, was compatible with deep space environment and required almost negligible energy to be depolymerised directly from a solid to gas. Both parallel and coaxial geometries were investigated and a linear dependency of the specific impulse to the discharge energy was observed in the tested range from 1 to 40 J discharge. In an attempt to increase the performance of the thrusters they examined how the specific impulse would change by varying the length of a nozzle. It was found that higher specific impulses were produced when the length of the nozzle was decreased.

Vondra and Thomassen (22), in 1972, studied the performance of a 2 J and a 20 J PPT, describing several experiments carried out with the intent to increase the efficiency and impulse bit. Changes in the geometry of the electrodes and fuel feed system were made and a new propellant feeding system, called 'side-fed', was developed. It was verified that by changing the space between the two PTFE bars d it was possible to control the mass ablated per shot, changing the specific impulse and impulse bit. Figure 7 shows a diagram of the side-fed PPT. It was demonstrated that by varying the distance d it was possible to achieve an optimum impulse bit. Charring was observed in a region of the bars after 10^4 shots and it was hypothesized that there was no arc passing on that region to ionise the carbon atoms deposited there from the exhaust gas.
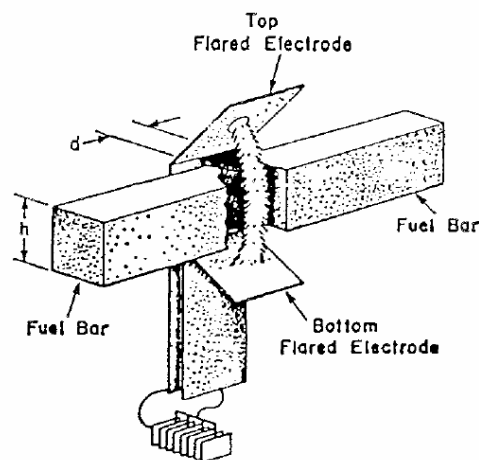
Figure 7: Side-fed PPT with flared electrodes (22).

In 1973, Solbes and Vondra (23) studied the effect of changes in various electric parameters on thruster performance. Based on a rectangular PPT and PTFE fuel they varied the capacitance between 0.66 μF and 6 μF, the voltage V from 500 V to 2000 V, the resistance R from 0 to 0.8 Ω, and the inductance L from 50 nH to 650 nH. They measured the thrust and the fuel consumption

for each configuration. A pendulum was used as a thrust stand on and the thruster was fired in synchronism with the motion of the pendulum. The results from this work showed that for a fixed configuration, i.e. inductance (L), capacitance (C) and resistance (R), the impulse bit and mass ablated per pulse were proportional to the discharge energy[16], as shown in Figure 89. But they also observed that changing R, L or C, in general yields changes in impulse bit, mass ablated, specific impulse and efficiency. Based on these experiments, they developed semi-empirical relationships to calculate the performance of the thruster based on its electrical and geometrical characteristics.
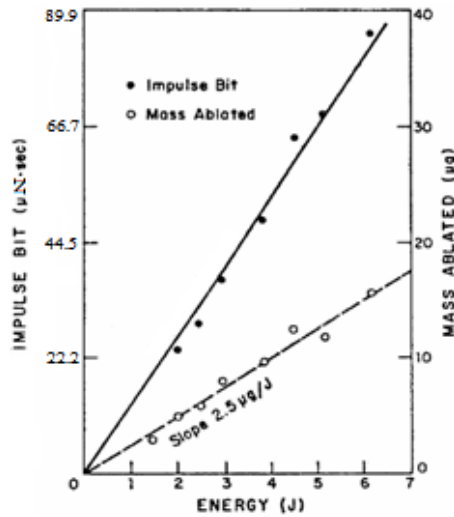
Figure 8: Impulse bit and mass ablated versus discharge energy for a fixed 4µF capacitor. Adapted to SI from reference (23).

Following the geometry experiments and parametric studies, in 1976 Palumbo and Guman (24) performed a parametric study with variations inter-electrode spacing and angles. Importantly, they investigated the PPT performance with different thermoplastics: Celcon, Halar, and

---

[16] The discharge energy in question is the energy E stored in the capacitor, which is $E = \frac{1}{2}CV^2$

unsintered Halon, but found that the best propellant overall was the PTFE. Some tests with Tefzel did show a 63% increase in specific impulse and a 13% increase in thrust efficiency, but also yield a decrease in thrust to power ratio (from 21.07 mN/kW to 16.05 mN/kW) and again made Tefzel less attractive than PTFE as a propellant. It was also tested PTFE seeded with 10% and 30% of LiOH[17] and InBr[18], but no increase in performance was found. In fact, PTFE seeded with LiOH could not be evaluated as it caused erratic behaviour on the thruster. Both rectangular breech-fed and side-fed were tested. They concluded that, with the same initial conditions, the breech-fed geometry yields higher thrust efficiency, due to the higher specific impulse generated – up to 5300 s specific impulses were reported[19]. It observed, especially for the breech-fed geometry, that the performance - in this case specific impulse, efficiency and thrust to power ratio - increased with increasing the angle between the electrodes up to an optimum at 20°, then it decreased rapidly. They also observed that, with fixed discharge energy and capacitance, a reduction in the inter-electrode space caused a more oscillatory discharge, decreasing thrust efficiency.

In 2000, Gulczinski III et al. (25) presented a miniaturised PPT. This so called 'micro-PPT' resembled a coaxial PPT, but had no igniter and no propellant feed system – ideally the electrodes would recede in approximately the same rate as the PTFE. The absence of the igniter yielded an order of magnitude of reduction in the thruster size and operational power level. A non-optimised proof-of-concept design had approximately half of the thrust-to-power ratio that

---

[17] Lithium Hydroxide.

[18] Indium Bromide

[19] These results were never reproduced by other research groups and are above all other reported performances.

of the flight qualified LES-8/9 PPT with a sixty times reduction in mass. Two distinct versions were developed: a triggered micro-PPT and a self-triggering micro-PPT. None of these thrusters had a spark plug. The triggered version had a 1:3 step up transformer with a capacitor on both primary and secondary circuits. It had a switch on the primary that was activated by a 5 Volt TTL[20] pulse. Upon receiving the trigger signal, the primary capacitor was discharged and the capacitor on the secondary circuit was charged until the voltage on the propellant surface was higher than the dielectric strength of the PTFE, when the secondary capacitor was discharged on the propellant. In contrast, the self-triggered version had no triggering circuit and only had one capacitor directly attached to the electrodes of the discharge chamber and initiated the discharge as soon as the voltage in the charging capacitor exceeded the breakdown voltage. Both thrusters were prototypes. Very long lifetime tests invariably ended in a failure mode, as expected. The failure mode was different for each version. The triggered design presented some preferential discharge paths that led to a significant waste of propellant and the self-triggered version would stop discharging when the breakdown voltage was higher than that available to charge the capacitor. The self-triggering was considered more successful due to its simplicity, but had intrinsic shot to shot variations due to breakdown voltages not being constant during operation. It was outlined the importance of the discharge energy to area ratio to avoid charring. It was also observed that current densities at the inner electrode should be high enough to allow it to recede with the propellant face. It was clear that the design trade-off was between the propellant area, inner electrode diameter, electrode material, discharge energy, and voltage.

---

[20] TTL stands for Transistor-Transistor Logic. Commonly, a TTL signal is defined as "low" or "0" if it is between 0V and 0.8V with respect to ground and "high" or "1" if it is between 2.2V and 5V.

Markusic et al. in 2000 presented a new geometry for the PPT, known as Z-Pinch, based on a Z-pinch configuration used in gas-fed devices. As a proof-of-concept, they built and tested three prototypes, namely AZPPT1-3. The main goal of this effort was to increase the performance of the PPTs and the main advantages stated were: mechanical simplicity, structural compactness amenable to miniaturisation, lower exhaust beam divergence, higher thrust-to-power ratio, and high propellant utilization efficiency. The last version tested, AZPPT-3, was claimed to have a specific impulse of 574 s, efficiency of 7.5% and thrust-to-power ratio of $28\,\mu N/W$.

2.2.2 Flight Qualification and Testing of PPTs

Guman and Nathanson (26), in 1970, presented the design built and flight qualification of a PPT for the LES-6 satellite. This PPT was designed to provide east-west station keeping for the spin stabilised, synchronous satellite. It employed four PPTs and tests indicated that issues of contamination and electromagnetic interference were not a problem for this communication satellite. The thrusters weighted 1391g each and used only one power conditioner with four outputs. Firing at 666 mHz the four thrusters produced 17μN thrust. The specific impulse was 500s with 25% due to gas dynamic contribution.

Also, Vondra et al. (27) in 1971 presented diagnostics performed on the LES-6 PPT, showing slightly different values than Gumman and Nathanson (26), and reported a specific impulse of ~300 s, with an impulse bit of ~31μNs, showing that 30% of the energy was lost in capacitor dissipation and plume divergence of ~36° with an ionisation no greater than 10%. They stated that, based on the velocity of the ions, the thrust from the ions alone could conceivably account for all of the thrust. They also performed Doppler measurements, shown in

Table 2, and observed that all excited ions travelled faster than the mass-averaged velocity and that the speed increased with the ionisation level[21], remarking the complexity of the plasma on the PPT.

Table 2: LES-6 species velocities from Doppler measurements (27).

Species	Velocity, km/s
C	10 ± 5
C^+	25 ± 5
C^{++}	——
C^{+++}	35 ± 5
F	10 ± 5
F^+	20 ± 5
F^{++}	——
F^{+++}	30 ± 5

In 1974, Guman and Williams (4), presented the synchronous meteorological satellite (SMS) propulsion system, built on the experience of the LES-6 PPT. The new PPT was reported as being capable of throttling over the range of 92.5µNs to 203.7µNs at a constant specific impulse of 405s. The flight qualification procedure was shown, detailing the vibration and acceleration tests. Interestingly, during a thermo-cycling test one of the flight test units failed with a short-circuit, caused by a radial crack in the capacitor due to the low temperature (between -40°C and -20°C). This capacitor was sealed with hard epoxy, which upon failure allowed air entrapped between the layers of foil and Mylar of the capacitor to be slowly pumped out. The capacitor kept working until its pressure was reduced to a critical value and a breakdown occurred within

---

[21] This is due to the Lorentz force (F) being proportional to the electric field (E), magnetic field (B) and, more important to the point, to the charge of the ion(q): $F = q(E + vB)$.

the capacitor. After replacing the hard epoxy end-seals with a flexible polyurethane potting compound the thruster performed satisfactorily.

Still in 1974, Vondra and Thomassen (28) presented a PPT for the LES-8/9. Designed to work in a set of six units, the PPTs were to be used in orbit acquisition, east-west station-keeping, three-axis attitude control and station changes. Each of the six thrusters had fuel for 7320 Ns total impulse and generated 300 µN thrust at 25W and 1000s specific impulse.

In 1993, Rudikov et al. (29), presented a design for a PPT for use in a 500 kg satellite for maintaining the attitude and pointing during a period of 10 years. With discharges in the range of 220 J to 320 J, the thruster had a lifetime of $2\text{-}3\times10^7$ pulses and produced a total impulse of 2.5×10^5 Ns, consuming up to 13 kg of PTFE. The estimated mass of the thruster was 50-60 kg. After analysing the standard coaxial and rectangular designs they concluded that the volume of the final thruster would be excessive for 13 kg of PTFE and a new geometry was developed, consisting of two half-rings of PTFE having a rectangular radial cross-section, allowing significant savings in volume. It suggests that employing PPTs in missions with a considerably high total impulse requires alternative discharge chamber geometries.

Cassady et al. (30) presented in 2000 the design of a miniaturised PPT for application in formation flying. These nano-satellites produced 70 µNs of impulse bit and had masses between 10kg and 20kg. These satellites were the smallest spacecrafts to fly with a propulsion system up to that point. As a starting point they had the NASA EO-1[22] PPT and had a goal to miniaturise all the components of the EO-1 PPT to make the new thruster. Before deciding on the PPT, they

---

[22] The NASA EO-1 PPT flown on NASA Earth Orbiting 1 Satellite and was launched in 1998.

compared it with a cold gas thruster (model Moog 58E135), and due to the increased specific impulse and reduced total mass of the PPT it was decided that a PPT was going to be used.

For comparison, Figure 9 shows the specific impulse and impulse bit for several flight and laboratory PPTs.
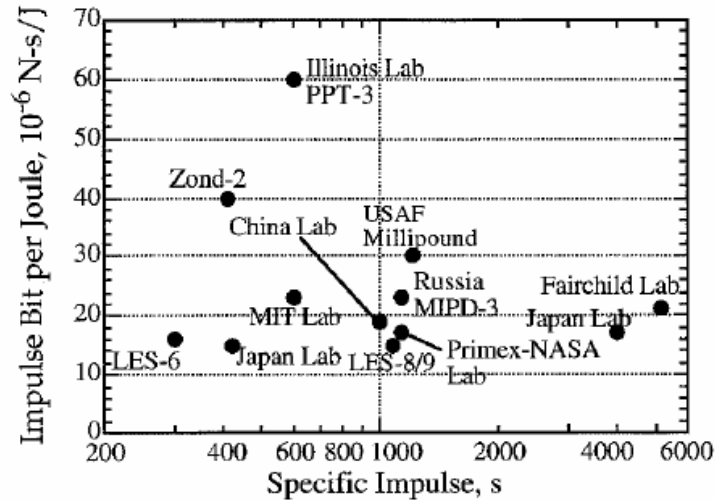
Figure 9: Impulse bit per joule versus specific impulse for various flight and laboratory PPTs (14).

2.2.3 Plume Studies

Thomassen and Vondra, in 1972, studied the exhaust velocity of the PPT (31). They measured the velocity of the ions and excited neutrals, but not the unexcited neutrals. Using a Faraday cup they measured a maximum of 10% of propellant ionisation. The ionised propellant was hypothesized to be responsible for nearly all the thrust for the PPT. They measured an average ion velocity of $\cong 30\ km/s$. They measured the speed of carbon and fluorine both singly, doubly and triply ionised. It was found that species with higher levels of ionisation had higher speeds.

24

In 1973 Thomassen and Tong (32) presented measurements of the exhaust of a PPT using a multiple-pass optical interferometer. Their measurements indicated that, contrary to previous findings, the ionisation level was 40% and not 10%. They also found values for the thermal and drift velocities of 9.3 km/s and 27.9 km/s, which were in agreement with previous experiments.

In 2004, using current mode quadruple Langmuir probe, Gatsonis et al. (33) measured electron temperature, electron density, and the ratio of ion speed to the most probable thermal speed in the plume of a rectangular plate laboratory PPT operating at 5 J, 20 J and 40 J. The measurements were made at 10 cm, 15 cm and 20 cm from the propellant surface and at angular locations up to 40° on both perpendicular and parallel planes to the centreline of the thruster. They measured temperatures at 10 cm from the surface in the range of 10 eV to 18 eV during the rise of the current discharge, but it remained below 5eV for the rest of the discharge. They reported maximum electron densities at 10 cm of 10^{20}, $7x10^{20}$, $1.5x10^{21}$, per cubic metre for 5 J, 20 J and 40 J discharge energy, respectively. They also reported measured ion-speeds at 10 cm of approximately 30 km/s at the beginning of the pulse and below 10 km/s near the end of the pulse.

2.2.4 Propellant and Ablation Studies

In 1996 Spanjers et al. (34) built a modified LES 8/9 PPT to investigate propellant inefficiencies. They developed a laser interferometer system able to measure plasma electron density and, of more interest to this work, high-density neutral gas. This laser interferometer system was used in conjunction with a high speed broadband emission imaging system. Based on the broadband

emission, able to detect excited neutrals[23], it was observed PTFE vaporization for at least 300μs after the end of the current discharge. The authors pointed out that it was possible that the PTFE vaporization continues past this time, as long as the PTFE is at a temperature above its sublimation point. They were the first to directly observe the late-time ablation. They introduced the concept of a two speed flow for the PPT. One for the high speed ionized flow, responsible for around 21% of the mass, travelling at 40km/s to 50 km/s and the other accounting for the late-ablation and 79% of the mass, travelling at 300m/s. They defined the total efficiency of the PPT as the product of the energy efficiency[24], propellant utilization efficiency and power processing unit efficiency. Based on their tests, it was concluded that the propellant efficiency remained constant with increased energy, and that for an arbitrarily high energy discharge the maximum achievable efficiency would be the fraction of mass travelling at high speed, i.e., 21%. Also based on their experiments, for a fixed PPT geometry and discharge energy, they recommended the use of lower capacitance – and consequently higher voltages – to achieve higher levels of ionization and exhaust speeds of the ionized portion of the exhaust. They suggested future works to focus on attempts to reduce neutral gas formation, i.e., late ablation.

---

[23] Excited neutrals are neutrals that have higher energy than a certain reference state (also called ground state). In this state these neutrals were detectable by the high speed broadband emission imaging diagnostic system used in conjunction with the interferometer.

[24] The energy efficiency defined in this work was: $\eta_E = \frac{KE_f + KE_s}{\eta_{PPU} E_0}$, where KE_f is the kinetic energy of the fast ions, KE_s is the kinetic energy of the slow late-ablation, η_{PPU} is the efficiency of the PPU and E_0 is the capacitor stored energy.

Based on the MACH2 code[25], in 1996, Mikellides and Turchi (35) developed a numeric model of the PPT that included the late time ablation. They were able to calculate the mass flow rate from the solid propellant, ablated mass, thrust and impulse bit. The rectangular geometry LES-6 PPT was selected for the simulations, with discharge energy ranging from 1.21J to 4J. The results obtained for current and voltage of the discharge were in good agreement with the experimental results. The most significant outcome of this research was that they actually found a discrepancy with the experimental results for the ablated mass, despite the impulse bit results agreeing with the experiments, where the impulse bit increases linearly with the discharge energy. The total ablated mass during a pulse was greatly underestimated. They raised the hypothesis that the majority of the ablated mass was, in fact, being produced between the discharges. The reason for this is that, as the discharges take place, the propellant temperature increases gradually, to a point where it produces a highly significant mass flow rate between discharges. They calculated steady state mass flow rates for PTFE in different temperatures, as show in Table 2.

Table 3 – PTFE Mass flow rate for different temperatures (35)

PTFE Temperature (K)	Mass flow rate (µg/s)
500	0.546
520	19.13
662	1.66×10^5

---

[25] The MACH2 code was developed by Mission Research Corporation and it is able to solve time-dependant magnetohydrodynamic (MHD) equations.

Taking into account estimated temperatures of the LES-6 PPT propellant, they were able to account for the remaining ablated mass. With the simulations showing that the heat deposited by the plasma created during the discharge was not sufficient to increase the propellant temperature as observed, they deduced that other surrounding sources were providing the extra energy. Their observation was reinforced by the fact that the electrodes - that are in direct contact with the propellant - were observed to be at elevated temperatures, during previous experimental investigations. It was recommended that finding a way of dissipating the heat away from the PTFE - or avoiding the heat to reach the propellant – could improve the propellant efficiency significantly.

Spanjers et al. (17), in 1998, investigated the effect of the PTFE temperature on the efficiency of the PPT. The influence of the average temperature of the propellant on the ablation rate and, most importantly, on the late ablation was studied. It was concluded that the late ablation is ejected at near the sound speed associated with the boiling temperature of PTFE ($\sim 300 \ m/s$). They tested a 20J laboratory PPT and varied the frequency of the discharge to achieve different power levels. By varying the power level from 5W to 60W – which implies a change in the discharge frequency from 0.25Hz to 3Hz - it was observed an increase in propellant consumption of 31% per discharge, a decreased thrust efficiency of 25% and a decrease in specific impulse of 28%, while the propellant temperature increased from 42°C to 135°C. It was verified therefore that an increase in the PTFE temperature caused an increase in the propellant consumption rate per discharge, but no decrease in the impulse. It was suggested that a method of dissipating the heat away from the propellant should be part of the spacecraft thermal design and of future PPT designs.

Continuing previous works, still in 1998, Spanjers et al. (18) investigated the particulate emission from a 20J rectangular PPT operating at 1Hz. They placed aluminium witness plates distributed vertical and horizontally to capture impacting particles. A total of eleven plates were placed around the PPT discharge chamber. Each disk was 6cm from the centre of the propellant face. They also made measurements with a high speed broadband emission imaging system. They estimated that around 40% of the propellant would be exhausted in particulate form. They hypothesized that the particulates could be originated from the deposition of heat below the PTFE surface, this energy would then heat trapped vapours and create a high pressure gas under the surface creating eruptions of the vapours and producing particulates from the surface. Another possibility raised was that propellant could have condensed on the electrodes during several discharges and could be ejected as particulates by vaporization occurring below the coated surface. They calculated a 70% possible increase in efficiency if the particulate emission was completely eliminated. It is worth mentioning that all the material collected by the witness plates were accounted as being generated by particulate emission, with the exception of a portion considered to come from the stainless steel electrodes. However, it should be noted that it is possible that electromagnetically accelerated propellant may have created deposits of fluorine or carbon on the surface of the witness plates, in which case the accounted total particulate mass could be overestimated.

Kamhawi et al. (36), in 2000, investigated an inverse-pinch configuration PPT, both experimentally and theoretically. This PPT consisted of a central conducting electrode, an annular PTFE propellant module, an external annular bell shaped electrode and an extra ring electrode at the exit plane, insulated from the bell shaped electrode. The main goal was to obtain a PPT where the majority of the propellant was accelerated electromagnetically, while keeping

the steady state temperature of the propellant below the PTFE decomposition temperature[26]. To achieve this, they developed an inductively driven PPT where a different from the usual series LRC circuit was utilised. Figure 10 shows a schematic of the circuit presented in this work.
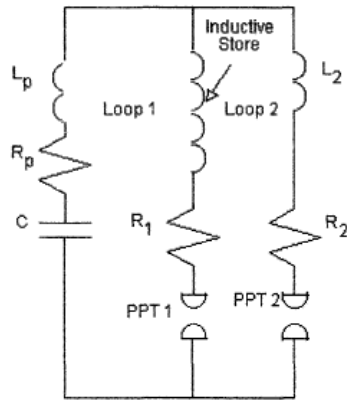
Figure 10 – Inductively driven PPT circuit (36).

In this design, the discharges on the so-called PPT1 and PPT2 started and ended at approximately the same time, with duration of approximately 15µs. The advantage pointed out by the utilization of the two discharges was that it could reduce the current reversals - improving the life-time of the capacitor - and provide extended current pulses to electromagnetically accelerate the majority of the propellant. They concluded that if the PTFE was kept below the decomposition temperature mentioned, higher values of efficiency could be achieved. Amongst the simulated configurations, the most efficient had 9.25% efficiency. And it was identified that approximately 55% of the total input energy was dissipated in the external circuit as joule heating. The experimental work was conducted in two different vacuum facilities and at two different base pressures: 6.65×10^{-6} mbar (5×10^{-6} torr) and 1.33×10^{-3} mbar (1×10^{-3} torr). They tested two different configurations. The results of these experiments show agreement with the

---

[26] In this work an "effective" decomposition temperature was accepted as being 673K (around 400°C).

simulations for current discharge and voltage. However, the expected uniform ablation of the propellant was not observed in the case of the PPT operating at lower pressure. Operating at higher background pressures of 6.65×10^{-3} mbar (5×10^{-3} torr), high speed images taken at the current peak show that the one of the configurations had a much more uniform discharge current, while the other had a localized current discharge. Localized discharges yield non-uniform ablation and therefore poor propellant utilization and lower total efficiency.

In 2001, Keidar et al. (37) analysed the PTFE surface charring of a micro-PPT. They found that the charring area contained mainly carbon and concluded that the carbon char is formed as a result of carbon flux returned from the plasma rather that an incomplete PTFE decomposition. It was also observed a layer of metal under the carbon char. This metal layer was said to come from the electrodes. They also found that the current density and PTFE temperature have peaks near the electrodes, which would explain the preferential ablation of these areas. By comparing the temperature field and the ablation rate distribution with photographs of the PTFE they observed that the area with minimum surface temperature and ablation rate corresponded to the charring area, hypothesizing the charring could be related to a temperature effect.

Antonsen et al. (38) in 2005 presented real time measurements of the PTFE surface temperature after the discharge for a coaxial micro-PPT with 6.35mm outer diameter and 4.35J. They used high speed cameras to allow for visual interpretation of the arc in terms of non-axisymmetric arc spoking effects. This effort was especially interesting in evaluating the late time ablation. They observed exponential temperature decay and demonstrated that, for this particular thruster, the portion of the late ablation would be $23 \pm 11\%$ with a specific impulse of ~60s. Measurements for higher discharge energy and different geometries were not performed.

2.3 Conclusion of the Literature review and relevance of the present work

The most relevant PPT research and development has been reviewed. As a useful reference, Table 4 shows the characteristics of many developed PPTs.

It was possible to verify the importance of the late ablation problem for this type of thruster. In fact, it is reported as the main cause of the PPT low thrust efficiency. On all reported efforts that aimed at studying the late ablation it was clear the attempt to mitigate to production of the late ablation. These works pointed in several directions where improvement in performance can be obtained by keeping the propellant temperature down. However, although it is possible to reduce the late ablation by operating at lower power, the late ablation will always be produced.

It is not known of any research that was focused on accelerating the late ablation. For the first time, in this present work, the focus in set on accelerating the late ablation instead of trying to minimise it.

Table 4: Characteristics of Several PPTs. Expanded and Modified from reference (14).

PPT Thruster	E_0	I_{sp}	I_{bit}	I_{bit}/E_0	$\Delta m/E_0$	$\Delta m/A$	E_0/A	Δm	A
	(J)	(s)	(μNs)	$(\mu Ns/J)$	$(\mu g/J)$	$(\mu g/cm^2)$	(J/cm^2)	(μg)	(cm^2)
LES-6	1.85	300	26	14	4.8	3.3	0.687	8.88	2.69
SMS	8.4	450	133	15	3.4	3.9	1.15	28.6	7.32
LES-8/9	25	1000	300	12	1.14	4.56	4.0	28.5	6.25
TIP-II (NOVA)	20	850	375	19	2.3	5.7	2.47	46	8.07
MIT Lab	20	600	454	23	2.8	4.3	1.53	56	13.0
MIPD-3	100	1130	2250	23	2.0	4.3	2.15	200	46.5
Millipound	750	1210	22300	30	2.5	27.7	11.08	1875	67.7
Primex (NASA)	43	1136	737	17	1.5	2.6	1.73	64.5	24.8
IL PPT-3 Lab	7.5	600	450	60	10.0	36.0	3.60	75	2.08
Japan Lab	30.4	423	469	15	3.7	6.4	1.73	112	17.6
China Lab	23.9	990	448	19	1.9	5.3	2.79	45.4	8.57

E_0 is discharge energy, I_{sp} is specific impulse, I_{bit} is the impulse bit, Δm is the average ejected mass per pulse and A is the exposed area of propellant between the electrodes.

Chapter 3

3. Late Ablation Acceleration Mechanism

As the goal of this research is to accelerate the late ablation, it is convenient to illustrate the production of the late ablation.
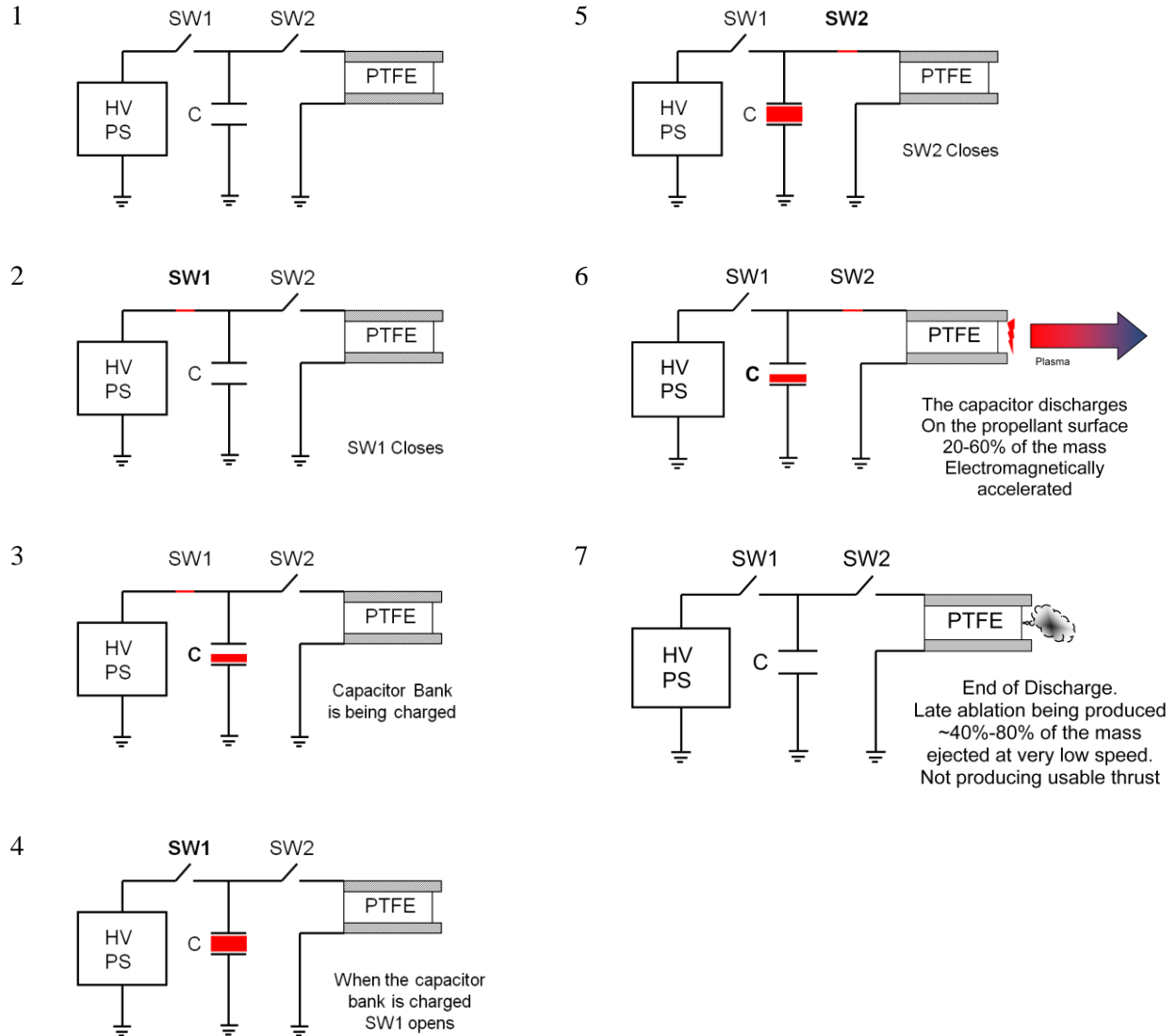
Figure 11: A standard PPT charge/discharge sequence showing late ablation. HV PS = High Voltage Power Supply. SW1 and SW2 are switches. C is the capacitor.

After the main discharge, the mass flow rate from the sublimating propellant is increasingly smaller, as the sublimation rate is proportional to the propellant temperature (39) and the temperature of the propellant reduces after the discharge.

The most immediate solution for this problem would be to smoothly modulate the current of the main discharge to match the mass evolution of the propellant, reducing the current gradually at the end of the discharge, in order to accelerate most of the sublimating propellant. Ideally this technique would employ a high-voltage high-current transistor, in order to be able to operate at typical discharge voltages and currents of PPTs, usually between 1kV-3kV and 20kA-40kA, respectively. Unfortunately, at the time this research was carried out no such device was available to validate this method.

A new method had to be created to achieve such goals with existing technology. The new mechanism had to be able to produce discharge(s) that ideally would match the mass evolution of the late ablation. Additionally – and of extreme importance - if these additional discharges were to take place in the same set of electrodes as the main discharge, close to the propellant surface, the extra generated heat would again promote more late ablation after the end of the secondary discharge(s). It was clear that the secondary discharge(s) had to be triggered from another set of electrodes, downstream. Therefore, in this work two separate discharges are used: a main discharge that takes place at the propellant surface and a secondary discharge that takes place downstream, away from the propellant.

Two possible mechanisms were envisioned: high frequency burst and double discharge. Both mechanisms utilise a modified PPT discharge chamber, hereby called two-stage PPT or TS-PPT. In this way it is possible, for the first time, to divide the two main processes in the PPT thrust

production: ablation and acceleration. Figure 12 shows a schematic view of the TS-PPT discharge chamber.
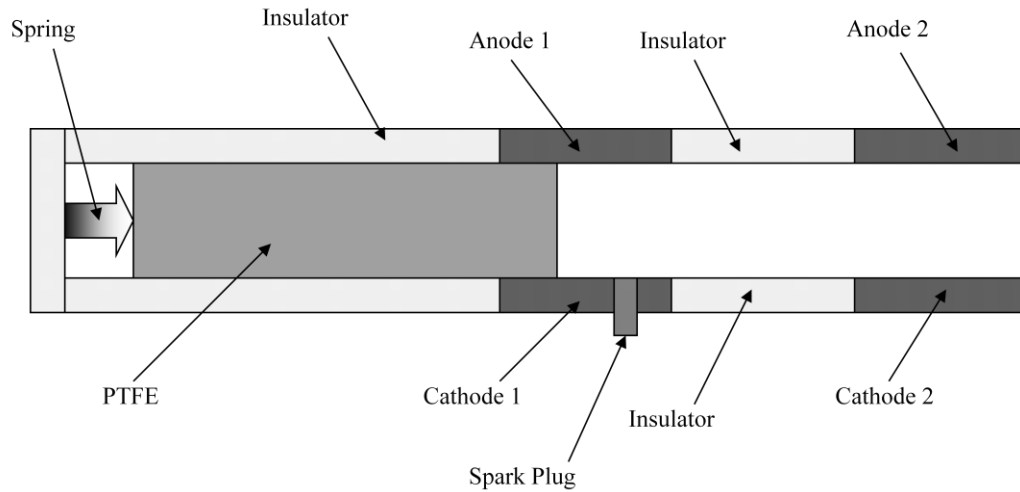
Figure 12: TS-PPT discharge chamber. The new concept of the discharge chamber, dividing the ablation and acceleration processes of the production of the thrust.

In this configuration two discrete pulses occur. A first pulse in the first set of electrodes and a secondary pulse (or pulses) on the second set of electrodes. The first pulse has the main function of producing mass to be accelerated by the secondary discharge, but also gives a significant initial speed to the propellant during the discharge. The first discharge will produce late ablation, as expected. This late ablation will serve as the propellant for the second discharge that will take place downstream.

The second discharge takes place relatively far from the propellant surface and will not produce late ablation[27], and will instead be used to accelerate the late ablation and possibly part of the main discharge plasma[28].

As the propellant total consumption is directly and linearly proportional to the main discharge energy and taking into account the average power of operation of the first pair of electrodes and the consequent steady state propellant temperature, it is possible to use this discharge chamber configuration to precisely dose the propellant mass that will take part in the impulse bit of the PPT.

3.1 Simple Analytic Model of the Late Ablation Acceleration Mechanism

In this work a stronger emphasis is given to the experimental part, but it is useful to have some important relationships defined when analysing the TS-PPT. It must be noted that this model was originally developed for this work and relies solely in the basic definitions of propulsion and a few empirical results from experimental works done by others.

---

[27] As there is a flow of propellant in the downstream direction, convection was not taken into account. Also conduction is discarded as it is assumed that the secondary electrodes are thermally insulated from the propellant and other components in contact with the propellant. The radiation from the secondary discharge is assumed as having a small contribution on the deposition of heat into the propellant that could yield to the production of late ablation.

[28] If the secondary discharge is initiated while there is current flowing in the primary discharge and the plasma produced by the primary discharge reaches the secondary electrodes, this configuration will function momentarily as a two-stage PPT, further increasing the plasma exhaust speed.

3.1.1 The TS-PPT working with a single stage.

If the TS-PPT utilises solely its primary electrodes, it will behave as a conventional PPT[29]. It is then possible to measure the average mass bit lost during a single pulse[30]. Based on empirical equations for rectangular PPTs (35), we can assume a mass variation per pulse in the form

$$\Delta m(\varepsilon_1, T_P) = \alpha_1 \varepsilon_1 + \beta T_P{}^\sigma = m_E + m_G = \frac{m_i - m_f}{N} \tag{3.1}$$

where Δm is the average total mass lost during a single discharge cycle, ε_1 is the discharge energy of the primary discharge, T_P is the steady state temperature of the propellant immediately before the first discharge, m_i is the initial mass of the propellant before the first discharge, m_f is the final mass of the propellant after the last discharge and N is the number of single discharges used to calculate the average mass loss per discharge[31], α_1, β, σ are constants obtained experimentally, m_E is the mass that is accelerated electromagnetically during the first discharge and m_G is the mass of the gas dynamically accelerated propellant.

It is also possible to calculate the impulse bit due to the main discharge.

$$I_{bit_1}(\varepsilon_1, T_P) = \int_0^{t_2} F_P \, dt = \int_0^{t_1} F_{P_1} \, dt + \int_0^{t_2} F_{P_2} \, dt \tag{3.2}$$

---

[29] Friction with the walls is not being considered here for the simplicity of the argument.

[30] This is done typically by measuring the propellant weight before and after a certain number of discharges and obtaining the averaged mass bit as the total mass lost divided by the number of discharges.

[31] The expression $\Delta m = \frac{m_i - m_f}{N}$ is useful when analysing experimental data.

where I_{bit_1} is the impulse bit solely due to the first discharge, F_P is the total force exerted by the exhausting products of the first discharge, t_1 is the time in which the primary capacitor, connected to the primary electrodes, is fully discharged and there is no longer current flowing on the primary electrodes, t_2 is the total time during which the propellant is sublimating[32], F_{P_1} is the force due to the electromagnetically accelerated particles and F_{P_2} is the force due to the gas dynamically accelerated mass, intrinsic in the first discharge. Part of this gas dynamically accelerated mass will come after the discharge as late ablation and part will be produced during the discharge as not necessarily all propellant is ionized and electromagnetically accelerated during the discharge.

The thrust efficiency, defined as the ratio of the total kinetic energy and the discharge energy is given by:

$$\eta_{1A} = \frac{\sum_{i=1}^{EP} m_{ep_i} v_{ep_i}{}^2 + \sum_{j=1}^{GP} m_{g_j} v_{gp_j}{}^2}{2\varepsilon_1} \tag{3.3}$$

where m_{ep_i} and v_{ep_i} are the mass and velocity of the specie i that was electromagnetically accelerated and m_{gp_j} and v_{gp_j} are the mass and velocity of the particle j that was gas dynamically accelerated and EP and GP are the number of electromagnetically accelerated species and the number of gas dynamically accelerated particles.

We can then define the specific impulse for the first stage:

---

[32] The propellant sublimates during and after the discharge, so $t_2 > t_1$.

$$I_{s_{SS}} = \frac{I_{bit_1}}{g_0 \int_0^{t2} \dot{m}\, dt} \tag{3.4}$$

where g_0 is the standard acceleration of gravity at sea level equal to $9.8066 \frac{m}{s^2}$ and $\dot{m}$ is the mass

flow rate of the propellant. We can also define the total mass ablated in a single discharge,

$\int_0^{t2} \dot{m}\, dt$ as Δm, in such way that:

$$I_{s_{SS}} = \frac{I_{bit_1}}{g_0 \Delta m} = \frac{\int_0^{t1} F_{P_1}\, dt + \int_0^{t2} F_{P_2}\, dt}{g_0 \Delta m} \tag{3.5}$$

And the thrust efficiency can then be defined (40) in terms of the impulse bit and the specific

impulse:

$$\eta_{1B} = \frac{1}{2} g_0 I_{s_{SS}} \left(\frac{I_{bit_1}}{\varepsilon_1} \right) \tag{3.6}$$

3.1.2 Adding the Second Stage to the TS-PPT

By adding the second stage of the TS-PPT it is possible to impart further energy to the exhaust

without increasing the total mass ablated, as Δm does not depend on the second discharge, as

observed from:

$$\Delta m(\varepsilon_1, T_P) = \alpha_1 \varepsilon_1 + \beta T_P{}^\sigma = \tau_E + \tau_G = \frac{m_i - m_f}{N} \tag{3.7}$$

where τ_E is the mass that is accelerated electromagnetically during the first discharge and τ_G is

the mass of the gas dynamically accelerated propellant.

The impulse bit of the first stage (or primary discharge) was calculated before as:

$$I_{bit_1}(\varepsilon_1, T_P) = \int_0^{t_2} F_P \, dt = \int_0^{t_1} F_{P_1} \, dt + \int_0^{t_2} F_{P_2} \, dt \tag{3.8}$$

And the impulse bit of the second stage (or secondary discharge) can be calculated as:

$$I_{bit_2}(\varepsilon_2, \Delta m) = \int_{t_3}^{t_5} F_S \, dt = \int_{t_3}^{t_4} F_{S_1} \, dt + \int_{t_3}^{t_5} F_{S_2} \, dt = \int_{t_3}^{t_5} \left(F_{S_1} + F_{S_2}\right) dt \tag{3.9}$$

Where ε_2 is the energy of the secondary discharge, F_S is the total force due to the secondary discharge, t_3 is the instant where the secondary discharge starts, t_4 is the time where the secondary discharge ends, t_5 is the time where no more gas dynamic forces are produced, F_{S_1} is the thrust force due to the electromagnetically accelerated species in the secondary discharge and F_{S_2} is the thrust force due to the gas dynamically accelerated particles in the secondary discharge. It should be noted that there is no late ablation production due to the secondary discharge. Both electromagnetic thrust and gas dynamic thrust are produced during the secondary discharge.

For convenience, we can now define the total mass accelerated electromagnetically and the total mass accelerated gas dynamically and electromagnetically:

$$m_E = \phi \Delta m \tag{3.10}$$

$$m_G = (1 - \phi) \Delta m \tag{3.11}$$

where ϕ is the portion of the mass accelerated electromagnetically.

Similarly to the single discharge PPT, the thrust efficiency of the two stages of the TS-PPT can be calculated by:

$$\eta_{2A} = \frac{\sum_{i=1}^{EP} m_{ep_i} v_{ep_i}^2 + \sum_{j=1}^{GP} m_{gp_j} v_{gp_j}^2 + \sum_{k=1}^{ES} m_{es_k} v_{es_k}^2 + \sum_{o=1}^{GS} m_{gs_o} v_{gs_o}^2}{2(\varepsilon_1 + \varepsilon_2)} \tag{3.12}$$

where m_{ep_i} and v_{ep_i} are the mass and velocity of the specie i that was electromagnetically accelerated in the primary discharge and m_{gp_j} and v_{gp_j} are the mass and velocity of the particle j that was gas dynamically accelerated in the first discharge and EP and GP are the number of electromagnetically accelerated species and the number of gas dynamically accelerated particles, respectively, in the primary discharge. m_{es_k} and v_{es_k} are the mass and velocity of the specie k that was electromagnetically accelerated in the secondary discharge and m_{gs_o} and v_{gp_o} are the mass and velocity of the particle o that was gas dynamically accelerated in the secondary discharge and ES and GS are the number of electromagnetically accelerated species and the number of gas dynamically accelerated particles, respectively, in the secondary discharge and ε_1 and ε_2 are the energy of the primary and secondary discharges, respectively.

Also, from the principle of conservation of mass:

$$\sum_{i=1}^{EP} m_{ep_i} + \sum_{j=1}^{GP} m_{gp_j} = \sum_{k=1}^{ES} m_{es_k} + \sum_{o=1}^{GS} m_{gs_o} = m_E + m_G = \phi \Delta m + (1 - \phi) \Delta m = \Delta m \tag{3.13}$$

It is then possible to define the specific impulse for the TS-PPT:

$$I_{s\,TS} = \frac{I_{bit_1} + I_{bit_2}}{g_0 \int_0^{t_5} \dot{m}\, dt} \tag{3.14}$$

As the source of propellant is only due to the first discharge $\int_0^{t_5} \dot{m} \, dt = \int_0^{t_2} \dot{m} \, dt$, since $\dot{m}(t) = 0$ for $t > t_2$ in a single discharge cycle. It is important to note that, although the times described are sequentially numbered, t_1, t_2, t_3, etc, they do overlap. For example, t_2 is greater than t_3. This nomenclature was chosen to simplify the notation. Figure 13 shows a time diagram of the discharge cycle of the TS-PPT. This diagrams shows a generic case where $t_5 > t_4$. Ideally $t_5 = t_4 = t_2$ and therefore the secondary discharge accelerates all the sublimating propellant.
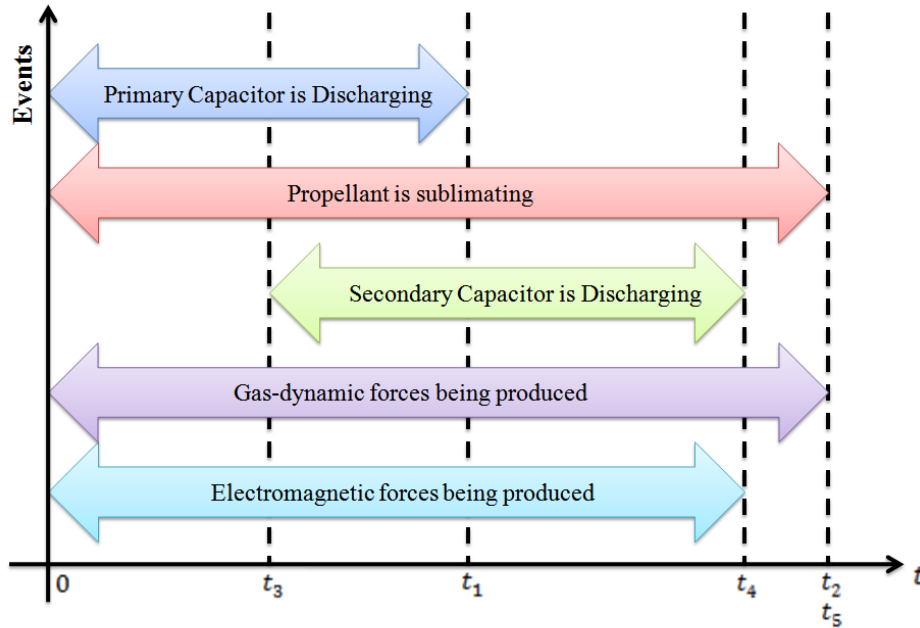
Figure 13: Time diagram of a discharge cycle of the two-stage PPT.

It is then possible to write the specific impulse for the TS-PPT as:

$$I_{s\,TS} = \frac{I_{bit\,1} + I_{bit\,2}}{g_0 \int_0^{t_2} \dot{m} \, dt} \tag{3.15}$$

But as $\int_0^{t_2} \dot{m} \, dt \stackrel{\text{def}}{=} \Delta m$, then

$$I_{s\,TS} = \frac{I_{bit\,1} + I_{bit\,2}}{g_0 \Delta m} = \frac{\int_0^{t_1} F_{P_1}\, dt + \int_0^{t_2} F_{P_2}\, dt + \int_{t_3}^{t_4} F_{S_1}\, dt + \int_{t_3}^{t_5} F_{S_2}\, dt}{g_0 \Delta m} \tag{3.16}$$

And the efficiency of the TS-PPT can be written as:

$$\eta_{2B} = \frac{1}{2} g_0 I_{s\,TS} \left(\frac{I_{bit\,1} + I_{bit\,2}}{\varepsilon_1 + \varepsilon_2} \right) \tag{3.17}$$

3.2 Parametric Study of the Efficiency for the TS-PPT

It is finally possible to do a simple parametric study of the efficiency of the single stage and two-stage PPT. Based on experimental results (14), it is known that the total impulse bit varies linearly with the discharge energy. For the sake of simplicity in this analysis, let us assume that the propellant has reach a constant temperature, T_p, and we will simply write the impulse bit as a function of the discharge energy:

$$I_{bit\,1}(\varepsilon_1) = \varphi \varepsilon_1 \tag{3.18}$$

where φ is obtained experimentally.

Let us also assume that the impulse bit of the second stage will have a similar behaviour:

$$I_{bit\,2} = \breve{\varphi} \varepsilon_2 \tag{3.19}$$

44

For analysis purposes, let us assume that $\check{\varphi} = \varphi$, and then

$$I_{bit\,2} = \varphi \varepsilon_2 \tag{3.20}$$

The assumption of $\varphi = \check{\varphi}$ is considered conservative at this point, as in the second discharge no energy is used for depolymerisation of the PTFE and there is no heat loss to the solid propellant, as the discharge is further for the propellant surface, not considering radiation.

Also, as previously defined, Δm is a function of ε_1 and T_P. Let us also assume that the propellant temperature, T_P, is constant and therefore $\beta T_P{}^\sigma$ is constant, and that $\alpha = \alpha_1 + \frac{\beta T_P{}^\sigma}{\varepsilon_1}$. We can then write:

$$\Delta m(\varepsilon_1) = \alpha \varepsilon_1 \tag{3.20}$$

It is now possible to write the efficiency expressions based on the energies ε_1 and ε_2. Starting from the expression for the specific impulse for the single stage previously defined as:

$$I_{s\,SS} = \frac{I_{bit\,1}}{g_0 \Delta m} \tag{3.21}$$

And the expression for the specific impulse for the two- stage previously defined as:

$$I_{s\,TS} = \frac{I_{bit\,1} + I_{bit\,2}}{g_0 \Delta m} \tag{3.22}$$

We then have the equivalent expressions with the appropriate substitutions:

$$I_{s\,SS} = \frac{\varphi \varepsilon_1}{g_0 \alpha \varepsilon_1} = \frac{\varphi}{g_0 \alpha} \tag{3.23}$$

And

$$I_{s\,TS} = \frac{\varphi\varepsilon_1 + \varphi\varepsilon_2}{g_0\alpha\varepsilon_1} = \frac{\varphi(\varepsilon_1 + \varepsilon_2)}{g_0\alpha\varepsilon_1} = \frac{\varphi}{g_0\alpha}\left(1 + \frac{\varepsilon_2}{\varepsilon_1}\right) \tag{3.24}$$

We can also calculate the efficiency of the single stage and two-stage in a similar way. Starting from the original expressions for the efficiency, as defined previously:

$$\eta_{1B} = \frac{1}{2}g_0I_{s\,SS}\left(\frac{I_{bit\,1}}{\varepsilon_1}\right) \tag{3.25}$$

And

$$\eta_{2B} = \frac{1}{2}g_0I_{s\,TS}\left(\frac{I_{bit\,1} + I_{bit\,2}}{\varepsilon_1 + \varepsilon_2}\right) \tag{3.26}$$

Applying the substitutions we have:

$$\eta_{1B} = \frac{1}{2}\frac{(\varphi\varepsilon_1)^2}{\alpha\varepsilon_1{}^2} = \frac{\varphi^2}{2\alpha} \tag{3.27}$$

And

$$\eta_{2B} = \frac{1}{2}\frac{(\varphi\varepsilon_1 + \varphi\varepsilon_2)^2}{\alpha\varepsilon_1(\varepsilon_1 + \varepsilon_2)} = \frac{1}{2}\frac{[\varphi(\varepsilon_1 + \varepsilon_2)]^2}{\alpha\varepsilon_1(\varepsilon_1 + \varepsilon_2)} \tag{3.28}$$

Or, simplifying,

46

$$\eta_{2B} = \frac{\varphi^2}{2\alpha}\left(1 + \frac{\varepsilon_2}{\varepsilon_1}\right) \tag{3.29}$$

As an example we can substitute α and φ for experimental data obtained for the LES 8/9 PPT $(34)^{33}$. We then have:

$$\alpha = 1.14\frac{\mu g}{J} \tag{3.30}$$

And

$$\varphi = 12\frac{\mu Ns}{J} \tag{3.31}$$

We then substitute these values on the expression for the efficiency:

$$\eta_{2B} = \frac{\left(12\frac{\mu Ns}{J}\right)^2}{2\left(1.14\mu \times 10^{-3}\frac{kg}{J}\right)}\left(1 + \frac{\varepsilon_2}{\varepsilon_1}\right) \tag{3.32}$$

We can have $\frac{\varepsilon_2}{\varepsilon_1}$ as a parameter called γ and doing the calculation:

$$\eta_{2B} \cong 63.158 \times 10^{-3}(1 + \gamma) \tag{3.33}$$

---

[33] While the LES8/9 PPT is a single stage PPT, its performance on the first stage is valid for this analysis. And even more valid because the goal of this analysis is to study trends in the efficiency varying ε_1 and ε_2 and, more importantly, α and φ are constants.

Therefore, the efficiency of the first stage alone is around 6.3%. With the second stage the efficiency will increase as γ goes up. This should hold true for TS-PPTs with an optimised second stage, where the specific thrust for the second stage can be comparable to the specific thrust of the first stage, φ. In this parametric study $\varphi = \breve{\varphi}$ was considered. However, if $\varphi \neq \breve{\varphi}$, and in the worst case $\varphi > \breve{\varphi}$, it is still possible to achieve higher specific impulses depending of the choices of ε_1 and ε_2, although the efficiency of the thruster will be reduced.

With the hypothesis stated, comparing the efficiency of the two-stage PPT with the single stage PPT it is possible to see that higher values of efficiency and - more importantly - specific impulse than those of the single stage PPT can be obtained when $\varepsilon_2 > 0$ and the specific thrust for the second stage is comparable to the specific thrust of the first stage.

We can make another simple comparison for a case where the same total discharge energy is employed in both single stage and two-stage PPT. In this case, let us assume that:

$$\varepsilon_{1_{two-stage}} = \varepsilon_{2_{two-stage}} = \frac{\varepsilon_{1_{single-stage}}}{2} \tag{3.34}$$

And

$$\varepsilon_{1_{two-stage}} + \varepsilon_{2_{two-stage}} = \varepsilon_{1_{single-stage}} \tag{3.35}$$

Then, it can be seen that:

$$\eta_{2B} = \frac{\varphi^2}{2\alpha}\left(1 + \frac{\varepsilon_{1_{two-stage}}}{\varepsilon_{2_{two-stage}}}\right) = \frac{\varphi^2}{\alpha} \tag{3.36}$$

And then, comparing with the efficiency of the single stage:

$$\eta_{2B} = 2\eta_{1B} \tag{3.37}$$

The efficiency of the two-stage PPT, in this case, is twice the efficiency of the single-stage PPT, as expected from simply looking at the expression for η_{2B}.

Differently than the case for the single stage, the two-stage PPT can achieve higher efficiencies, depending on the choice of ε_1 and ε_2.

Chapter 4

4. Implementation of the Late Ablation Acceleration Mechanism

As observed by Antonsen et al. (38) the temperature of the propellant decays as a negative exponential. The propellant temperature returns to the steady state temperature in the following fashion:

$$T_p = T_0 + \zeta e^{-\xi t} \tag{4.1}$$

where T_0 is the steady state temperature of the PTFE at the beginning of a discharge, ζ and ξ are constants that can be obtained experimentally.

Based on the theoretical analysis shown in the previous chapter it was verified that the implementation of the late time ablation acceleration mechanism can be achieved in more than one way. As one of the main attractive points of the original PPT was its simplicity, special attention was given to keeping the mechanism as simple as possible. Two ways of accelerating the late ablation were considered and one was chosen to be implemented.

4.1 High Frequency Burst Method (HFB-PPT)

The High Frequency Burst method, also here referred to as HFB-PPT, is one of the considered mechanisms to achieve the acceleration of the late ablation. The principle of operation of the HFB-PPT is to generate subsequent high frequency discharges after the main discharge. The main challenge to implement this concept is the switching device that must be capable of

switching at high frequency, high voltage and at high currents. A device called IGBT - Insulated Gate Bipolar Transistor - was found as being a candidate for this role and a new system employing such device was then considered.

With the HFB-PPT method several secondary discharges are employed in order to allow a greater portion of the sublimating propellant to be electromagnetically accelerated. This pulsed method would distribute the secondary discharge energy in several pulses to match the mass evolution of the late ablation. A variant of a technique known as PWM(41) - Pulse Width Modulation – could be used to modulate the energy of the secondary discharges. This PWM-like technique can allow the control of the average power of the discharge. This discharge modulation could use IGBTs as switches, but differently from a standard PWM signal, there would be no repeatable cycles inside a given burst. Instead the duty cycle of each pulse would decrease to match the expected mass evolution from the PTFE surface. Figure 14 gives an example of an arbitrary discharge and propellant temperature for a regular PPT, based on previous works (38) (34). In black is the TTL control signal (5V=ON/0V=OFF) for the spark plug system that initiates the main discharge, in blue and red are arbitrary qualitative variations of the discharge current and propellant mass flow rate, respectively. In this hypothetical example the current starts from 0A and is raised to a steady high value, typically 20kA. The propellant is initially at room temperature (300K) and is raised to a high value (>1000K) by the discharge current. It can be seen qualitatively that the propellant takes a considerable amount of time to cool. During this time mass is being sublimated from the surface. Looking at this figure it is possible to have an idea of time-scales of the events. Typical PPT discharges last for 20μs, but the propellant can take 300μs and possibly more (38) to cool and stop sublimating.
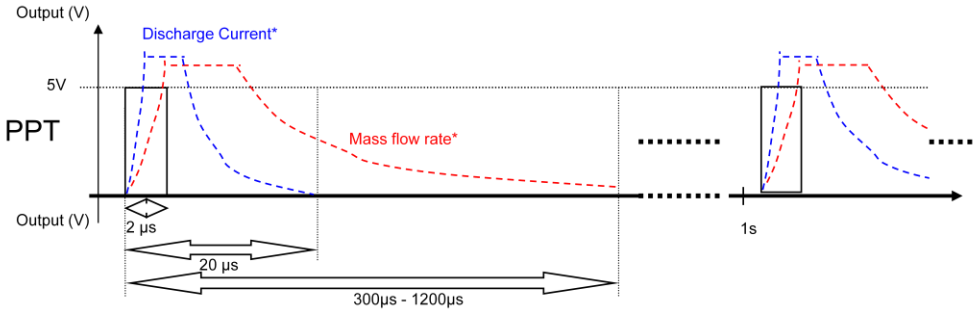
Figure 14: An example of an arbitrary discharge for a PPT firing at 1Hz. *Discharge current and Propellant mass flow rate are arbitrary qualitative variations only.

Because the relative smoothness of the distribution of power is dependent on the frequency of the modulation when using a PWM-like technique – which modulates the duty cycle of the on/off discharge signal - the first hypothesis was that the secondary pulses should occur at a relatively high frequency, compared to a standard PPT discharge frequency (typically 1Hz), to be able to efficiently electromagnetically accelerate most of the late ablation while varying the power in an attempt to match the ablation rate changes after the main discharge. The main reason for this is because of the relative long duration of the late ablation. The secondary discharges would occur as a high frequency burst, after the main discharge. This is the principle of operation of the high frequency burst pulsed plasma thruster – HFB-PPT.

To illustrate the operation of the HFB-PPT mechanism here described, Figure 15 shows the secondary discharge control pulses (black), hypothetical qualitative secondary discharge current (blue) and propellant mass flow rate (red) of a conceptual HFB-PPT discharge. The pulses are modulated to match the mass flow rate of the late ablation. Although this figure is for illustration purposes only, it shows the principle of operation of the HFB-PPT using a PWM-like technique.

52
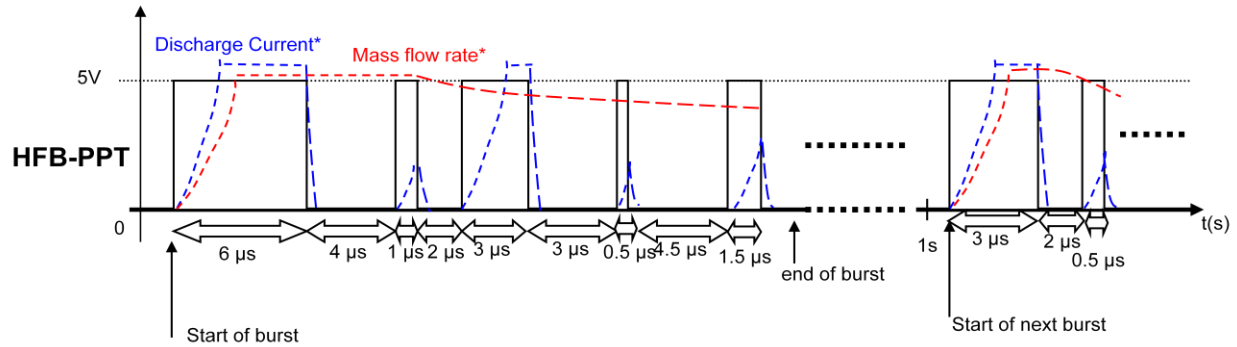
Figure 15: A conceptual HFB-PPT secondary discharges. *Discharge current and Propellant mass flow rate are arbitrary qualitative variations only to show the concept of the control system.

The downside of the HFB-PPT method is the necessity of operating the switching system at high frequency, high current and high voltage. Although the IGBT was found as a possible candidate to work as the switch, a control system was necessary to generate the control signals.

Because of the relatively high added complexity, another simpler method that could modulate the secondary discharge current was investigated.

4.2 Double Discharge Method

Due to the intrinsic complexity of the switching system of the HFB-PPT, an attempt was made to simplify the mechanism but still achieve the constraints of modulation of the secondary current discharge to follow the late ablation mass evolution.

When returning to the ideal solution of the transistor mentioned earlier in the beginning of the previous chapter, a simpler possible technique arises. This technique employs a single secondary discharge and is modulated by the first discharge and by the late ablation. The current is modulated by the electrical resistance of the products of the first discharge when they reach the secondary electrodes and varying the voltage of the secondary discharge capacitor. There is no switch in this method and the secondary discharge capacitor is always connected to the

53

secondary electrodes. During the main discharge – and therefore before the late ablation – the current flowing in the plasma due to the first discharge is expected to induce currents in the secondary electrodes. This is due to time variation in the magnetic field - in this case caused by varying current in the first pair of electrodes - inducing an electric field. The induced electric field is responsible for the expected modulation of the current. Figure 16 illustrates the mentioned induction.
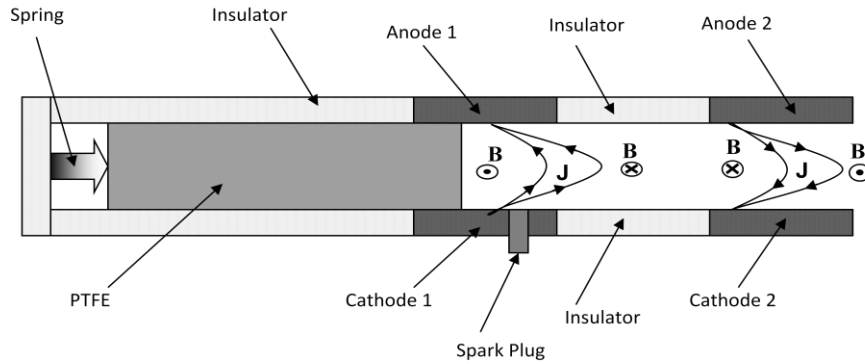
Figure 16: Changing magnetic field inducing a current in the secondary electrodes.

Also, the current in the secondary electrodes will depend on the resistance of the plasma between the electrodes.

$$I_s = \frac{V_{02}}{R_{P2}} e^{-t/R_{P2}C_2}$$

where V_{02} is the initial voltage of the secondary capacitor, R_{P2} is the total electrical resistance between the electrodes of the secondary discharge, C_2 is the capacitance of the secondary discharge capacitor and t is the secondary discharge time.

Therefore, the total current in the secondary electrodes should have the form of:

$$I_s = I_{MF}(t) + \frac{V_{02}}{R_{P2}} e^{-t/R_{P2}C_2}$$

where $I_{MF}(t)$ is the current due to the plasma induction, as mentioned above.

Figure 17 illustrates the expected behaviour of the Double Discharge Method. The first discharge is shown in blue and modulates the current on the second electrodes, shown in red. After the end of the first discharge the secondary discharge behaves similar to a capacitor discharging circuit. The time scales and current magnitudes shown serve as an example only, but are consistent with the experiments of this work.

Electric Current (kA)

$$I_{MF}(t) + \frac{V_{0_2}}{R_{P2}} e^{-t/R_{P_2}C_2}$$

$$\frac{V_{0_2}}{R_{P2}} e^{-t/R_{P_2}C_2}$$

20

10 I_1

20   40   100   200   Time (µs)

Primary Discharge and Secondary Discharge

Only Secondary Discharge
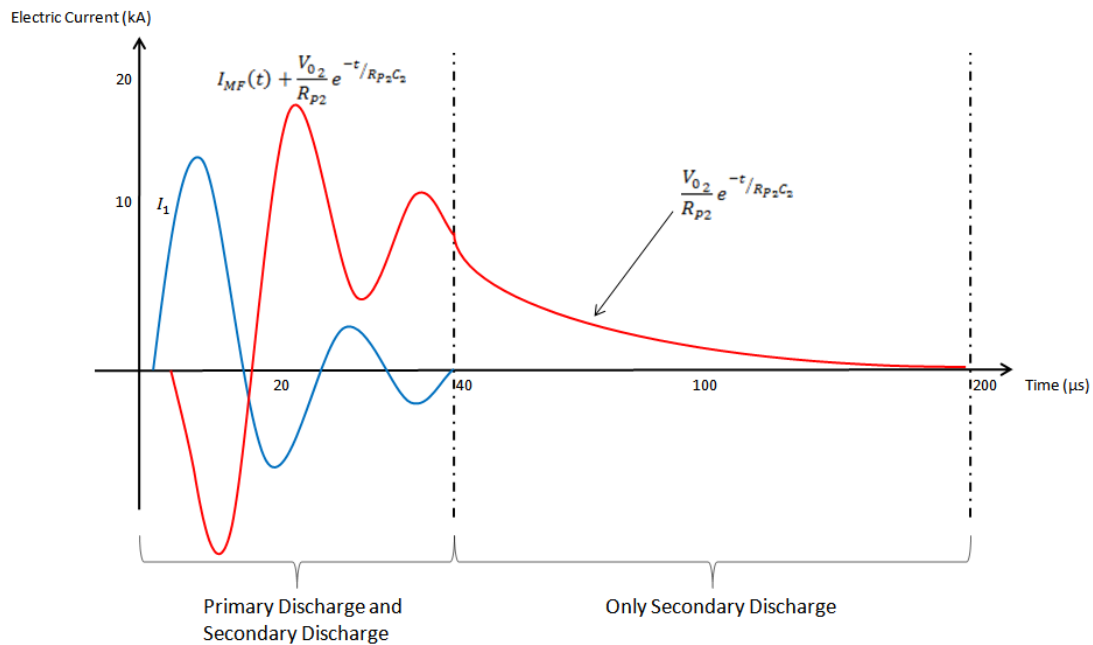
Figure 17: Expected discharge currents when using Double Discharge Method. In blue is the first discharge current and in red the secondary discharge current.

4.3 Summary of the Late Ablation Acceleration Mechanisms

Both mechanisms presented have the unique advantage of - for the first time - dividing the thrust production of the PPT in two non-exclusive phases: ablation and acceleration. This is achieved through the use of two sets of electrodes, instead of one – like in the conventional PPT. Two

candidate methods were analysed: high frequency burst PPT (HFB-PPT) and two-stage PPT (TS-PPT). The TS-PPT presented itself as a simpler solution and more suitable for the philosophy of the PPT and was chosen to be implemented. However, the HFB-PPT is still a valid idea.

Chapter 5

5. Test Facility

At the beginning of this research no suitable vacuum facility was available to perform the tests. A new facility was built on purpose for this research. A vacuum tank, originally used as a thermo-cycling chamber, donated by QinetiQ several years ago was set to be used as the vacuum chamber. Also a cryogenic pump donated by QinetiQ was to be used in this facility. A rotary pump was available from the Astronautics Research Group and was also used.

5.1 Building the Vacuum Facility

The vacuum facility was designed around the vacuum chamber donated by QinetiQ. This vacuum chamber was 1.2 m long and 0.8 m diameter, and was made of non-magnetic stainless steel. Figure 18 and Figure 19 show a diagram of the vacuum chamber with some custom made parts. Port 13 was used for connection with a cryogenic pump.

Due to the lack of lateral viewports, a mirror was placed on Port 11 underneath the chamber to allow for visualisation of the experiment. Ports 3 and 4 had custom made high voltage (10kV), high current (200A) feedthroughs. Port 5 was connected to the rotary pump. A vacuum gauge was connected to the Port 1.

The mechanical pump was an Edwards E2M80 Two Stage Rotary Vacuum Pump 3kW with ultimate pressure of 1×10^{-4} mbar and maximum pumping speed of $74 \frac{m^3}{h}$. The cryogenic pump was a CVI TorrMaster$^®$ TM250 Cryopump, water cooler, using Helium pressurised at 285 psig ($\cong$ 20.7bar) with a maximum pumping speed of $34,200 \frac{m^3}{h}$. For pressure measurement it

was used a Pfeiffer SingleGauge™ TPG 261 controller with a PBR 260 gauge able to measure pressures from 1×10^3 mbar to 5×10^{-10} mbar.

Port 13 had a custom size flange and to be able to mount the cryogenic pump a custom adaptor had to be designed and manufactured and also custom made o-rings had to made. To be able to operate the cryogenic pump efficiently a pneumatic gate valve was also used. Also, as due to the weight of the cryogenic head (approximately 86kg), the gate valve and the adaptor flange it was decided that simply bolting the components on Port 13 was not acceptable and a support was designed and built. Figure 20 and Figure 21 show the designed support with the components.

Also the laboratory itself had to be modified to provide three-phase electrical supply for the pumps, compressed air for the gate valve, exhaust for the rotary pump, electrical safety switches and controls and water for cooling the compressor of the cryopump.
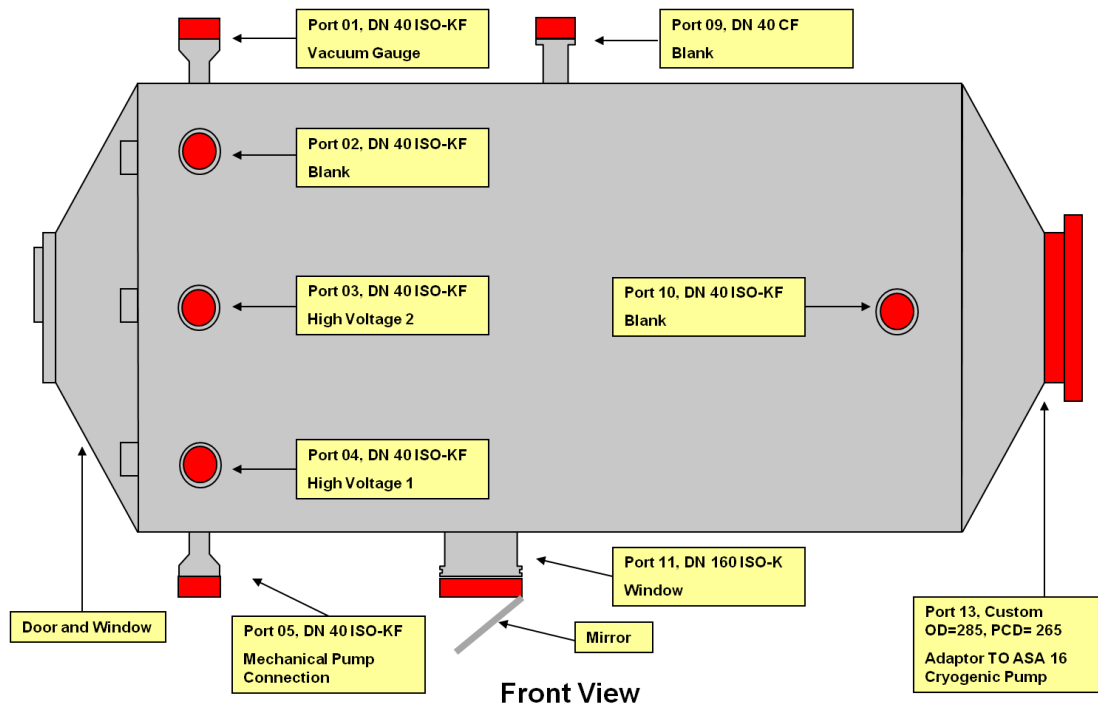
Figure 18: Schematic front view of the vacuum facility CPVF1, used for the tests.

58

Back View

Port 09, DN 40 CF
Blank

Port 01, DN 40
Vacuum Gauge

Port 08, DN 40 ISO-KF
Venting Valve

Port 10, DN 40 CF
Blank

Port 07, Custom
Thermocouple
Feedthrough

Port 06, DN 40 ISO-KF
Blank

Port 11, DN 160 ISO-K
Window

Port 13, Custom
OD=285, PCD= 265
Adaptor TO ASA 16
Cryogenic Pump

Mirror

Port 05, DN 40 ISO-KF
Mechanical Pump
Connection

Door and Window
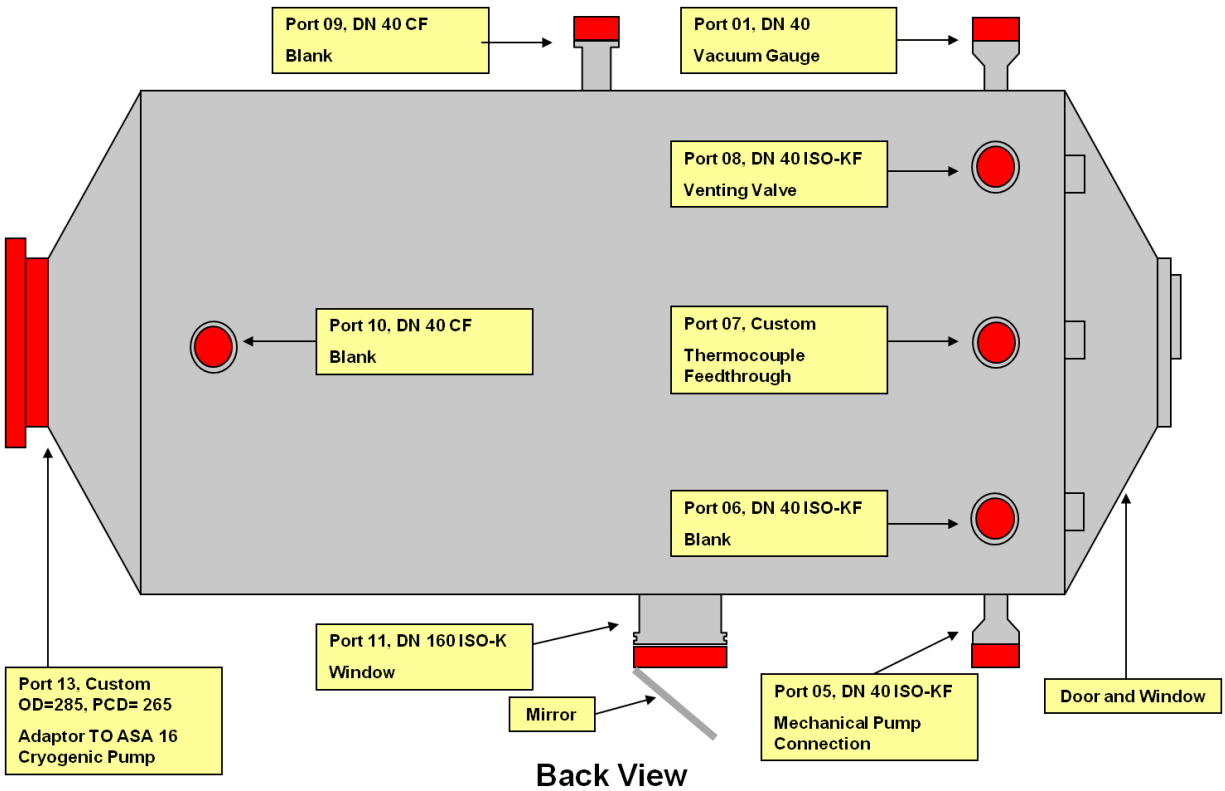
Figure 19: Schematic back view of the vacuum facility CPVF1, used for the tests.

This facility was named Cryogenic Pumped Vacuum Facility 1 (CPVF1) and is one of the vacuum facilities of the Astronautics Research Group Laboratories at the University of Southampton.

After finished tests indicated that the CPVF1 was able to reach a pressure lower than $1{\times}10^{-7}$ mbar after 20h, with no load and starting the cryogenic head from ambient temperature.

However, under normal use, when the cryogenic head reached its steady state temperature, with the gate valve closed, it was possible to open the chamber to perform maintenance, then use the rotary pump to bring the pressure down to $4{\times}10^{-3}$ (after 10 minutes) and by opening the gate valve of the cryogenic pump, achieve a pressure of $5{\times}10^{-6}$ after another 20 minutes only.

The results indicated that the CPVF1 was able to be used for PPT tests.

59
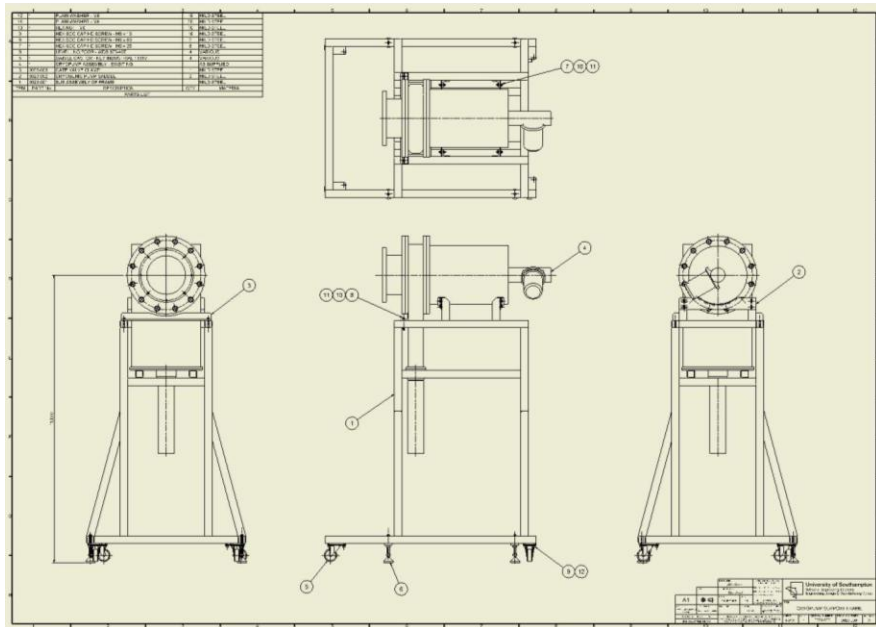
Figure 20: The designed support for the cryogenic head, gate valve and flange adaptor.
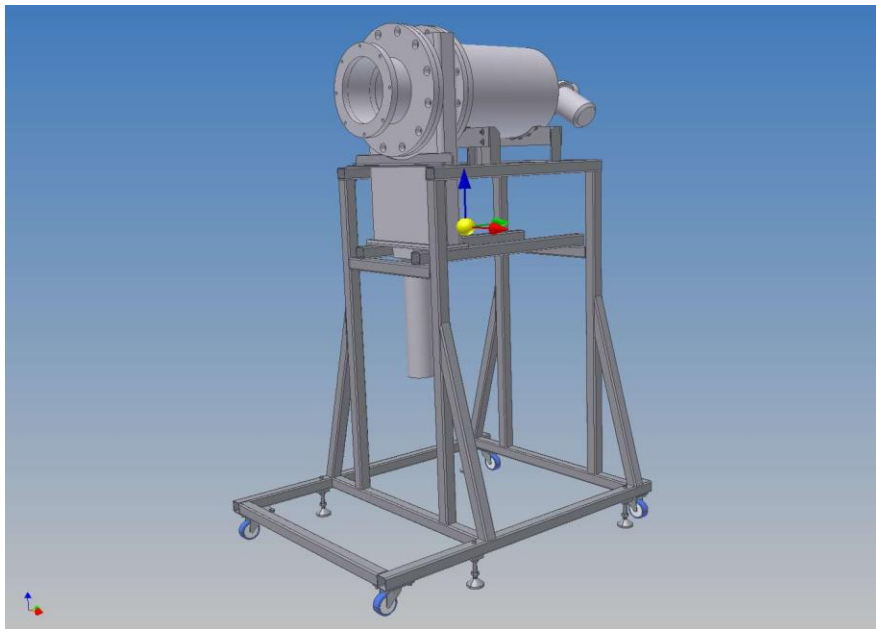
Figure 21: The Cryogenic head, the gate valve and the flange adaptor mounted on the designed support.

Figure 22 shows the facility finished, Figure 23 shows a detail of the cryogenic head, gate valve and the support and Figure 24 shows the cryogenic pump compressor. Figure 24 shows the pressure gauge controller and the pressure gauge.
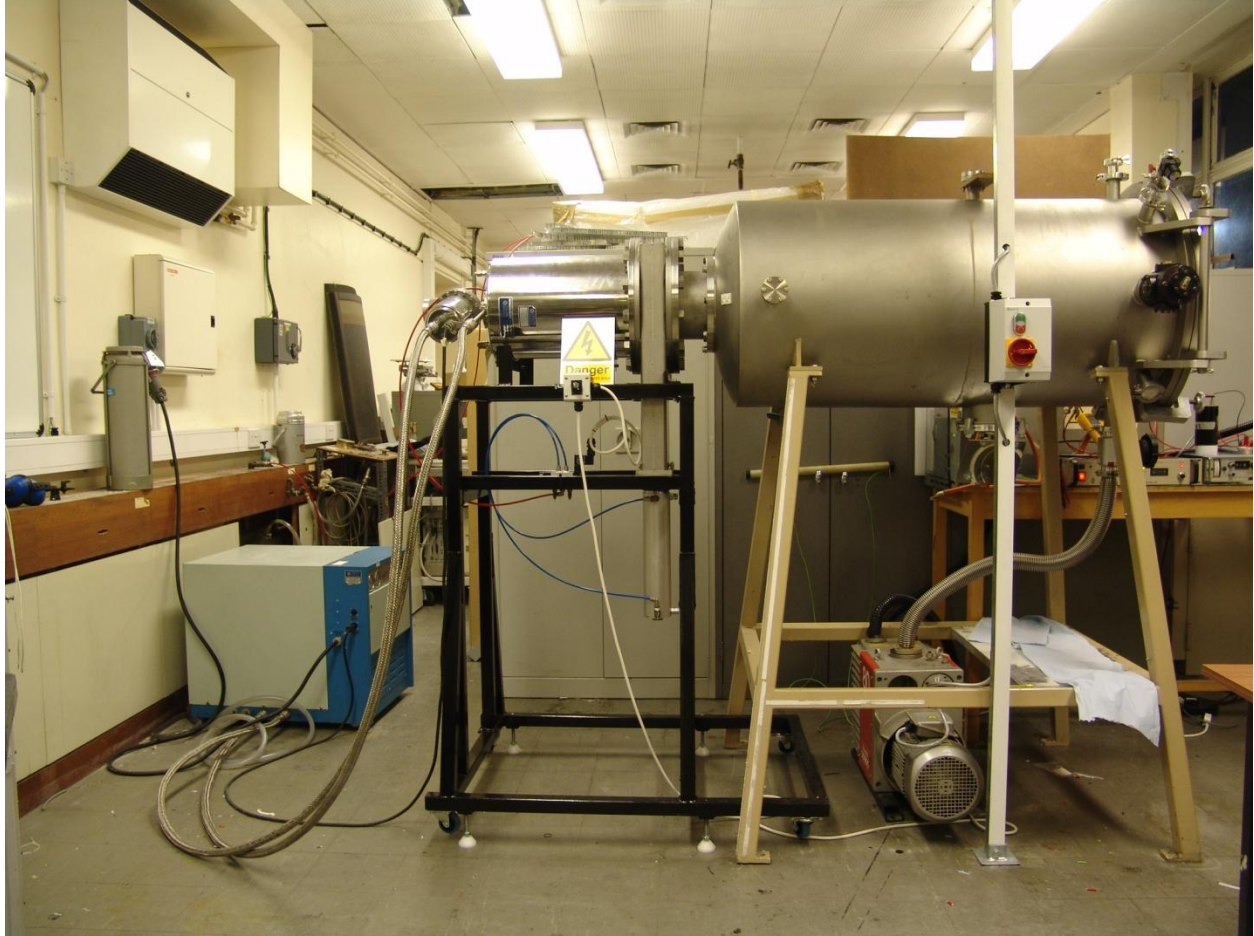
Figure 22:The Astro Group CPVF1 facility assembled at the University of Southampton.
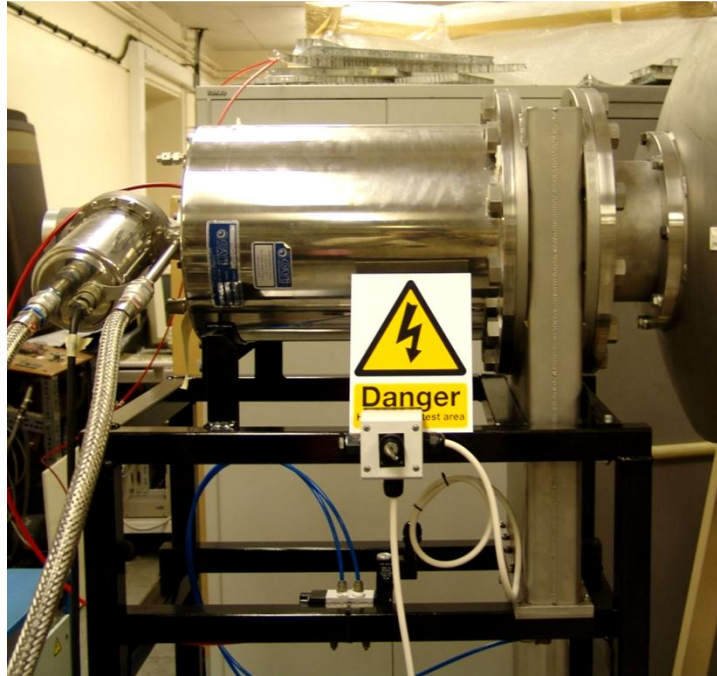
Figure 23: Detail of the cryogenic head, the gate valve and its pneumatic circuit and the designed flange adaptor and mechanical support.

Figure 24: The cryogenic pump compressor.

a)   b)

Figure 25: The Gauge controller (a) and the pressure gauge (b) installed on the facility.

5.2 Power Supplies

Two variable high voltage power supplies were used to charge the primary capacitor and the secondary capacitor. Two variable low voltage (0-12Vdc) power supplies were used to power the IGBT controllers, optical interface and the spark plug circuit.

The primary capacitor was powered by a Glassman EQ010R120-22 high voltage power supply, variable from 0V to 10kV and up to 120mA, as shown in Figure 26.

The secondary power supply was an Oltronix A2,5K-10HR, variable from 0V to 2.5kV and up to 10mA, as shown in Figure 27.

Figure 26: Primary capacitor power supply, model Glassman EQ10R120-22.

Figure 27: Secondary capacitor power supply, model Oltronix A2,5K10-HR.

Chapter 6

6. TS-PPT Implementation

The control system of the TS-PPT was developed in a research campaign at INPE – Instituto Nacional de Pesquisas Espaciais (The Brazilian National Space Research Institute) at the LCP - Laboratório de Combustão e Propulsão (Combustion and Propulsion Laboratory) – in Cachoeira Paulista – São Paulo – Brazil.

The TS-PPT comprises a discharge chamber, a switching system, a control system hardware and software, custom made peripherals, and capacitor banks.

6.1 System Overview

The PPT main component is the discharge chamber. This is also the case with the TS-PPT. Because of this the discharge chamber is used here to provide a system overview for the TS-PPT. The discharge chamber is the place where the solid propellant PTFE is housed against two electrodes, called primary electrodes. The primary electrodes are responsible for dosing the amount of propellant that will form the mass of a single discharge – or mass bit, Δm. Further downstream there are two more electrodes – the secondary electrodes – responsible for the acceleration process of the mass produced by the primary discharge. Due the linear variation of Δm with the primary discharge energy, the primary electrodes are able to dose the propellant though the use of a known energy for the primary discharge.

It must be noted that the rules of the primary electrodes and secondary electrodes are *non* exclusive. In fact, the primary discharge does accelerate the propellant, but for the TS-PPT philosophy, this is *not* its main role. Likewise, the secondary electrode discharge should not

contribute to any increase in the ablated mass, in a way that the total Δm should be independent of the secondary discharge. In practice, due to radiation, a very small amount of heat deposition on the propellant is expected due to the secondary discharge. The analysis in this work will not take this radiation effect into account. Figure 28 shows a schematic diagram of the discharge chamber.
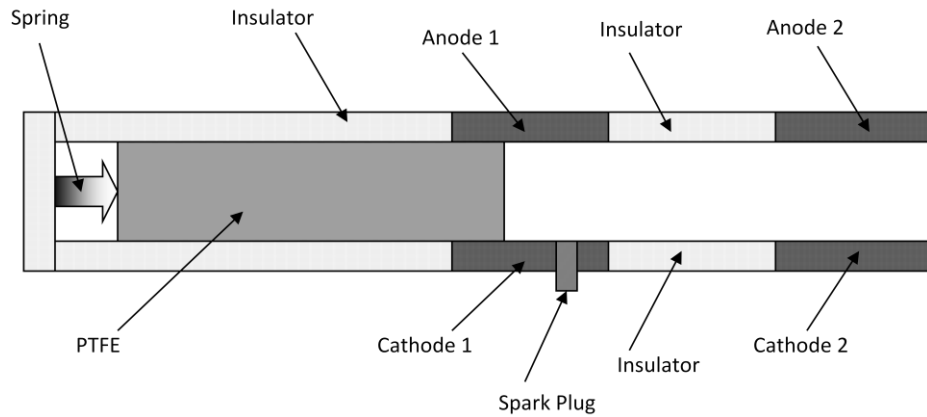
Figure 28: The TS-PPT schematic diagram.

The TS-PPT discharge chamber is connected to a custom designed circuit. This circuit comprises the primary capacitor, secondary capacitor, spark plug capacitor, DC-DC converter – or power supplies -, and digital control unit. A schematic of the TS-PPT discharge chamber connected to its circuit can be found on Figure 29. The digital control unit receives commands and is able to generate the appropriate signals to control the charge and discharge processes of the TS-PPT. The capacitor C1 is the primary capacitor, C2 is the secondary capacitor, C3 is the spark plug capacitor. The black numbered circles represents the switches. The Switch 1 controls the primary discharge, Switch 2 controls the secondary discharge and Switch 3 control the spark plug. The high voltage generated by the DC-DC converter – or power supplies – are used to charge the

capacitors. HV1 charges C1, HV2 charges C2 and HV3 charges C3. The DC-DC Converter can be powered by a 28Vdc bus, as shown, or while in the laboratory, by a 240Vac source.
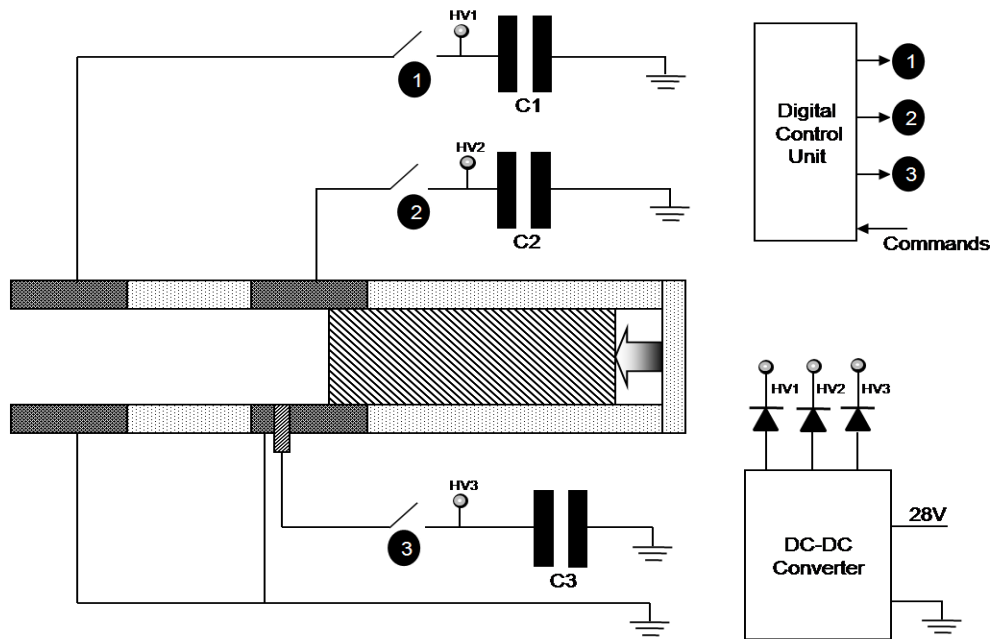
Figure 29: TS-PPT system schematic overview.

The operation of the system starts by charging all the capacitors, C1, C2 and C3. Then, as the digital control unit (DCU) receives the signal to perform a discharge cycle, it starts by generating a CLOSE signal Switch 1, so that C1 is connected to the secondary electrodes. The DCU then generates a CLOSE signal to Switch 2, connecting C2 to the primary electrodes. The last step involves generating a CLOSE signal to Switch 3 that will yield the discharge of C3 and produce a discharge on the surface of the spark plug, producing free electrons and ultra-violet radiation, a combination of which (14) will start the discharge of C2 on the surface of the propellant. As the plasma reaches the secondary electrodes, C1 will start to discharge. This whole cycle lasts for a very short period of time, between 200µs and 300µs.

In order to generate the control signals a PC104 computer was used and the switches were implemented with IGBTs, as mentioned earlier. Figure 30 shows a block diagram of the TS-PPT.
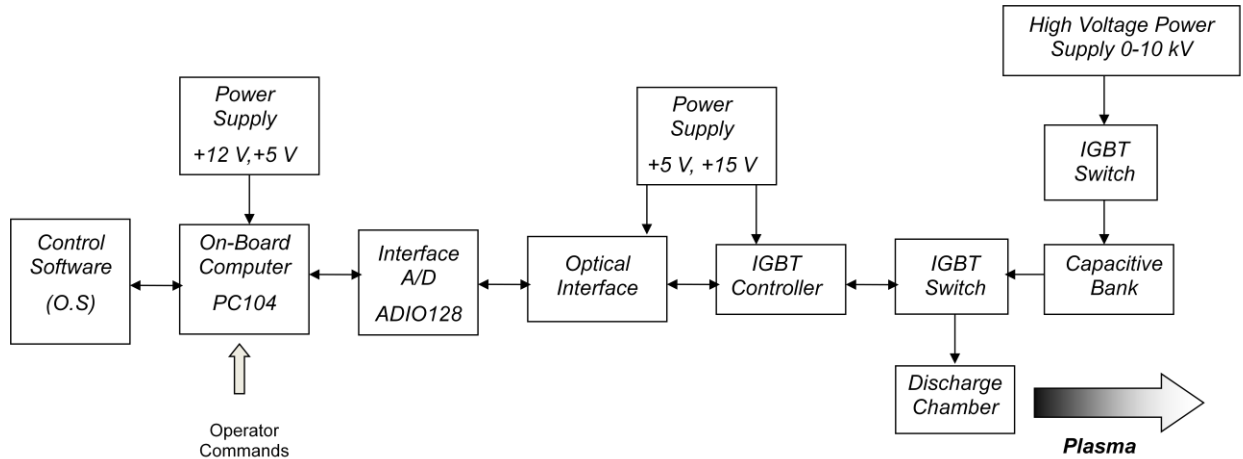
Figure 30: TS-PPT Block Diagram.

The Control Software is a custom made software in "C" Language to generate the pulses. The PC104 is a flight computer where this software runs and acts as the digital control unit - DCU. The analogue to digital (A/D) interface is responsible for sending and receiving signals from the switching system. The optical interface performs the electric insulation of the high voltage and low voltage logic control system. The IGBT controllers generate the proper signals to the IGBT switches and controls the charge and discharge of the capacitive bank.

Figure 31 shows the TS-PPT discharge sequence in a schematic way to illustrate the process on the discharge chamber.
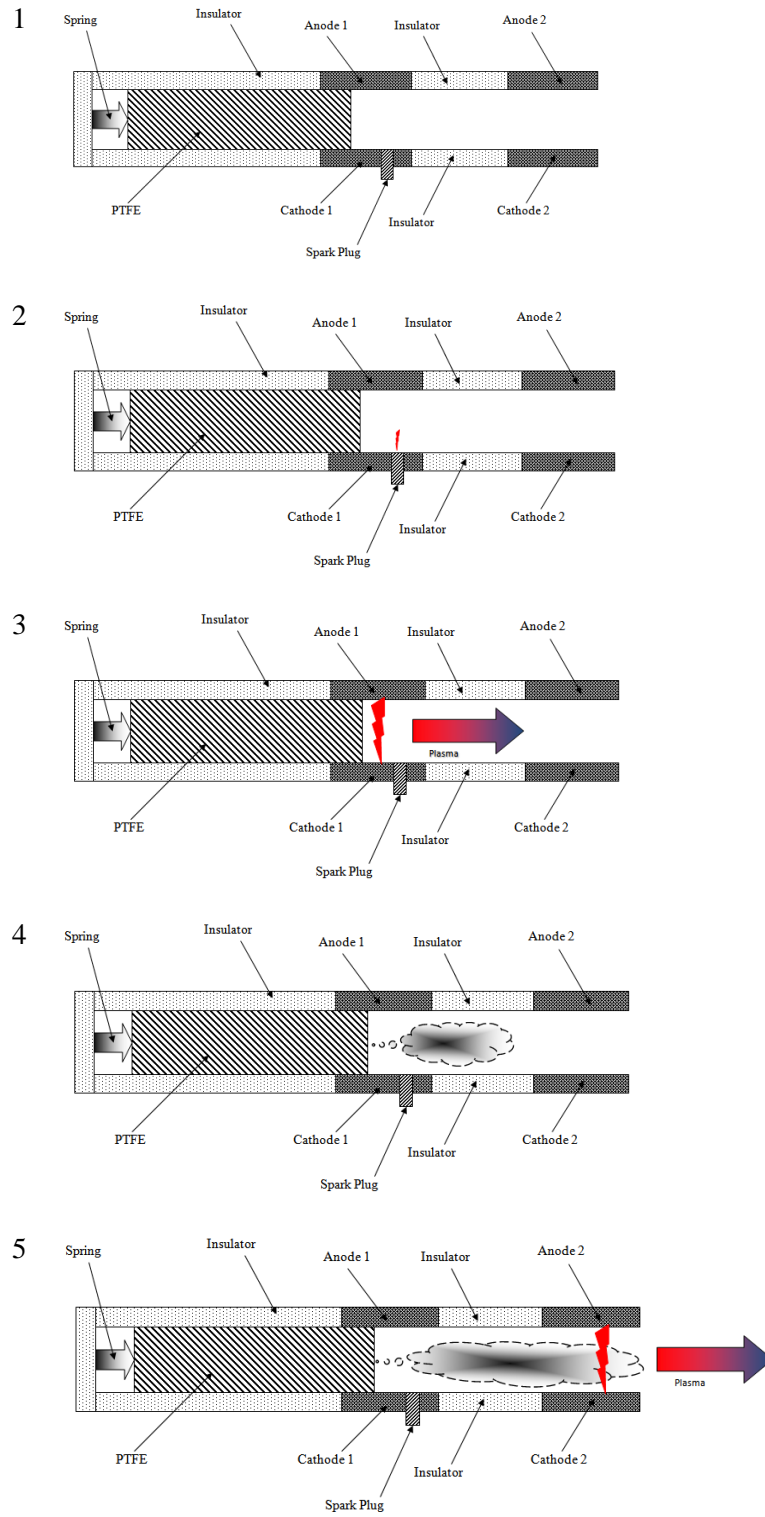
Figure 31: TS-PPT Discharge sequence schematics.

6.2 Switching System

The electronics of the TS-PPT differs significantly from the one on a conventional PPT. A PPT typically uses a SCR (Silicon Controlled Rectifier) as a switch to control the discharge of the capacitor that triggers the spark plug. The SCR is a device that after triggered cannot be turned off, until the current flowing is approximately zero – and the capacitor is fully discharged.

As a requirement, during the design of the TS-PPT it was decided that it should be possible to re-trigger the spark plug to aid the secondary discharges, meaning that the spark plug itself would be required to operate at a much higher frequency than on a conventional PPT. From an electrical point of view, charging the spark plug capacitor after each discharge at high frequency is less than ideal. A device that could discharge the spark plug capacitor in several discrete steps was necessary. Because this requirement is very similar to those of the secondary discharges of the HFB-PPT method, the same solution was applied by using an IGBT.

In this case, the IGBT had to be able to operate at high current (up to 25kA) and high voltage (up to 1.2kV). These requirements were set taking in account normal PPTs (14), as the main differences between PPTs and TS-PPTs are not maximum voltage and current, but how these are applied, i.e., several pulses instead of one pulse. A partnership with a main supplier of electronic components, Semikron Brazil, was established and a switching system was designed specifically for the TS-PPT. The supplied system can be seen in Figure 32. The original system comprise two capacitive banks, two IGBTs, two IGBT control boards, a cooling system and three diodes.

6.3 Control System Hardware

Due to the specific switching needs of the TS-PPT the control system also significantly differs from the one on a conventional PPT. While in the PPT normally there is only one input signal – typically a TTL (Transistor-Transistor Logic) pulse – to trigger the spark plug, the TS-PPT needs a rather more complex logic circuit.

The main function of the control system in the TS-PPT is to synchronise the discharge of the spark plug, main discharge and secondary discharges. In order for a control system to be considered it must be able to have independent control of each of the switches and be able to communicate with the controller boards of the IGBTs. Several systems were considered and a special computer system called PC-104 was selected as the control system and was acquired with two expansion boards to provide a total of 8 D/A ports, 8 A/D ports and 12 digital I/O ports. Figure 33 shows the control system assembled with the PC104. On the left side is the base board

with the CPU and interfaces and on the right side is a Compact Flash (CF) card slot. This system allow for TTL signals to be generated at a maximum frequency of 1 MHz (1 µs pulses).
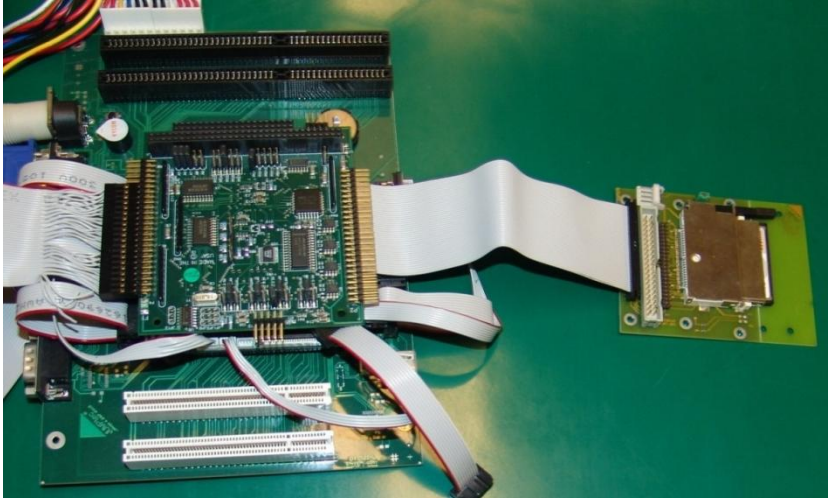
Figure 33: The HFB-PPT control system.

The PC-104 was time calibrated to allow for precise switching of the IGBTs. The calibration workbench can be seen in Figure 34. Pulses can be switched on/off with a ±1 µs precision.

Figure 34: The calibration workbench for the PC104 Control System.

6.4 Control System Software

To generate the required pulses to control the TS-PPT, a software in "C" Language (42) was developed. The goal of the software was to provide a flexible platform to allow different tests to be performed automatically. A picture of the software running on the PC-104 can be seen in Figure 35.

The programming of the software was carried out in a portable PC computer using a "C" compiler and then after compiling it is transferred to a CF card and inserted in the CF card slot in the PC-104 system. The PC-104 was equipped with a standard 104-keys keyboard and a VGA monitor to allow user interaction.

Figure 35: The software written in "C" language running on the PC-104 control system.

6.5 Power System Coupling

In order to allow the PC-104 computer to communicate with the IGBTs an interface had to be developed. This interface provides an optical insulation for the PC-104, converting its TTL signals to optical signals, avoiding direct electric connection from the control system to the power system. This is very important, since the PC-104 is a computer device, therefore sensitive to voltage fluctuations and strong electromagnetic fields and could be irreparably damaged if there was a failure in the power system that could allow contact of the cable connecting the PC-104 and the high voltages in the power system. Figure 36 shows the power system coupling for the TS-PPT.
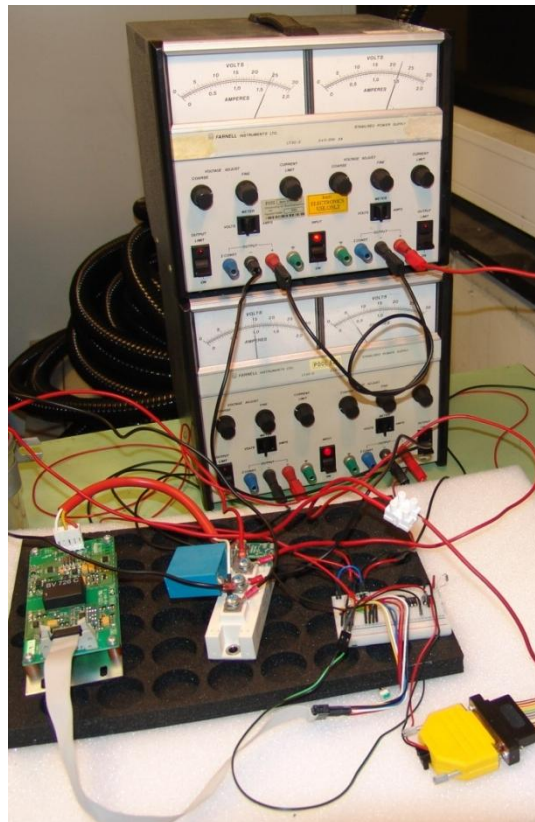
Figure 36: Custom made peripherals. On the black support: IGBT control board (left), IGBT (center), optical couplers (right) and auxiliary power supplies (background).

6.6 Capacitor Banks

Two capacitor banks were used. The main capacitor, used for the primary discharge, was a non-polarised BICC 7 kV, 110 µF, up to 2695J, fast discharge, heavily sealed, military specified capacitor. A picture of the primary capacitor can be seen in Figure 37. The secondary capacitor was an EPCOS 450V, 4700µF, up to 475J, as seen in Figure 38.

Figure 37: TS-PPT Main capacitor.
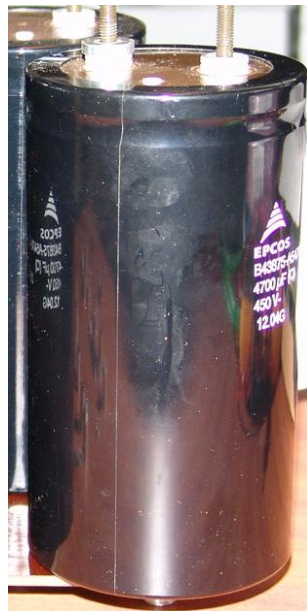
Figure 38: TS-PPT secondary capacitor.

6.7 Discharge Chamber

The most important single component on a PPT is the discharge chamber. This is also the case with the TS-PPT. The geometry of the discharge chamber dictates the overall characteristics of the PPT. Several PPT configurations were tested by others in an attempt to achieve higher performance (16) (23)(22) (24). Interestingly, two geometries are recursively used across the more than 40 years of development of the PPT: rectangular and coaxial.

It was decided that either a rectangular or coaxial geometry would be considered. However, ordinary PPT discharge chamber configurations could not be used without modifications because a new pair of electrodes had to be included. New designs were required and the main challenge was to allow the secondary discharges to occur in a different set of electrodes, relatively far from the surface.

As the absolute most common design for PPTs is the rectangular, this was the chosen geometry for the TS-PPT.

6.7.1 Rectangular Design

A rectangular design was conceived. This configuration resembles an ordinary rectangular spring fed PPT but has an additional pair of electrodes - namely *Anode 2* and *Cathode 2* – that are mainly responsible for the acceleration of the propellant. Based on the concept shown in Figure 28, the TS-PPT discharge chamber was designed and can be seen in Figure 39. The secondary

electrodes are relatively far from the propellant surface and have a divergent shape[34]. The spark plug is located slightly further away from the propellant surface than in a regular PPT, in an attempt to make it usable with the secondary electrodes.

To be able to mount the TS-PPT in the vacuum chamber a custom interface was designed and built, shown in Figure 40. Figure 41 shows the design of the discharge chamber on the interface inside the vacuum chamber and Figure 42 shows the actual TS-PPT discharge chamber mounted on the built interface inside the vacuum chamber during assembly[35]. Some figures show the thruster mounted perpendicular to the vacuum chamber axis, close to the wall; this was done only for photography reasons and not for testing.
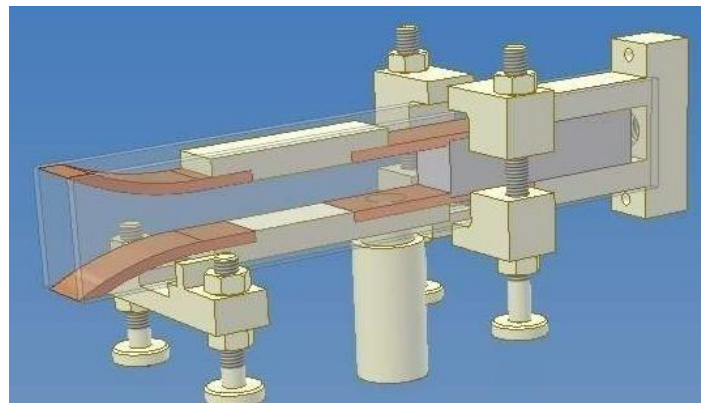
Figure 39: TS-PPT discharge chamber.

---

[34] The divergent shape of the secondary electrodes had the intent to improve the performance of the thruster for gas-dynamic accelerated propellant.

[35] In this picture, taken during assembly, only the primary electrode and the spark plug are connected.
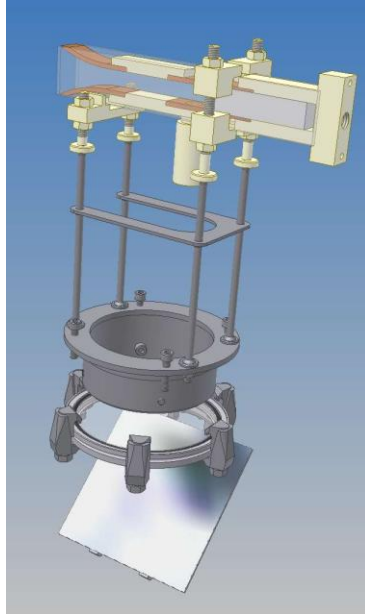
Figure 40: Design of the discharge chamber with the custom interface.
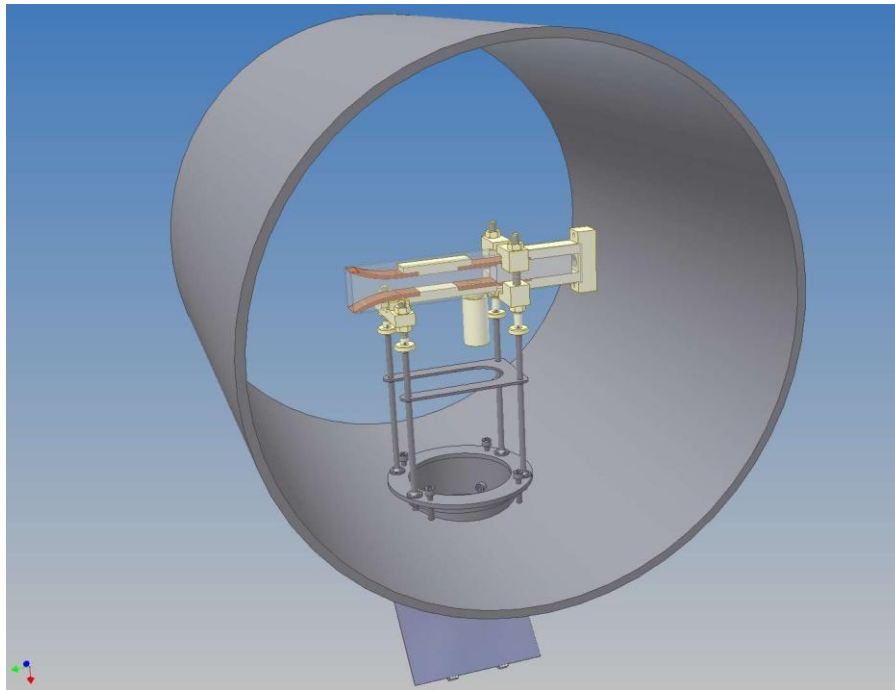
Figure 41: Design of the discharge chamber on the support inside the vacuum chamber.

Figure 42: TS-PPT inside the vacuum chamber being prepared to be tested.

The propellant module was a $25 \times 25 \times 102 \ (mm)$ bar of PTFE and was spring fed to the primary electrodes. The primary electrodes, made of copper, were $97 \times 25 \times 3 \ (mm)$. The secondary electrodes, also made of copper, were $85 \times 25 \times 3 \ (mm)$ and had a curvature radius of $54 \ mm$. The spark plug was inside a nylon receptacle in the cathode 1 and was an adaptation of an automotive spark plug, where the outer electrode was removed and a hollow cylinder of PTFE coated with carbon was placed between the electrodes, resembling a small coaxial PPT. In order to allow visual monitoring of the thruster operation, glass side walls were used as part of the structure of the TS-PPT discharge chamber.

Chapter 7

7. Experimental Results

7.1 Preliminary Tests

As the thruster itself was a completely new development, before initiating long tests with the TS-PPT it was necessary to validate each of its components. Preliminary tests were carried out to verify the operation of the spark plug circuit and the main electrodes circuit and also to obtain the value of the average mass bit consumption per cycle, Δm.

7.1.1 Spark Plug Tests

The first component tested was the spark plug. At first a conventional automotive spark plug was used, but during the tests, at a pressure of 4×10^{-6} mbar, it was observed that the breakdown voltage was in excess of 20kV. Obviously this spark plug was not made to operate in vacuum, but in fact in high pressures (> 1000mbar). A new idea to use a coaxial PPT as spark plug arose and the original automotive spark plug was then adapted into a coaxial PPT. Its curved top electrode was removed and a hollow cylinder of PTFE was used as an inter-electrode material. To further reduce the dielectric strength of the spark plug a thin layer of carbon was deposited on the surface of the PTFE. After the modifications the spark plug was able to operate at 3.6kV. Figure 26 shows the spark plug discharging at 4×10^{-6} mbar during the tests. The spark plug circuit included an auto-transformer (1:60) where a 0.15μF capacitor charged at 60V (0.27mJ) was discharged on its primary. The sparkplug discharge was controlled by an IGBT (Semikron SKM 145GAL174D) that received a signal from the IGBT control board (Semikron SKHI 10/17)

that in turn received a digital from the output of a control board on the PC-104 computer (Kontron SpeedMops Pentium III 700MHz PC104). The control signals were tested at high frequency and were capable of generating control pulses that last for 2μs and different signals could be as close as 3μs, as shown on Figure 44.
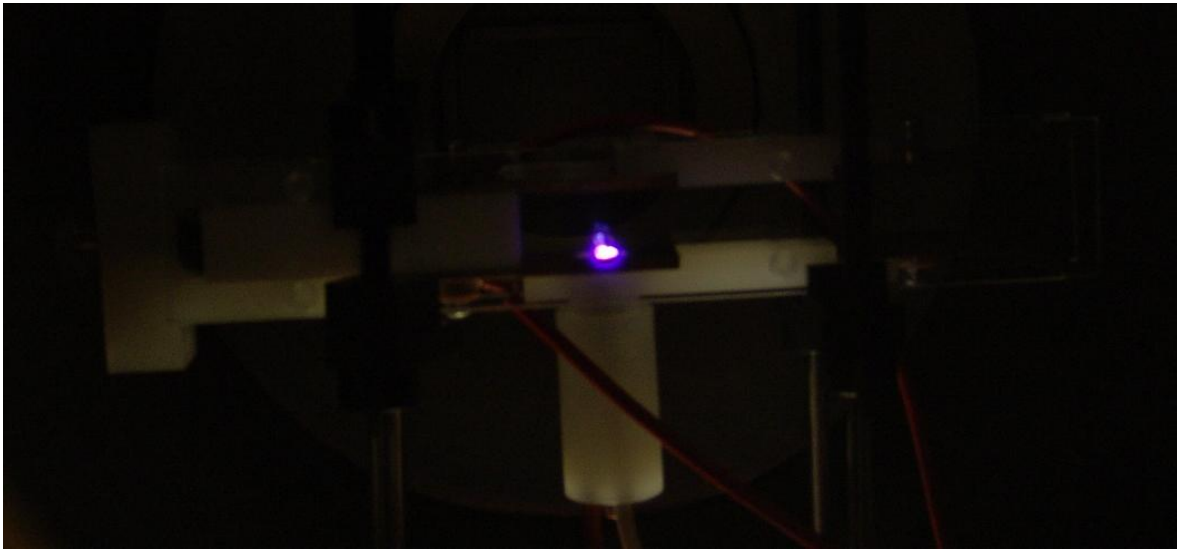
Figure 43: Spark Plug tests.
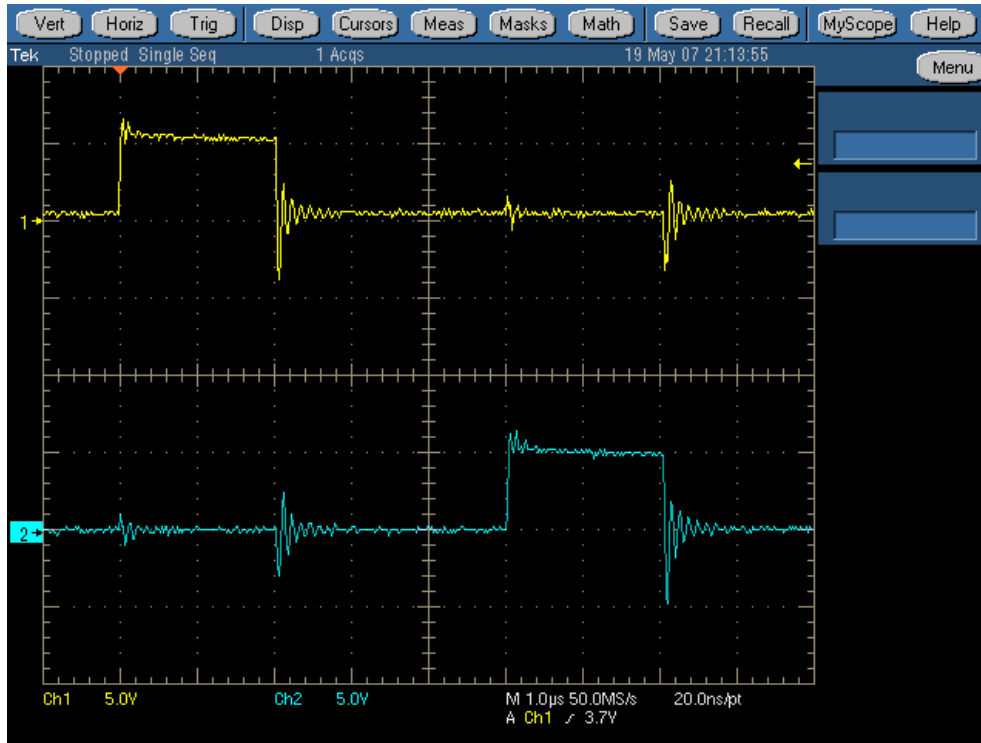
Figure 44: Control signals programmed in software running of the PC104.

7.1.2 Primary Discharge Tests

The primary electrodes were directly connected to the high voltage Glassman power supply, able to operate at up to 10 kV and up to 100mA. However, the main capacitor was able to operate at up to 7kV (110µF).

To find the operating points of the primary discharge it was necessary to analyse the ranges of energy density that the thruster would operate in order to both avoid charring on the propellant surface and avoid damage to the circuitry. Based on other studies (14), to avoid charring, the energy density should be higher than $0.687 \, J/cm^2$. It was decided to allow a large margin for the energy density and a minimum energy density of $9 \, J/cm^2$ was chosen.

Knowing that the surface area between the electrodes of the TS-PPT was $5.25 \, cm^2$ and, as a first approach, using $\varphi = 18 \frac{\mu Ns}{J}$, it was possible to generate a table of energy density and an

estimated impulse bit for several levels of discharge energy of the primary discharge. It is worth observing that this estimated impulse bit is uniquely due to the first discharge. Observing Table 5 it can be seen that when the primary capacitor is charged at $960V$, the energy of discharge is $50.69J$ and the energy density is $9.65\,J/cm^2$. This was the established minimum operating discharge energy for the TS-PPT first discharge. The upper limit chosen was $200J$ ($1910V$, $200.65J$, $38.22\,J/cm^2$) to avoid possible damage to the circuits due to unforeseen issues. In this table it was assumed a specific thrust of $18\mu Ns/J$ (43), as mentioned. For comparison, Table 4, on page 33, summarised data for several PPTs, including energy density and impulse bit.

Table 5: Energy densities and estimated impulse bit for a range of primary discharge energies.

Prospective Operating Voltage	$\varepsilon_{Cap} = \frac{1}{2}CV^2$	Propellant Area $= 5.25 cm^2$	Estimated Impulse Bit Primary Discharge Assuming $\varphi = 18\frac{\mu Ns}{J}$
Voltage (V)	Energy (J)	Energy/Area (J/cm^2)	(x10^{-6} Ns)
50	0.14	0.03	2.48
100	0.55	0.10	9.90
150	1.24	0.24	22.28
200	2.20	0.42	39.60
250	3.44	0.65	61.88
500	13.75	2.62	247.50
750	30.94	5.89	556.88
960	50.69	9.65	912.38
1000	55.00	10.48	990.00
1250	85.94	16.37	1546.88
1350	100.24	19.09	1804.28
1500	123.75	23.57	2227.50
1660	151.56	28.87	2728.04
1750	168.44	32.08	3031.88
1910	200.65	38.22	3611.62
2000	220.00	41.90	3960.00
2140	251.88	47.98	4533.80
2250	278.44	53.04	5011.88
2350	303.74	57.85	5467.28
2500	343.75	65.48	6187.50
2530	352.05	67.06	6336.89
2700	400.95	76.37	7217.10
2870	453.03	86.29	8154.53
3000	495.00	94.29	8910.00
3020	501.62	95.55	9029.20
4000	880.00	167.62	15840.00
5000	1375.00	261.90	24750.00
6000	1980.00	377.14	35640.00
7000	2695.00	513.33	48510.00

In order to operate the TS-PPT, it was necessary to first operate it as a regular PPT, i.e., only with the primary discharge. Operating with only the primary discharge also works as a validation tool for the electronics and control system of the TS-PPT.

In order to validate the electronics of the TS-PPT several tests were carried out at different discharge energy levels: $50J$, $100J$, $150J$ and $200J$. Higher values of energy were avoided during this test phase. As the reference for the discharge energy is the capacitor voltage, due to the precision of the voltmeter used (Fluke 87), the actual discharge energies were: $50.69J$, $100.24J$, $151.56J$ and $200.65J$. However, due to other sources of error - like the voltmeter itself and capacitance - they will be here referred to as $50J$, $100J$, $150J$ and $200J$. All discharges were triggered by the spark plug circuit.

Figure 45 shows a TS-PPT discharge at $960V$, $50J$ and Figure 46 shows the voltage of the main capacitor during the discharge.
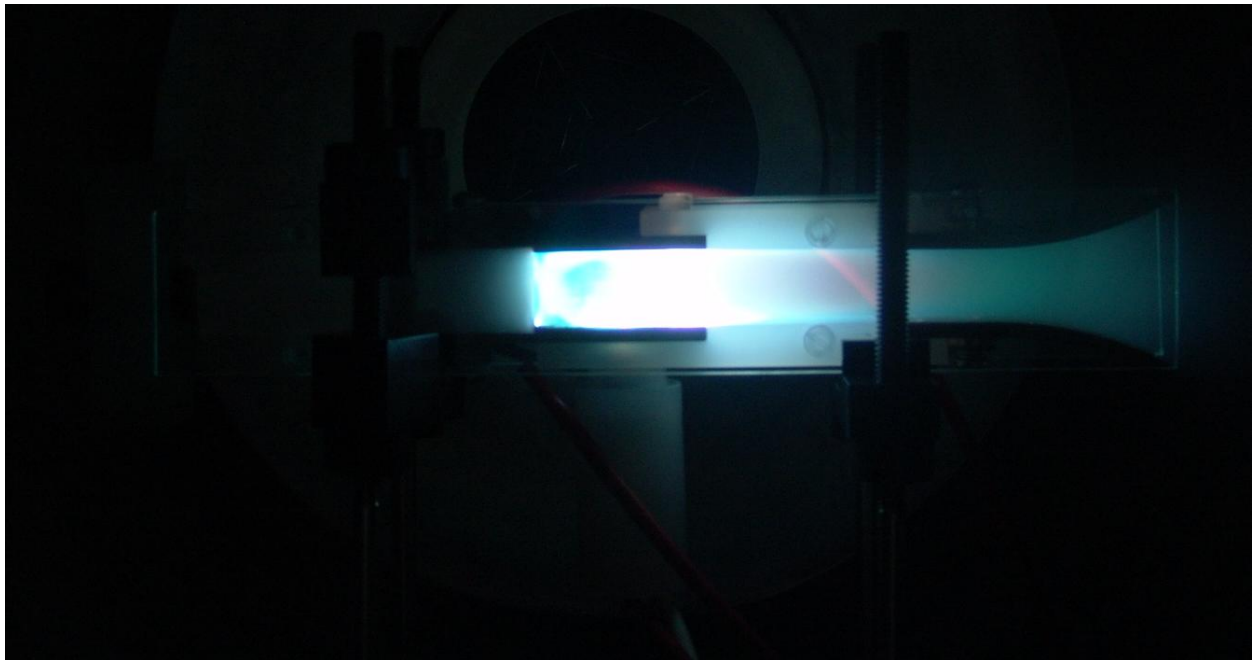

Figure 45: The TS-PPT discharging at 960V, 50 J.

85
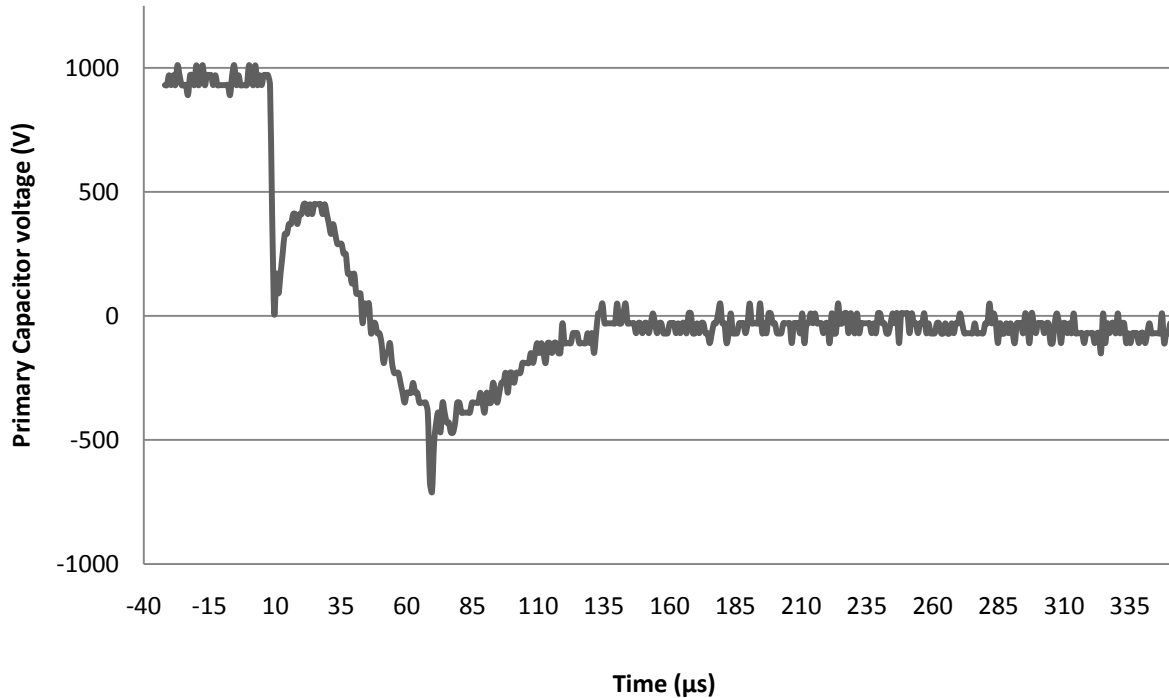
Figure 46: TS-PPT discharge voltage versus time at 960V, 50J.

The measurement of the voltage over time was done using a high voltage probe connected to a Tektronix TDS-5034B oscilloscope. It is convenient to note that the oscilloscope was configured to trigger 36µs before the discharge, therefore the time line starts with negative numbers. This was done to document the capacitor discharge voltage on the graph itself. It can be seen that the discharge type is typical of an under-damped RLC circuit and there is a portion of the discharge where the voltage is inverted in polarity. This represents a typical PPT discharge (14). It can also be seen an increase in the voltage after the discharge is initiated; this is probably due to the relatively high inductances in the circuit, as it was not optimised. This relatively high inductance does not affect the conclusions on this work as it is accounted for.

At this point it is possible to estimate the total inductance of the circuit, as:

$$T = 2\pi\sqrt{L \cdot C}$$

where T is the period of the discharge function (either current or voltage) over time, L is the total inductance (or equivalent inductance) and C is the capacitance of the circuit. It is worth noting that this is an approximation for the plasma discharge, although is commonly used to model the PPT discharge (44).

Looking at Figure 46 (and its source raw data), it is possible to determine the half period of the function shown (voltage over time) and therefore:

$$\frac{T}{2} = 46\mu s \pm 2\mu s$$

And therefore: $T = 96\mu s \pm 4\mu s$.

The primary capacitor capacitance is known, $C = 110\mu F$. Therefore, the approximate inductance of the circuit is:

$$L = \frac{T^2}{4\pi^2} \cdot \frac{1}{C}$$

And therefore

$$L \cong 2.43\mu H \pm 0.18\mu H$$

As expected, this is relatively high, compared to other PPTs[36], but again this thruster was not optimized, as this is not the objective of this research.

These comments and calculation are valid for all four levels of energy.

---

[36] Some PPTs have inductances as low as $50nH$ (14).

Figure 47 shows the TS-PPT discharging at 1350V (100J) and Figure 48 shows the voltage of the primary capacitor during the discharge.


Figure 47: TS-PPT discharging at 1350V, 100J.

Figure 48: TS-PPT discharge voltage versus time at 1350V, 100J.

Figure 49 shows the TS-PPT discharging at 1660V (150J) and Figure 50 shows the voltage of the primary capacitor during the discharge.
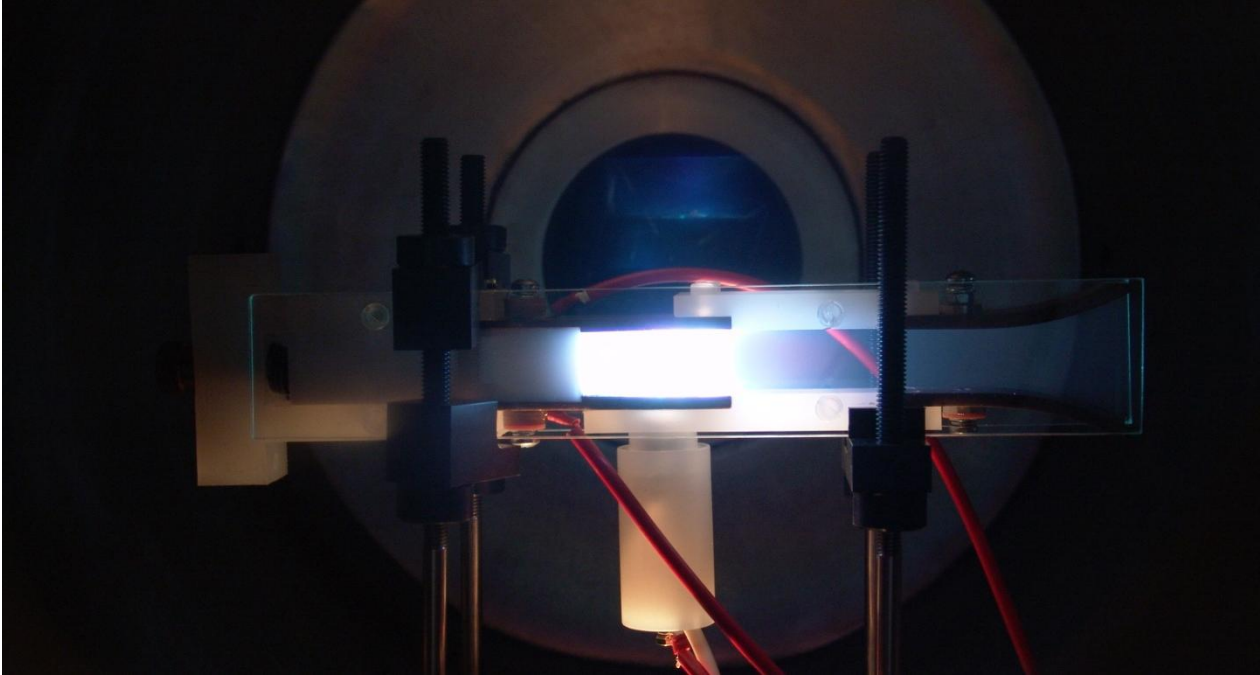
Figure 49: TS-PPT discharging at 1660V, 150J

Time (µs)
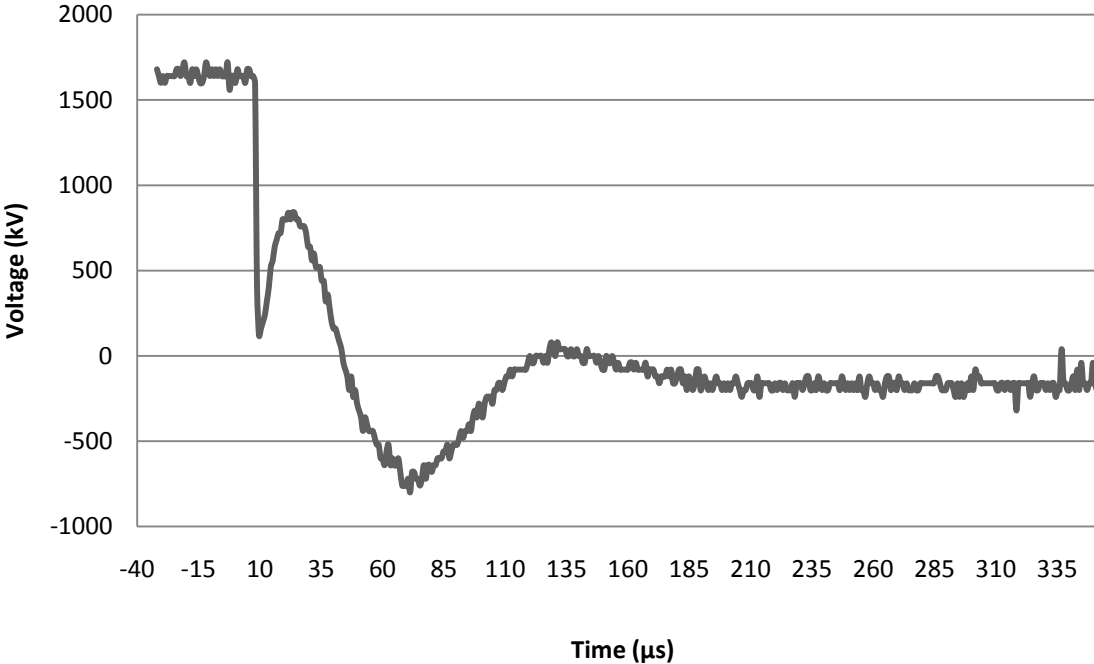
Figure 50: TS-PPT discharge voltage versus time at 1660V, 150J.

Figure 51 shows the HFB-PPT V1 discharge at 1910V (200J) and Figure 52 shows the voltage of the primary capacitor during the discharge.
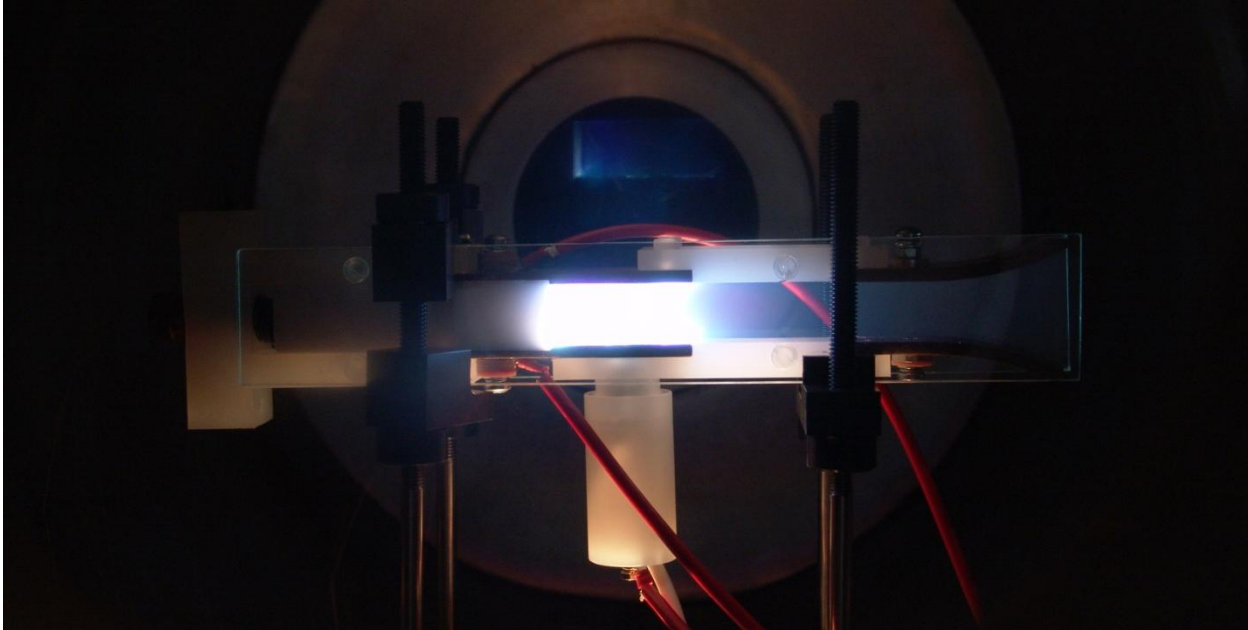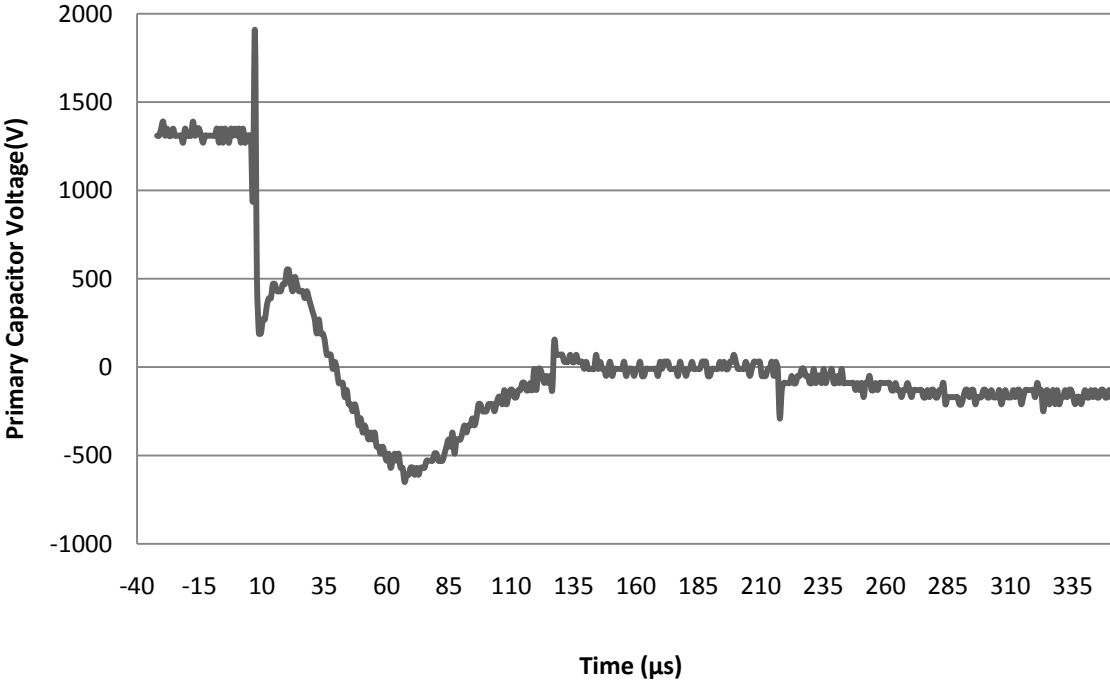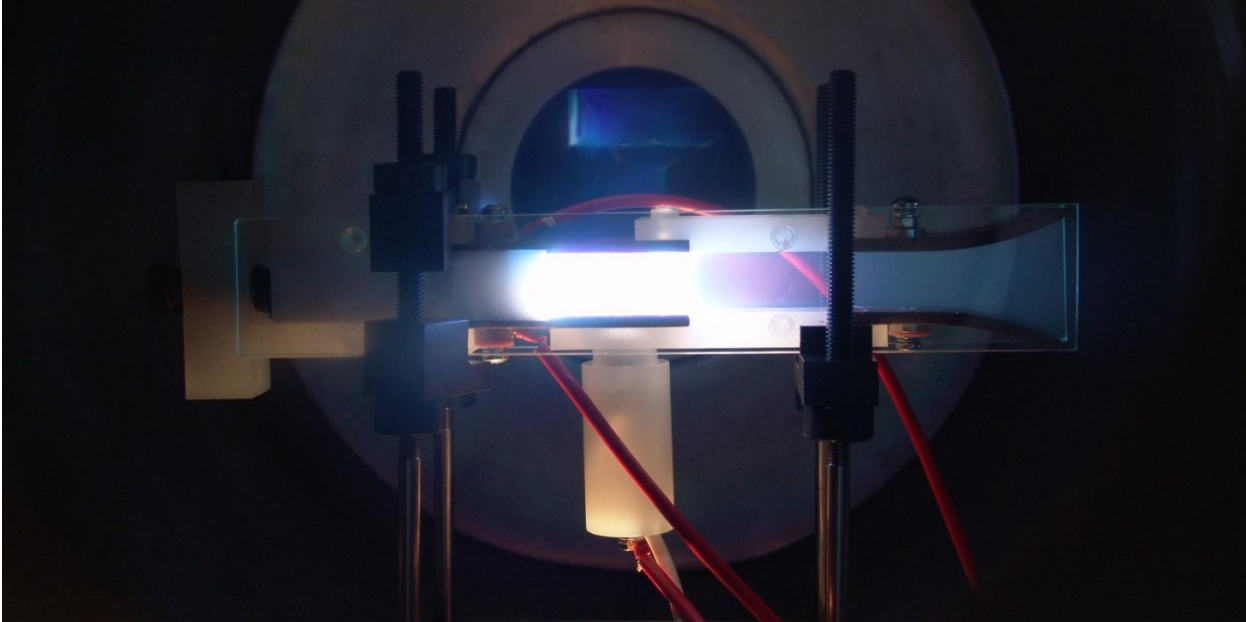

Figure 51: TS-PPT discharging at 1910V, 200J
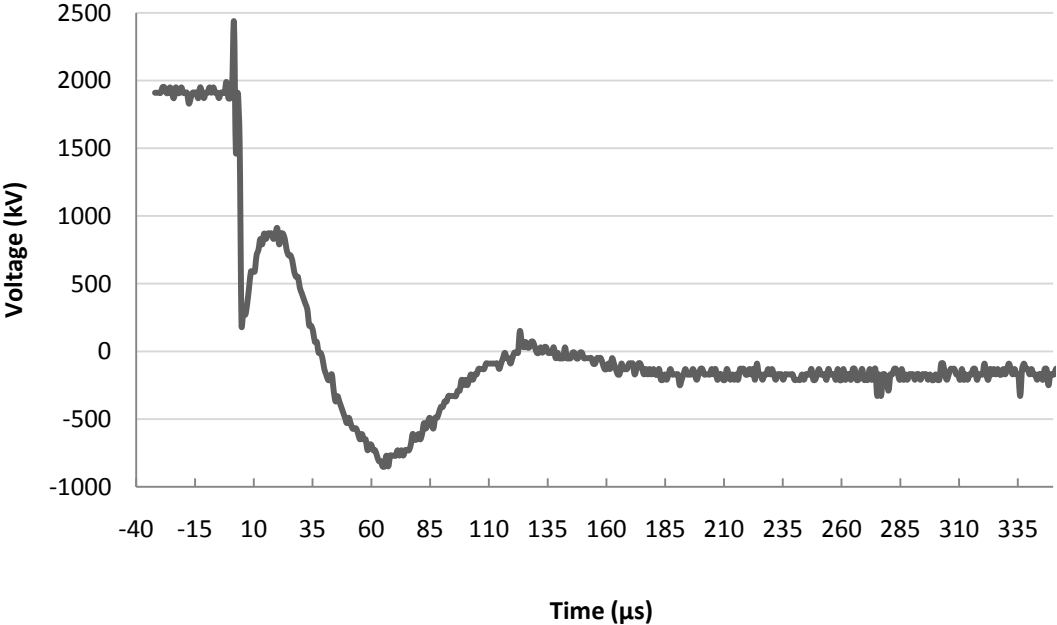
Figure 52: TS-PPT discharge voltage versus time at 1910V, 200J.

For comparison, Figure 53 shows the capacitor voltages for all four cases in one graph, where it is possible to see the change in amplitude, but the period of the discharges are practically the same.
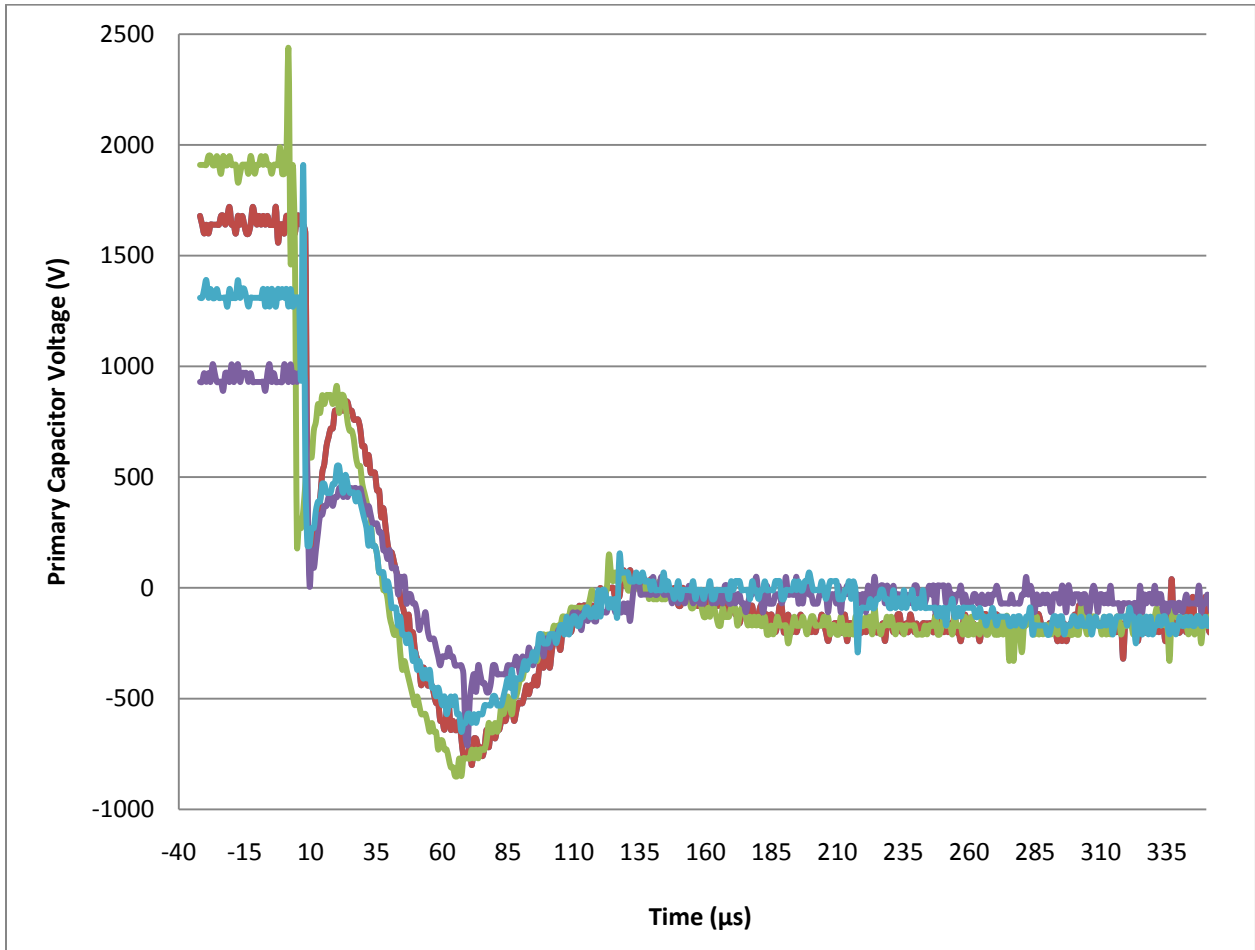
Figure 53: TS-PPT discharges. Four cases shown together for comparison.

As this was a newly designed and built thruster, these tests were very important and successfully validated the circuits and software of the TS-PPT.

91

7.1.3 Mass Variation Tests

While the main emphasis of this work is on a late ablation acceleration mechanism, it is useful, as a reference, to obtain the total mass ablated in a single pulse for the primary discharge. The mass ablated in a single discharge is an important characteristic of a PPT – and also of a TS-PPT – and was previously defined as Δm.

In these tests the TS-PPT will still work only with the primary discharge, as it is the primary discharge that discharges at the propellant surface and is responsible for ablating the mass.

While it is extremely difficult to measure the mass ablated in a single discharge due the small amount of mass involved (typically in the µg range), it is possible to calculate an average value, based on many discharges. This test typically requires hundreds or even thousands of discharges. In the process of obtaining the average mass ablated per single cycle, the TS-PPT electronics is also further tested.

To evaluate the average mass consumption per discharge a test was undertaken. The PTFE bar was weighed before and after the tests. Before weighting the PTFE it was kept in vacuum ($\sim4\times10^{-6}$ mbar) for at least 2h and immediately removed, weighed and returned to the vacuum condition. This procedure was done as a way to reduce uncertainties related to handling of the PTFE, as in case of contact hand digital prints oils would evaporate under vacuum. It was used a scale with a precision of ±0.01g. These tests were carried out using a primary discharge energy of 100J - with the exception of the first test that used 50J-, chosen as an energy in the middle range of the thruster to avoid stressing the TS-PPT before the most important dual discharge tests were carried out.

It is relevant to mention that the main purpose of the TS-PPT is to demonstrate the late ablation acceleration mechanism, therefore it was not optimised to operate for long hours, required for measuring the mass ablated per pulse.

In turn, due to the long time required to obtain a measurable mass variation, with the original TS-PPT configuration, it was observed that, after hundreds of pulses, interactions of the plume with the glass walls and nylon structure of the TS-PPT were creating a failure mode of operation. The nylon was carbonising and the glass had deposited in its surface a layer of copper. Because these two components were not important for this test they were removed and these tests were carried out with the main electrodes and the spark plug only.

The first test initiated with a weighted PTFE of $138.28g \pm 0.01g$, discharging 50J at 1Hz for 2h25m for a total of 8700 pulses. This test was aborted for removal of the glass side walls and nylon structure and the final PTFE mass measured was 138.22g with an average mass per discharge of 6.89 µg (0.1378 µg/J). It was found that the discharge frequency (1Hz) was too high and was not allowing the vacuum chamber pressure to return to its initial pressure ($\sim 10^{-5}$ mbar). The surface of the PTFE showed signs of charring, due to the relatively high pressure in the chamber and deposition of copper on the glass – discharges occurred on the glass surface.

The second test last for 5h59m, with a frequency of discharge between 74mHz and 148mHz, much lower than the first test. This frequency was adjusted in order to obtain a vacuum chamber pressure smaller than 6.0×10^{-5}mbar before each discharge. The discharge energy was $100J$, twice the energy of the first test. The initial PTFE mass was 138.16g, measured after leaving the PTFE in vacuum ($\sim 10^{-6}$ mbar) for more than 10h. A total of 2807 pulses were fired and the final PTFE mass was 138.07g, a total mass consumption of 0.09g. The average mass consumption was 32µg/pulse (0.32µg/joule).

Table 6 summarises the results of the mass ablation tests.

Table 6: Summary of the Mass Ablation Tests.

	Day 1	Day 1	Day 2	Day 2	Total
Start (time)	21:09:00	21:22:00	16:00:00	17:38:00	
Stop (time)	21:21:00	23:00:00	17:37:00	20:10:00	
Total (time)	00:12:00	01:38:00	01:37:00	02:32:00	**05:59**
Total (h)	0.2	1.633333	1.616667	2.533333	5.983333
Total (m)	12	98	97	152	359
Total (s)	720	5880	5820	9120	21540
Freq (Hz)	0.074	0.117	0.123	0.148	
Energy/Pulse (J)	100	100	100	100	
Total Pulses	53.208	687.96	717.024	1349.76	**2807.952**
Total Energy (J)	5320.8	68796	71702.4	134976	280795.2

Initial Mass (g)	138.16
Final Mass (g)	138.07
Mass Consumption (g)	0.09

Mass/Pulse (g)	**3.20518E-05**
Mass/Energy (g/J)	3.20518E-07

Charring of the PTFE was also observed on this test. A more careful analysis of the thruster, when the glass was removed, showed that the exposed area of PTFE between the electrodes was, in fact, dramatically bigger than expected. This was not noted before the tests and was caused by the removal of the glass that consequently exposed the sides of the PTFE and created a possible path for the discharges. Due to the increase in PTFE area between the electrodes the actual energy density was much lower than expected. This fact was accepted as responsible for the charring. Even under this condition the second test obtained a mass per joule ratio more than two times bigger than in the first test (2.32 times).

It is, nonetheless, useful to compare these results with other PPTs, as in this mode the TS-PPT is operating as a regular PPT. Other PPTs have a sublimated mass per joule ratio between 1.5µg/J and 4.8µg/J (with the exception of the IL PPT-3 Lab which is 10µg/J) against the 0.32µg/J

measured in this test. While it can be validly argued that the TS-PPT tested is a non-optimised

design, it is also true that the bigger than expected discharge surface was responsible for such

discrepancy. Figure 54 shows the PTFE surface after the tests and it can be seen that discharges
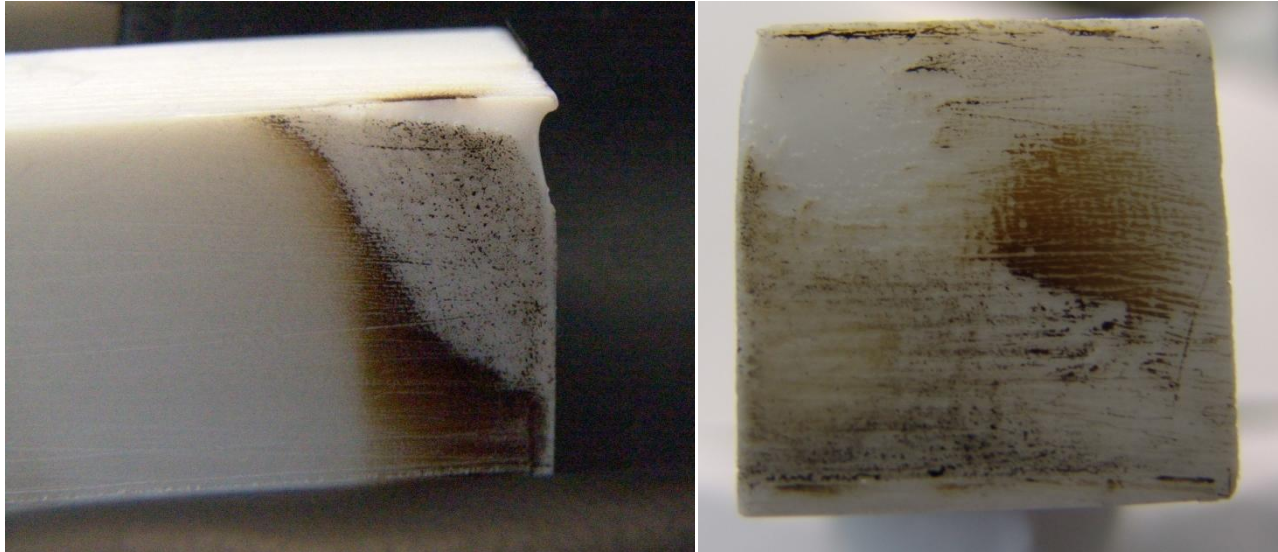
occurred on the sides of the PTFE bar, as discussed.

Figure 54: PTFE after the second test. Side view (left) and front view (right).

As the main objective of this research is to demonstrate the late ablation acceleration mechanism,

the mass variation results were taken as a reference only. Even with the observed charring, these

tests were useful to help improve future designs for the TS-PTP discharge chambers. It is good to

remember that this type of discharge chamber was never used before for a PPT, as the four

electrodes PPT is, in fact, based very much on the discharge chamber. In an optimised

configuration, higher values of Δm per Joule are expected.

7.2 Two-Stage Pulsed Plasma Thruster Tests

7.2.1 Introduction

Tests with the TS-PPT used a 110 µF capacitor for the primary discharge and a 4700µF capacitor for the secondary discharge. The high capacitance of the secondary discharge was chosen to investigate maximum durations of secondary discharges. Three different main discharge voltages were used: 1 kV, 1.5 kV and 2 kV, yielding $55J$, $123J$ and $220J$ for ε_1, respectively; and fourteen different secondary discharge voltages: 0, 3.75, 7.5, 15, 30 35, 50, 75, 100, 150, 200, 250, and 300 V, yielding $0J$, $0.0330J$, $0.132J$, $0.528J$, $2.11J$, $2.87J$, $5.87J$, $13.2J$, $23.5J$, $52.8J$, $94J$, $146J$ and $211J$ for ε_2. Importantly, as this is the two-stage method, a single second pulse was employed in all cases and there was no added delay between the first pulse and the second pulse. The intention with these tests was to observe how the currents and voltages of the secondary discharge behave with a single pulse and *zero* delay in the DCU. The low voltages applied to the secondary discharges were used to investigate the time of flight of the fastest portion of the plasma and the effects of the first discharge on the secondary discharge.

A suitable thrust balance was not available for use with the TS-PPT and although direct measurements of the impulse bit would have been welcome, they were not necessary to demonstrate the late ablation acceleration mechanism. As the main emphasis on this work was the electromagnetic acceleration of the late ablation, the electromagnetic impulse bit was calculated based on the current discharge measurements, as described in other work on with PPTs (45) (46) (47)(48)(49)(15)(50)(24)(40)(22)(38)(14).

The current measurements were taken with a Rogowski coil PEM CWT300, 0.1mV/A, 16MHz bandwidth. The accuracy of this equipment is ±1.05%. A total uncertainty of ±5% is used for

the values calculated from the current measurements and comprises the uncertainty of the Rogowsky coil, oscilloscope, voltmeters and power supplies metering.

7.2.2 Simple Time of Flight Measurement

As a reference, a simple time of flight measurement can be extracted when the secondary capacitor is charged at 0V. In this case the secondary current can be seen as a measurement tool for the first discharge. Although this is a new way of performing this measurement, the principle of operation is based on the Faraday law of induction. Figure 16 on page 54 shows a diagram of the TS-PPT with the fields and currents for reference.

Figure 55 presents a measurement of the current in the primary electrodes and on the secondary electrodes. As $0V$ is used as secondary capacitor voltage, a time of flight analysis can be made. In this case, it is useful to recur to the original raw data, shown in Figure 56 and, in more detail in Figure 57.
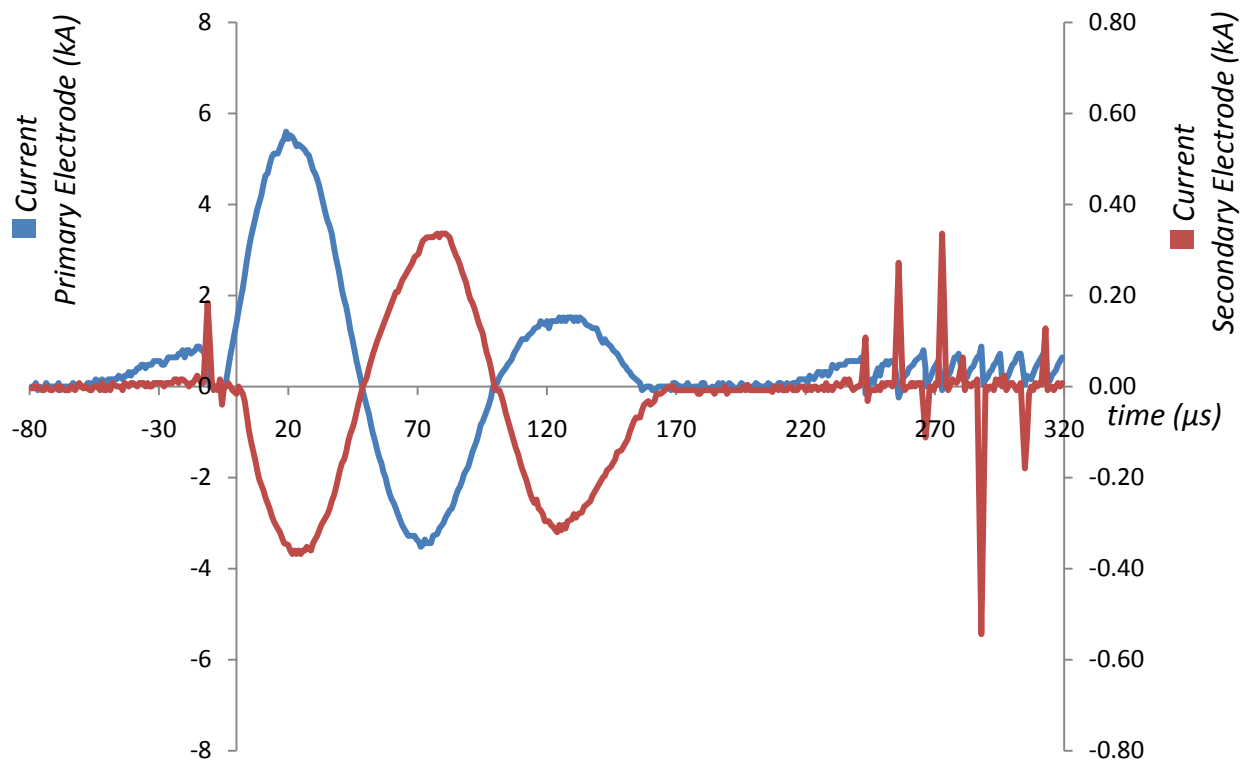

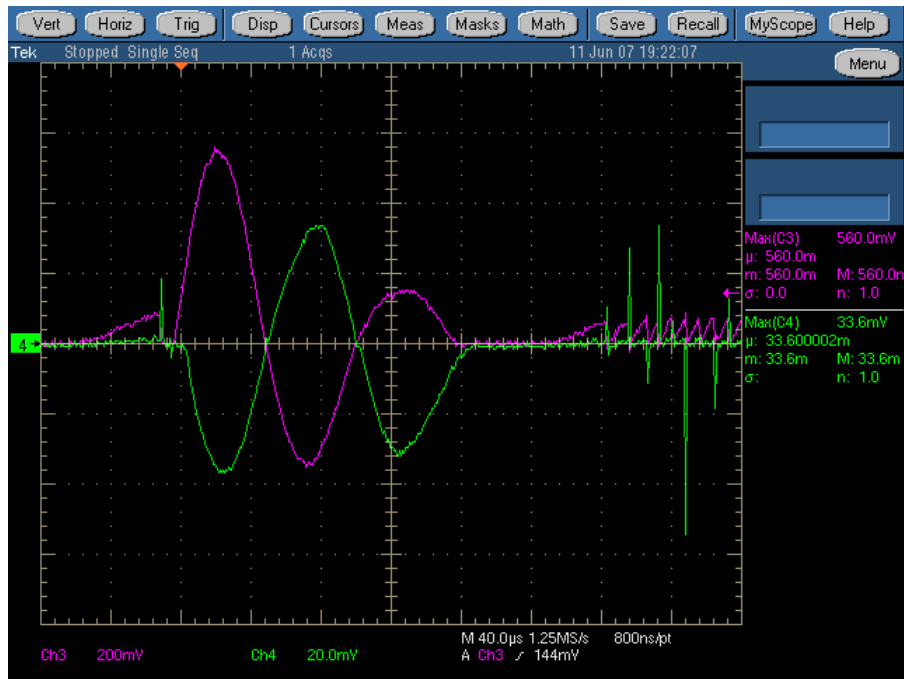**Figure 55: TS-PPT discharge 1kV (55J) Primary Discharge and 0V (0J) Secondary Discharge.**

98

Figure 56: TS-PPT Raw Data for discharge at 1kV (55J) Primary Discharge and 0V (0J) Secondary Discharge.
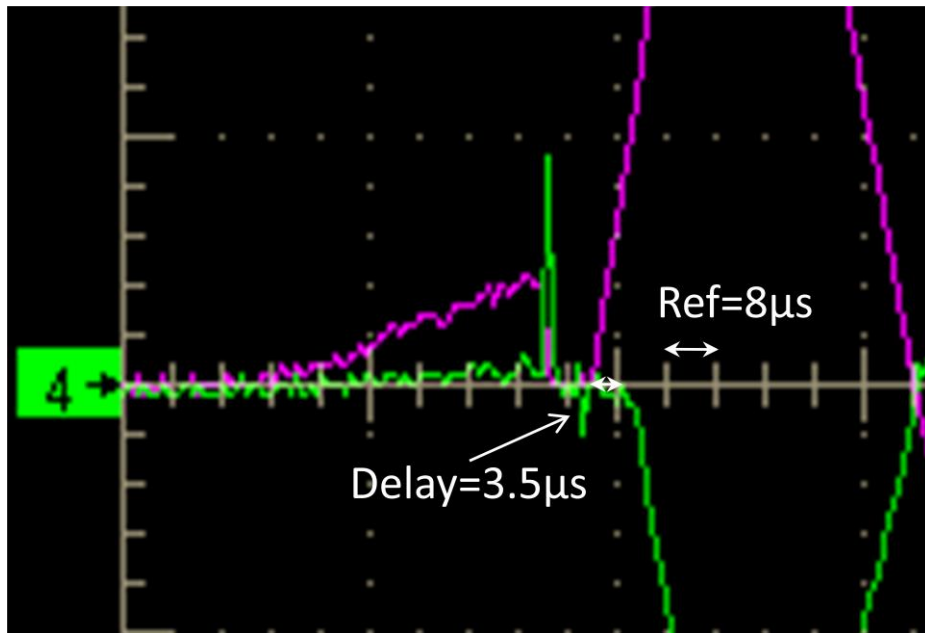

Figure 57: Detail of the RAW data for 1kV (55J) Primary Discharge and 0V (0J) Secondary Discharge for time of flight

analysis.

Looking at the TS-PPT discharge chamber, shown in Figure 58, it is possible to see the distance

between the primary electrodes and the secondary electrodes, equal to $50mm$.
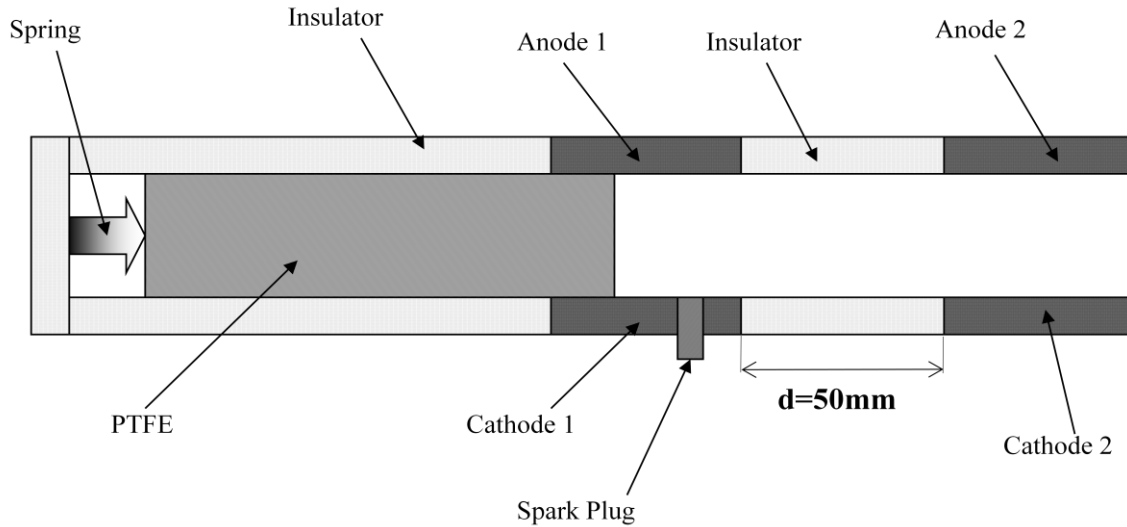

Figure 58: TS-PPT Discharge Chamber. Distance between primary and secondary electrodes.

Therefore, a simple calculation of the speed of the plasma can be done.

$$T_{flight} = 3.5\mu s \pm 1\mu s$$

$$d = 50 \times 10^{-3}m \pm 2 \times 10^{-3}m$$

$$S^* = \frac{d}{T_{flight}} = 14.28\frac{km}{s} \pm 4.65\frac{km}{s}$$

The value of S^* is a reference of the speed of the plasma, and should capture the fastest portion

of the plasma to reach the secondary electrodes that is able to break down the secondary

discharge. This result is within the same range observed in other researches (31)(14), and also

shown in Table 2 on page 22. A slightly lower value of S^* is attributed to the fact that it is

necessary a certain amount of free electrons in the region to allow the current to flow. As the

fastest portion of the plasma comprise only a small fraction of the total mass it is possible that the fastest portion is not able to trigger the discharge.

The induced electric field travels at the speed of light, but a current is only observed as the plasma reaches the secondary electrodes, after which the secondary discharge current is modulated by the primary discharge time varying self generated magnetic field.

7.3 Current Measurements of the TS-PPT

As described in section 7.2.1 on page 96, several current measurements were taken with voltages ranging from 1kV to 2kV for the primary discharge and from 0V to 300V for the secondary discharge.

At this point it is important to note that the following sections will solely describe the results of the tests and will have only very brief comments on them. A proper analysis of the results is done in Chapter 8, starting on page 125.

7.3.1 Measurements with primary capacitor at 1kV and secondary capacitor from 3.75V to 300V

This section presents the results obtained while measuring the primary discharge current and secondary discharge current for the TS-PPT. The secondary discharge capacitor voltage was gradually increased to observe its behaviour from 3.75V to 300V, while the primary discharge capacitor voltage was kept at 1kV.

From Figure 59 to Figure 70, it is shown the behaviour of both the primary discharge current and secondary discharge current, while varying the secondary discharge capacitor initial voltage, and therefore its discharge energy.
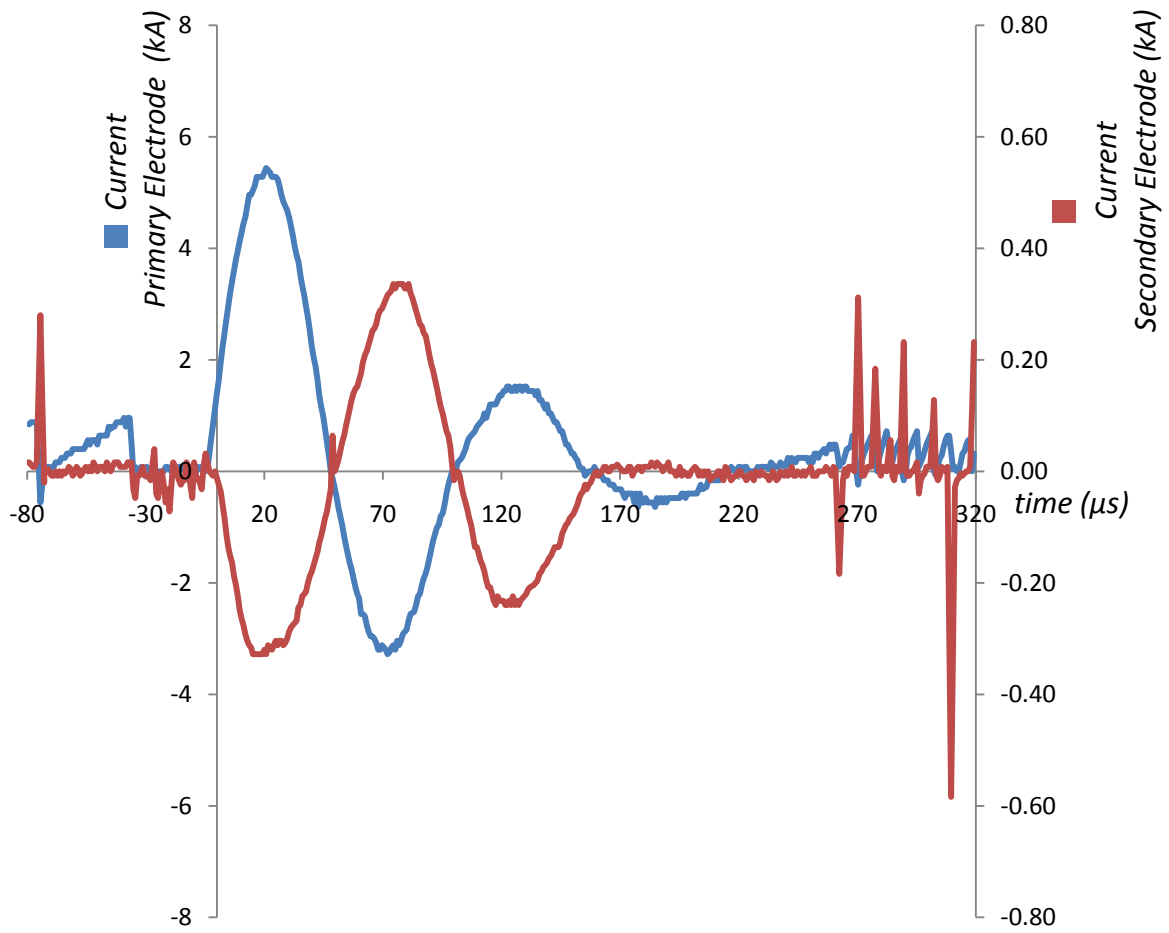
Figure 59: TS-PPT discharge 1kV (55J) Primary Discharge and 3.75V (0.033J) Secondary Discharge.
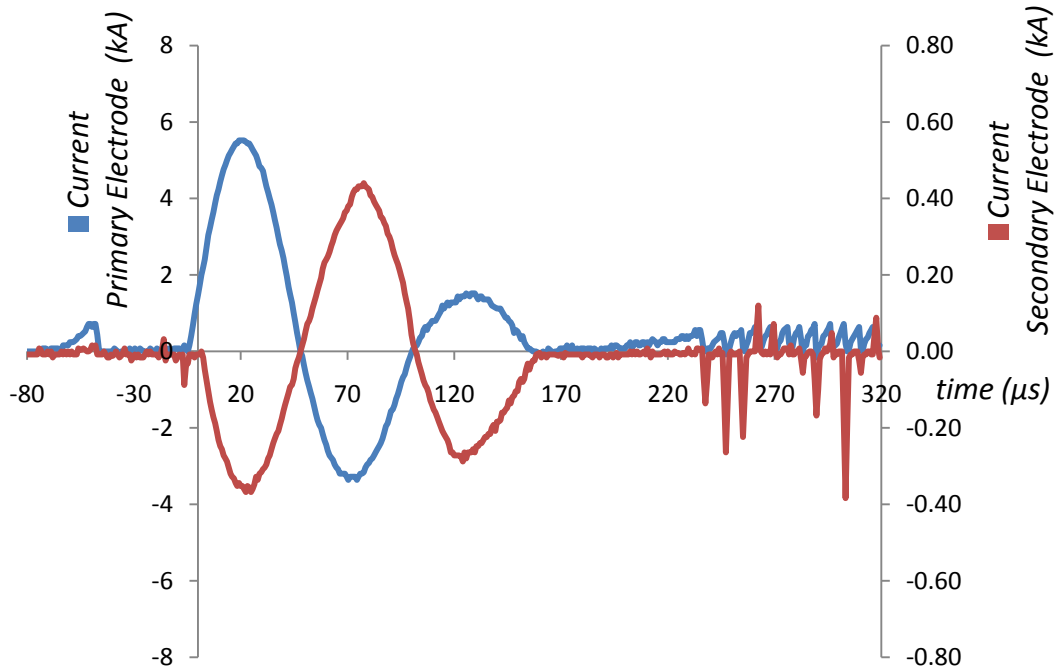
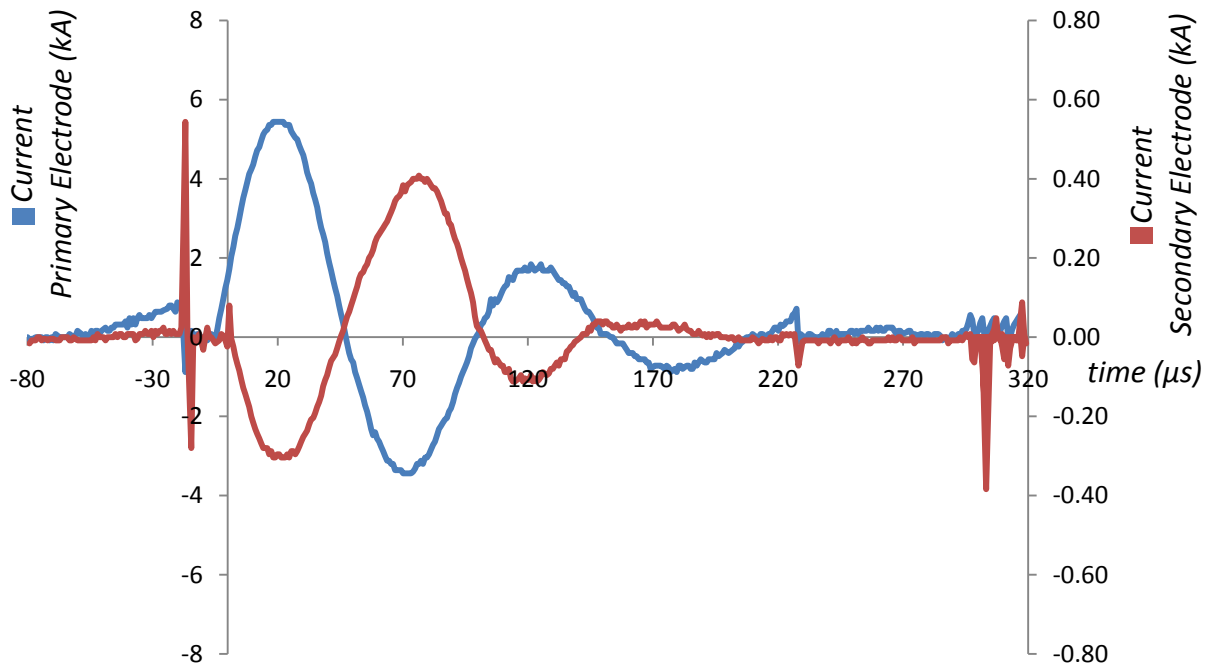**Figure 60: TS-PPT discharge 1kV (55J) Primary Discharge and 7.5V (0.132J) Secondary Discharge.**

Figure 61: TS-PPT discharge 1kV (55J) Primary Discharge and 15V (0.528J) Secondary Discharge.
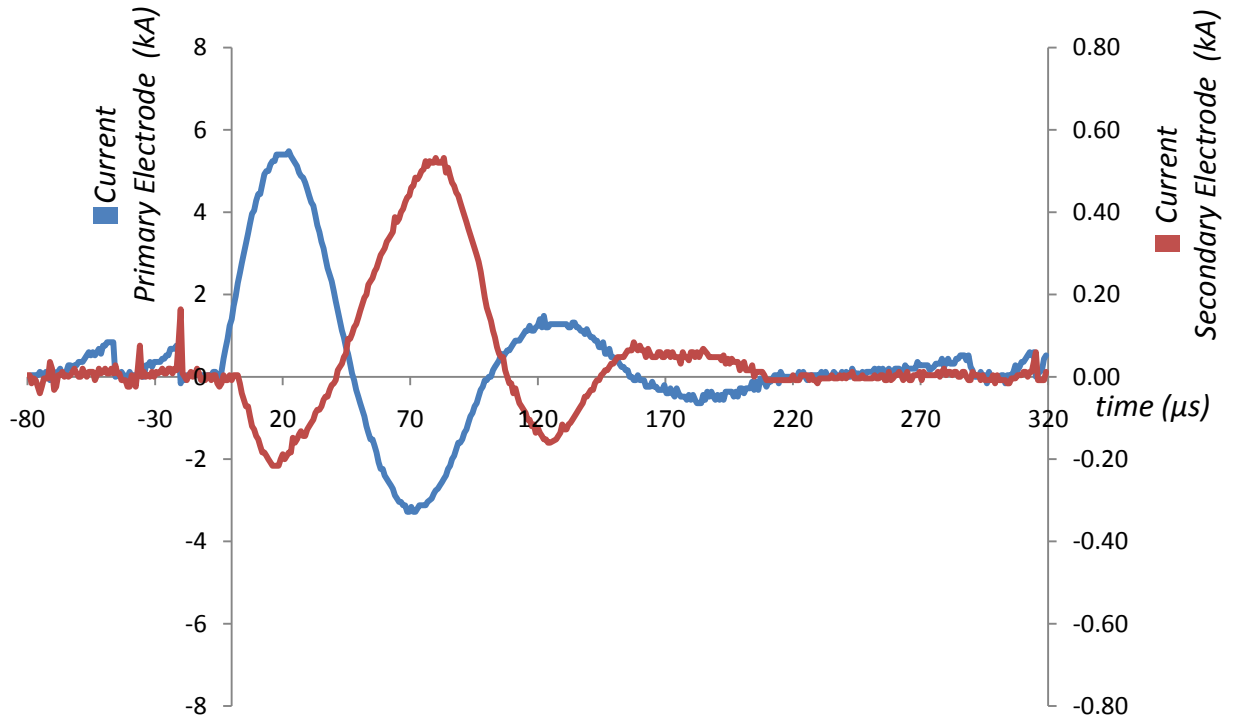
Figure 62: TS-PPT discharge 1kV (55J) Primary Discharge and 30V (2.11J) Secondary Discharge.

Figure 63: TS-PPT discharge 1kV (55J) Primary Discharge and 35V (2.88J) Secondary Discharge.

105

Figure 64: TS-PPT discharge 1kV (55J) Primary Discharge and 50V (5.85J) Secondary Discharge.

Figure 65: TS-PPT discharge 1kV (55J) Primary Discharge and 75V (13.2J) Secondary Discharge.
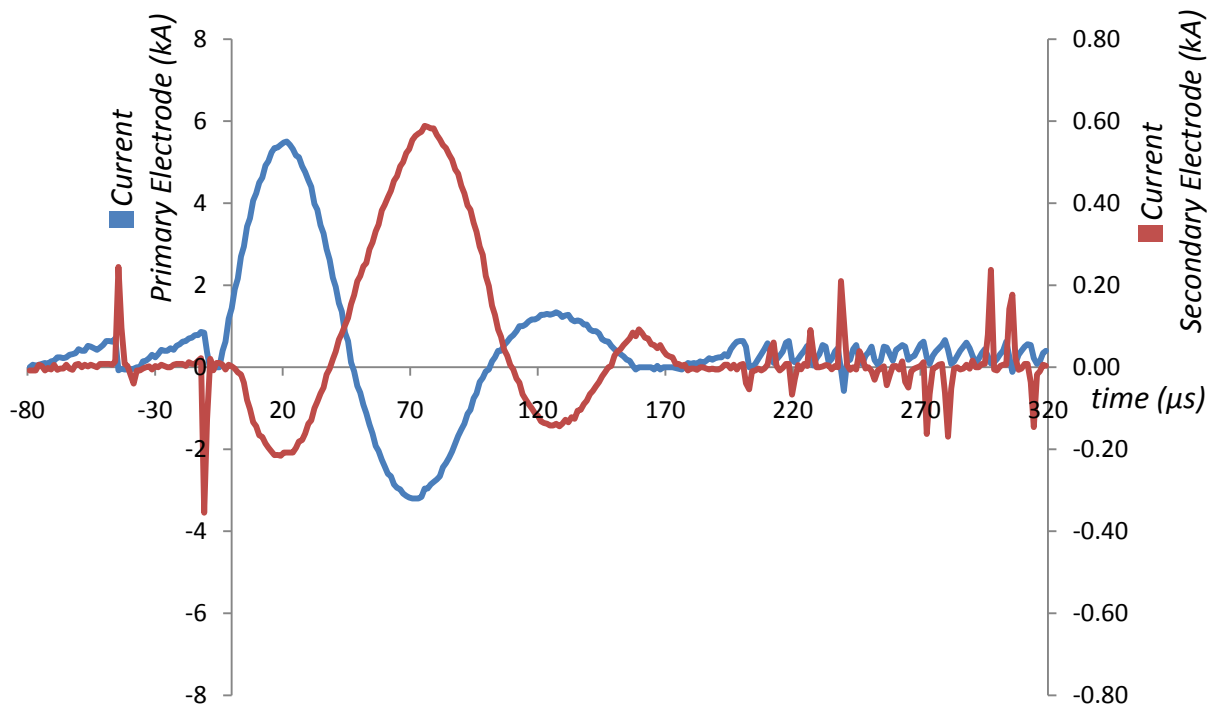
106

Figure 66: TS-PPT discharge 1kV (55J) Primary Discharge and 100V (23.5J) Secondary Discharge.

Figure 67: TS-PPT discharge 1kV (55J) Primary Discharge and 150V (52.87J) Secondary Discharge.
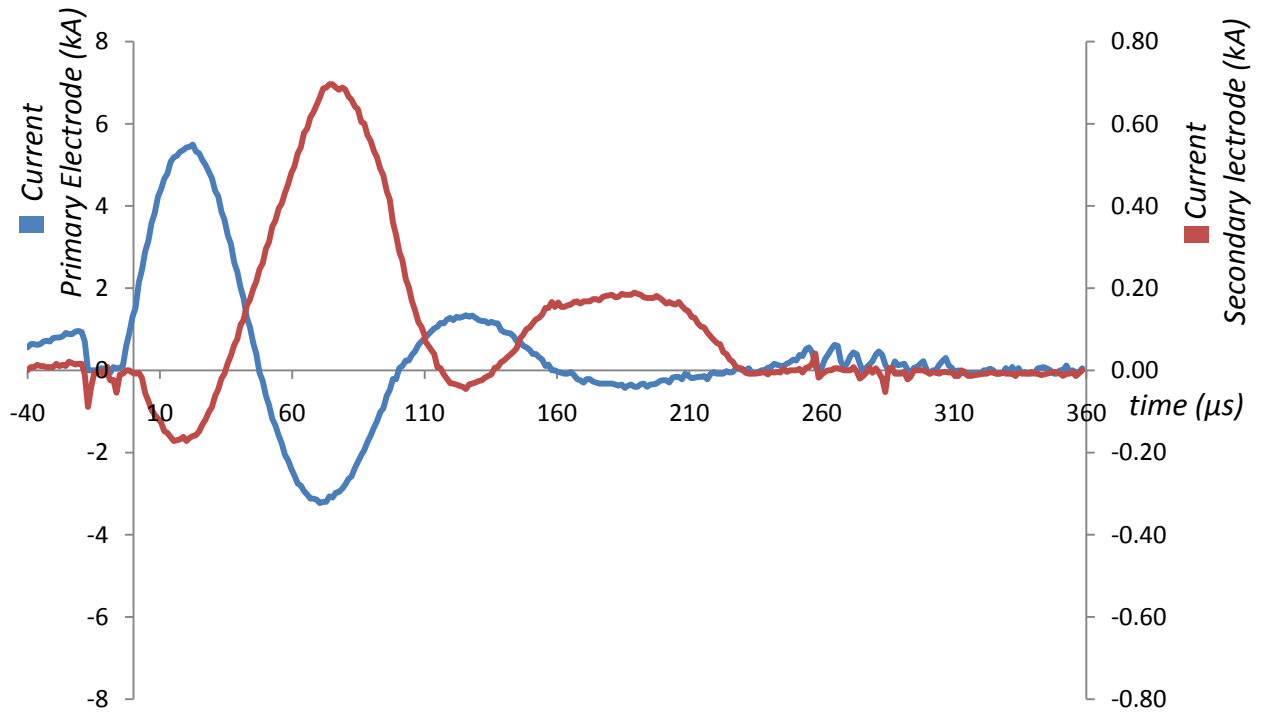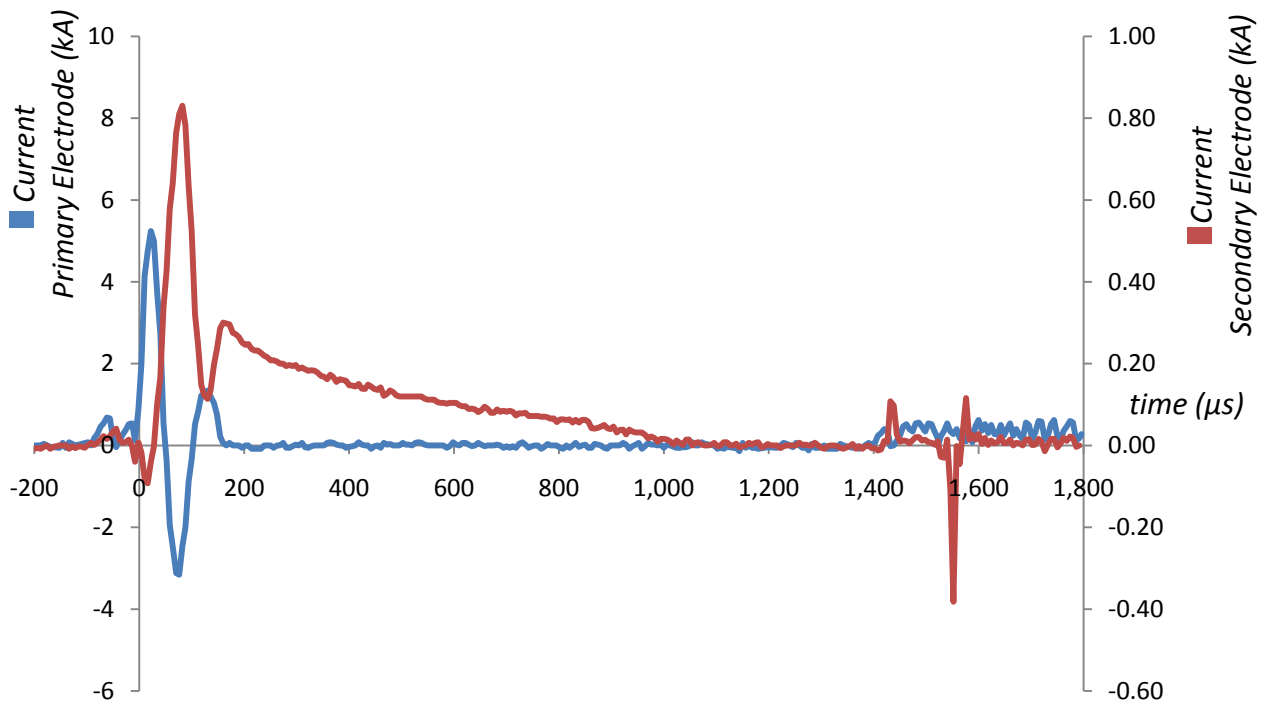
107

Figure 68: TS-PPT discharge 1kV (55J) Primary Discharge and 200V (94J) Secondary Discharge.
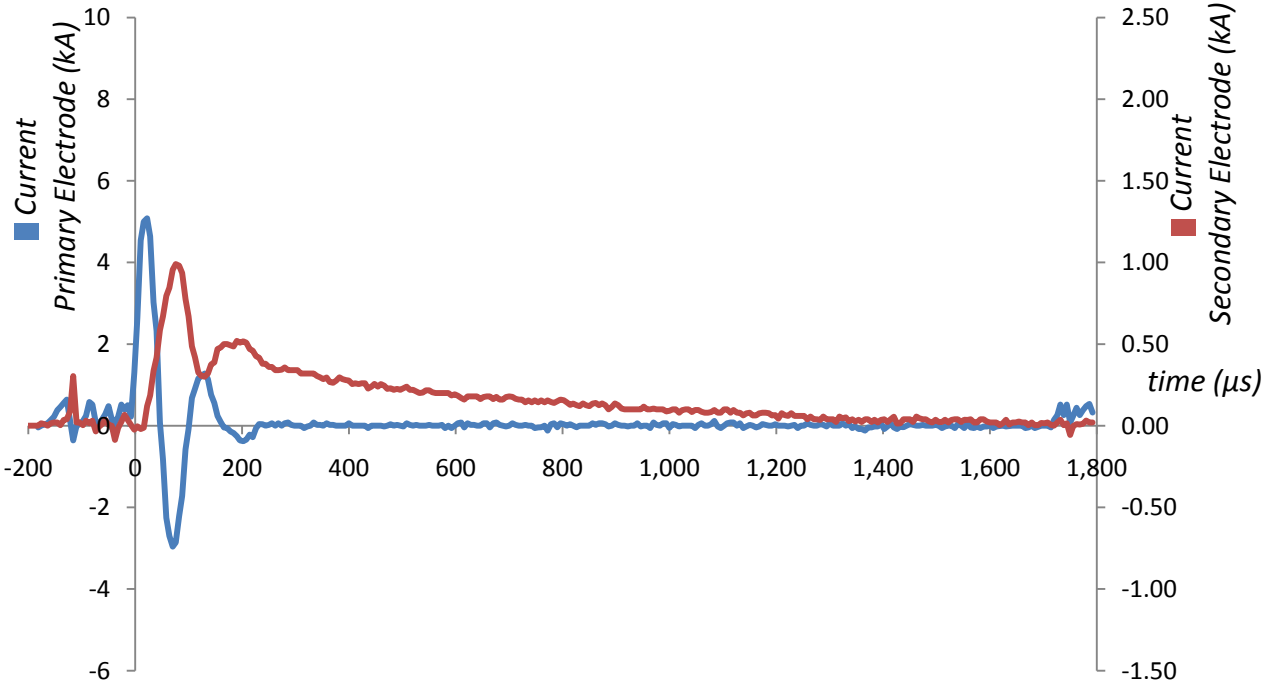

Figure 69: TS-PPT discharge 1kV (55J) Primary Discharge and 250V (146J) Secondary Discharge.

108

Figure 70: TS-PPT discharge 1kV (55J) Primary Discharge and 300V (211J) Secondary Discharge.

It was possible to see the behaviour of the discharge currents with the primary discharge capacitor at 1kV and the secondary discharge capacitor voltage varying from 3.75V up to 300V.

7.3.2 Measurements with primary capacitor at 1.5kV and secondary capacitor from 0V to 300V

In this section the results obtained while measuring the primary discharge current and secondary discharge current for the TS-PPT are presented when the secondary discharge capacitor voltage was gradually increased to observe its behaviour from 0V to 300V, the primary discharge capacitor voltage was kept at 1.5kV.

From Figure 71 to Figure 83, it is shown the behaviour of the primary discharge current and secondary discharge current, while varying the secondary discharge capacitor initial voltage, and consequently its discharge energy.
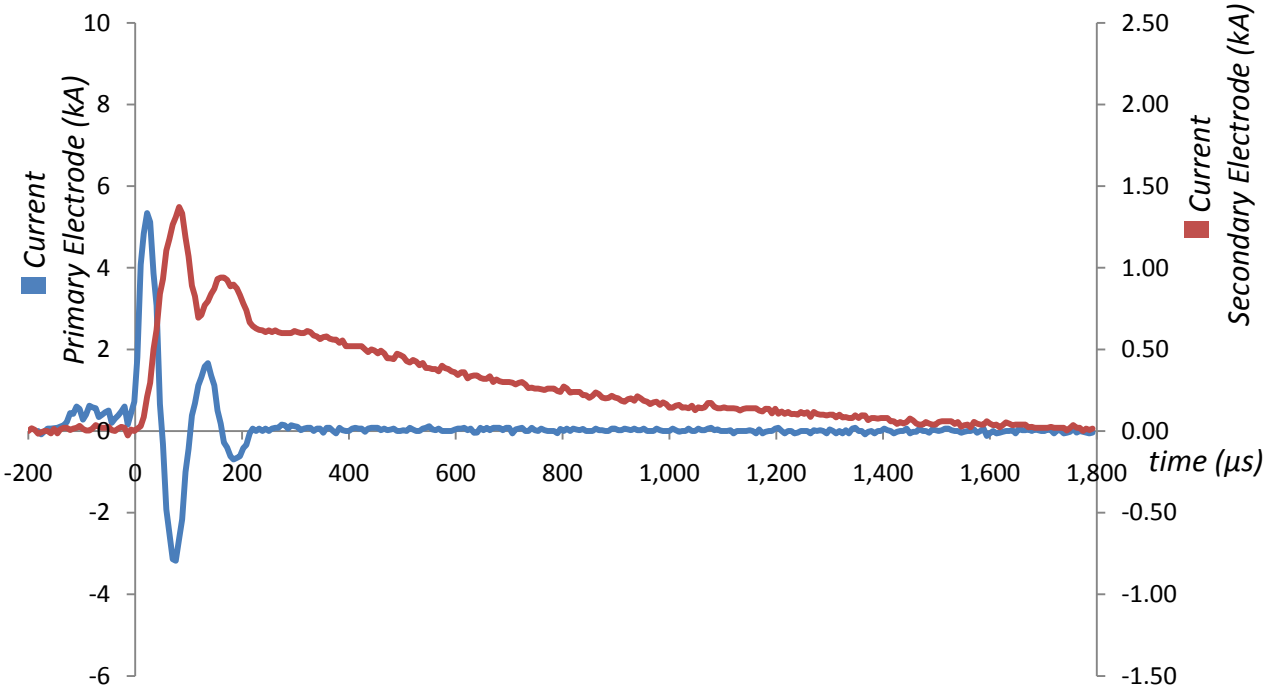

Figure 71: TS-PPT discharge 1.5kV (123J) Primary Discharge and 0V (0J) Secondary Discharge.

Figure 72: TS-PPT discharge 1.5kV (123J) Primary Discharge and 3.75V (0.33J) Secondary Discharge.
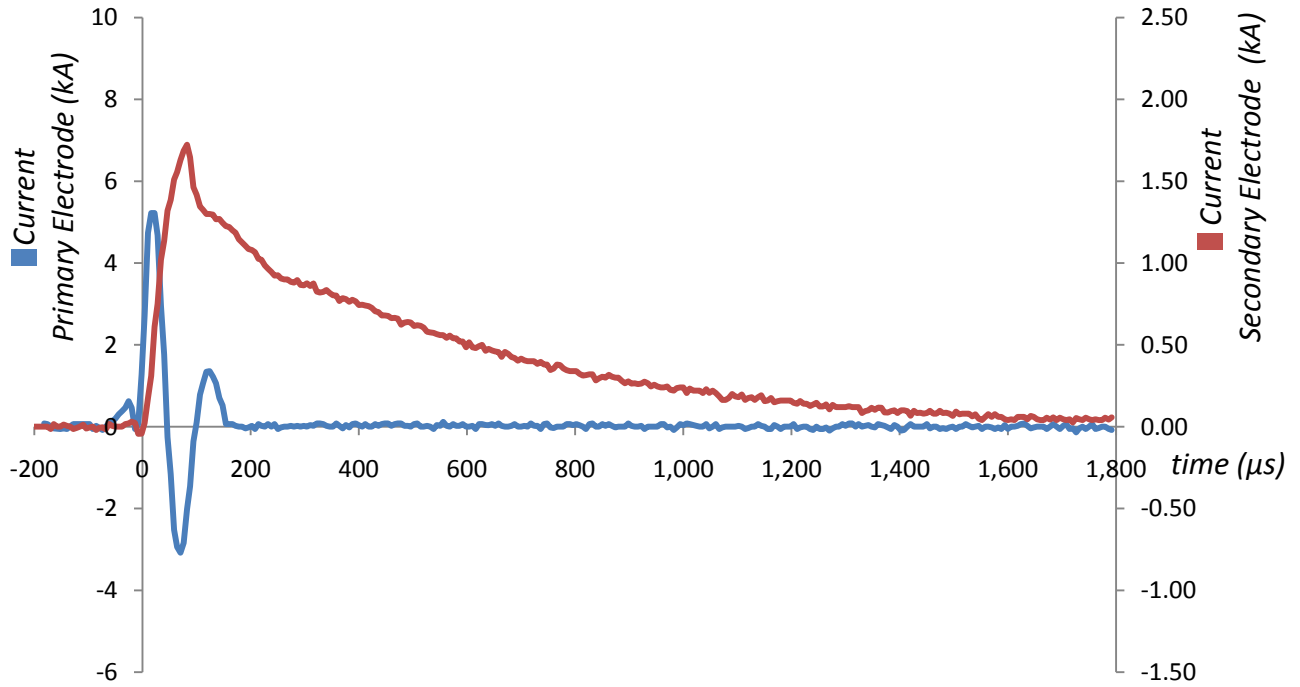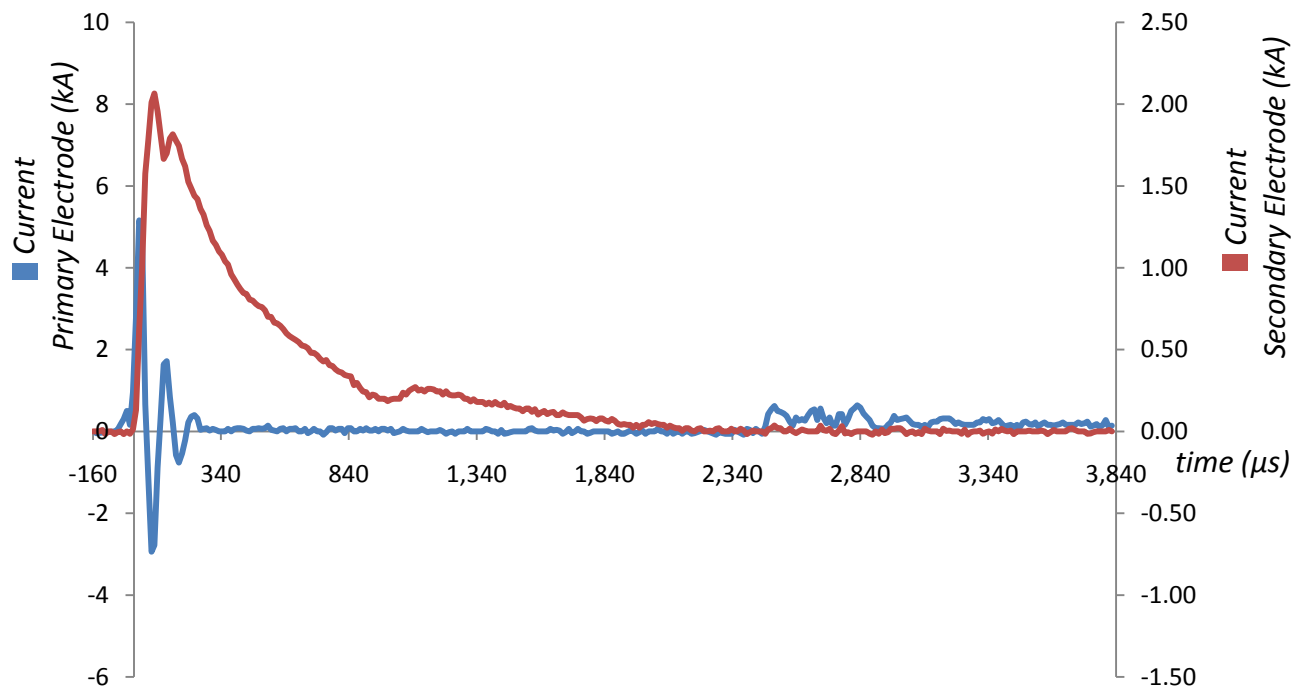

Figure 73: TS-PPT discharge 1.5kV (123J) Primary Discharge and 7.5V (0.132J) Secondary Discharge.

111

Figure 74: TS-PPT discharge 1.5kV (123J) Primary Discharge and 15V (0.528J) Secondary Discharge.

Figure 75: TS-PPT discharge 1.5kV (123J) Primary Discharge and 30V (2.11J) Secondary Discharge.

Figure 76: TS-PPT discharge 1.5kV (123J) Primary Discharge and 35V (2.87J) Secondary Discharge.
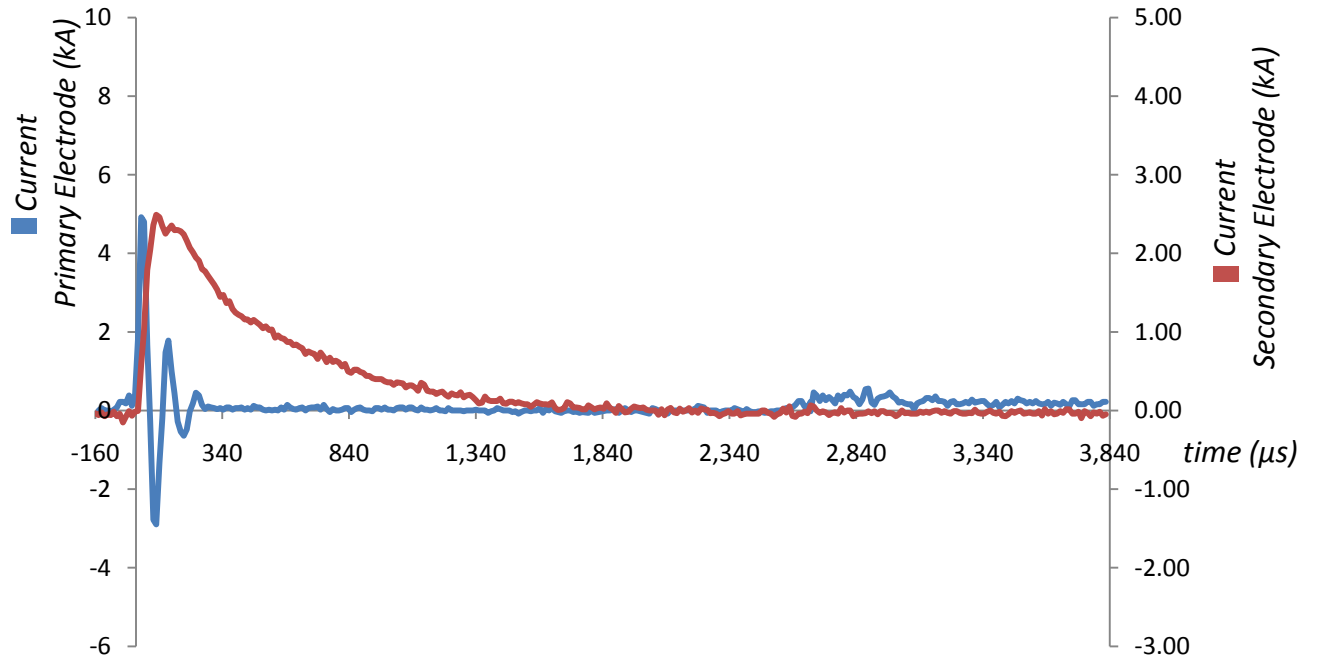

Figure 77: TS-PPT discharge 1.5kV (123J) Primary Discharge and 50V (5.87J) Secondary Discharge.

113

Figure 78: TS-PPT discharge 1.5kV (123J) Primary Discharge and 75V (13.2J) Secondary Discharge.

Figure 79: TS-PPT discharge 1.5kV (123J) Primary Discharge and 100V (23.5J) Secondary Discharge.

114

Figure 80: TS-PPT discharge 1.5kV (123J) Primary Discharge and 150V (52.8J) Secondary Discharge.

Figure 81: TS-PPT discharge 1.5kV (123J) Primary Discharge and 200V (94J) Secondary Discharge.
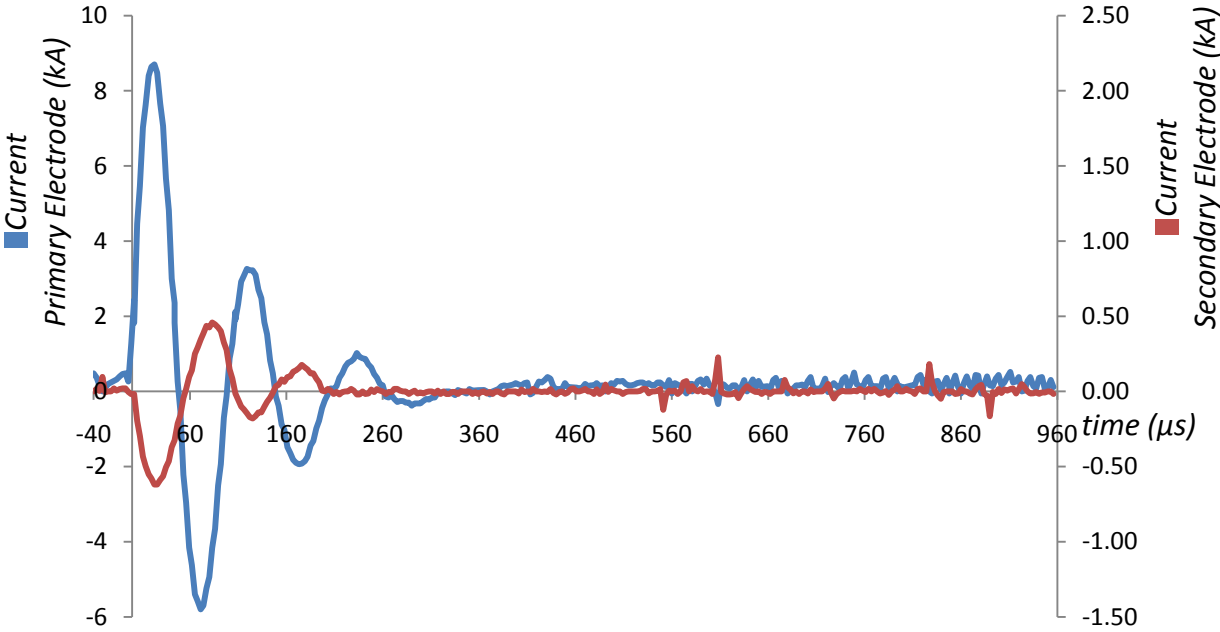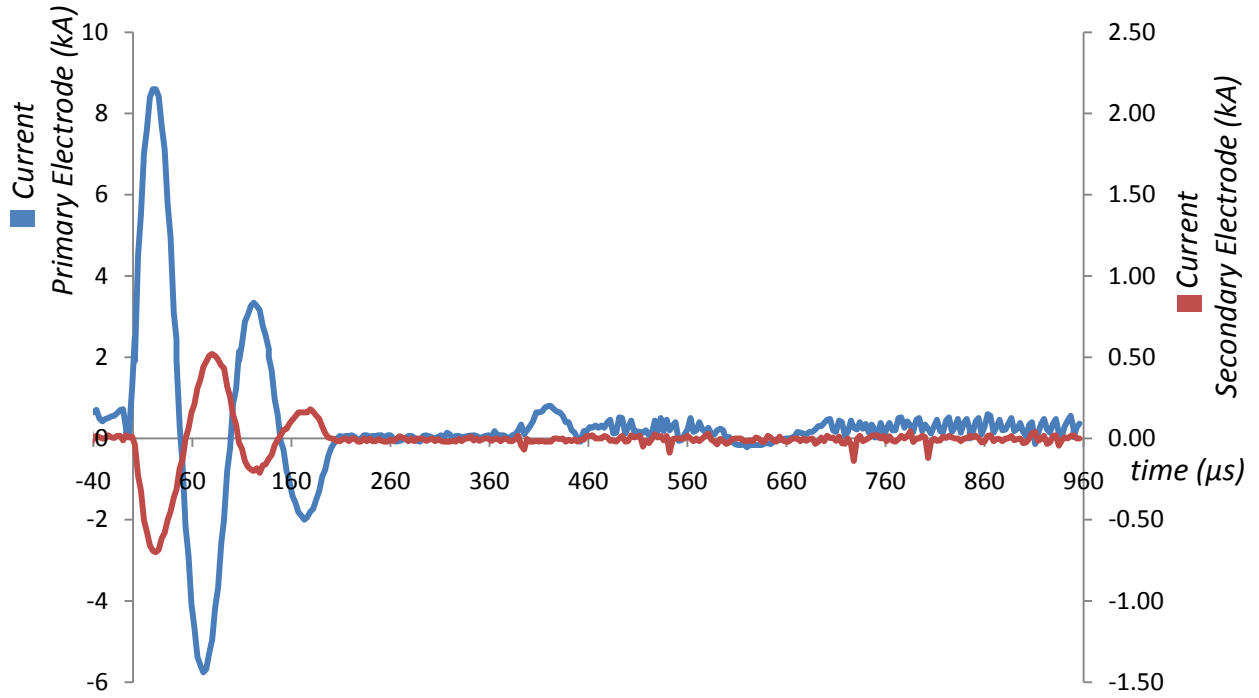
115

Figure 82: TS-PPT discharge 1.5kV (123J) Primary Discharge and 250V (146J) Secondary Discharge.

Figure 83: TS-PPT discharge 1.5kV (123J) Primary Discharge and 300V (211J) Secondary Discharge.

116

It was shown the behaviour of the discharge currents with the primary discharge capacitor at 1.5kV and the secondary discharge capacitor voltage varying from 0V up to 300V.

7.3.3 Measurements with primary capacitor at 2kV and secondary capacitor varying from 0V to 300V

Results obtained while measuring the primary discharge current and secondary discharge current for the TS-PPT are presented in this section. The secondary discharge capacitor voltage was gradually increased to observe its behaviour from 0V to 300V. The primary discharge capacitor voltage was kept at 1.5kV.

It is shown from Figure 84 to Figure 96, the behaviour of the primary discharge current and secondary discharge current, while the secondary discharge capacitor initial voltage – and its associated initial energy - was varied.
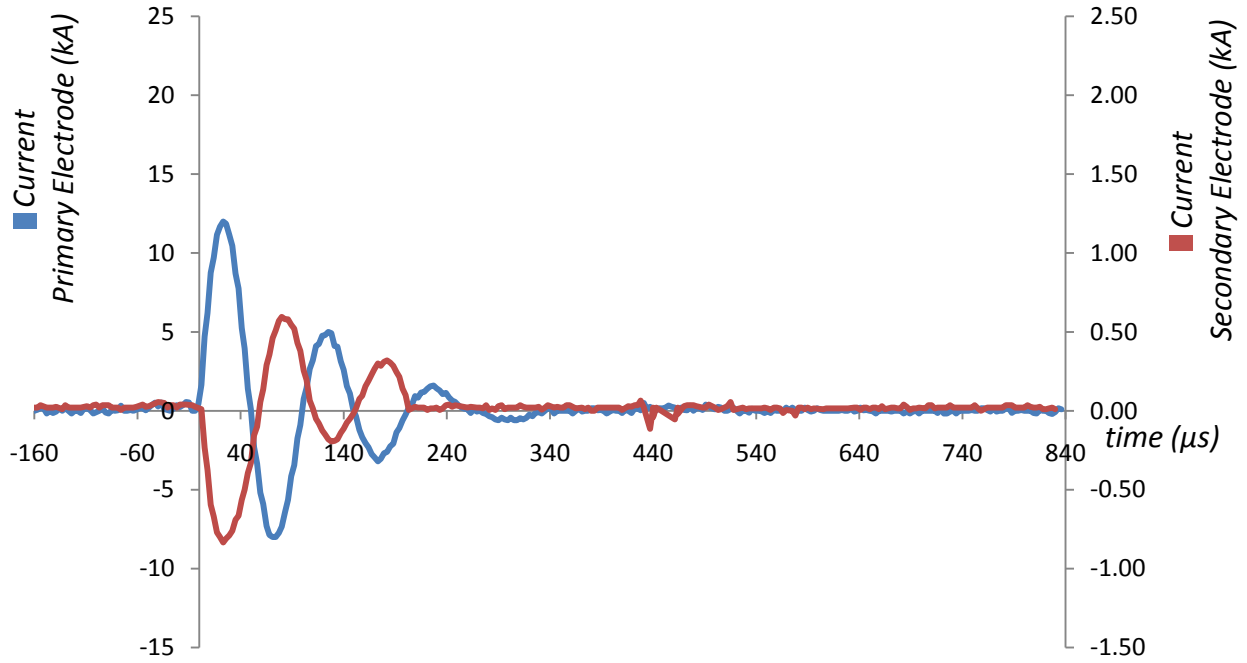
Figure 84: TS-PPT discharge 2kV (220J) Primary Discharge and 0V (0J) Secondary Discharge.
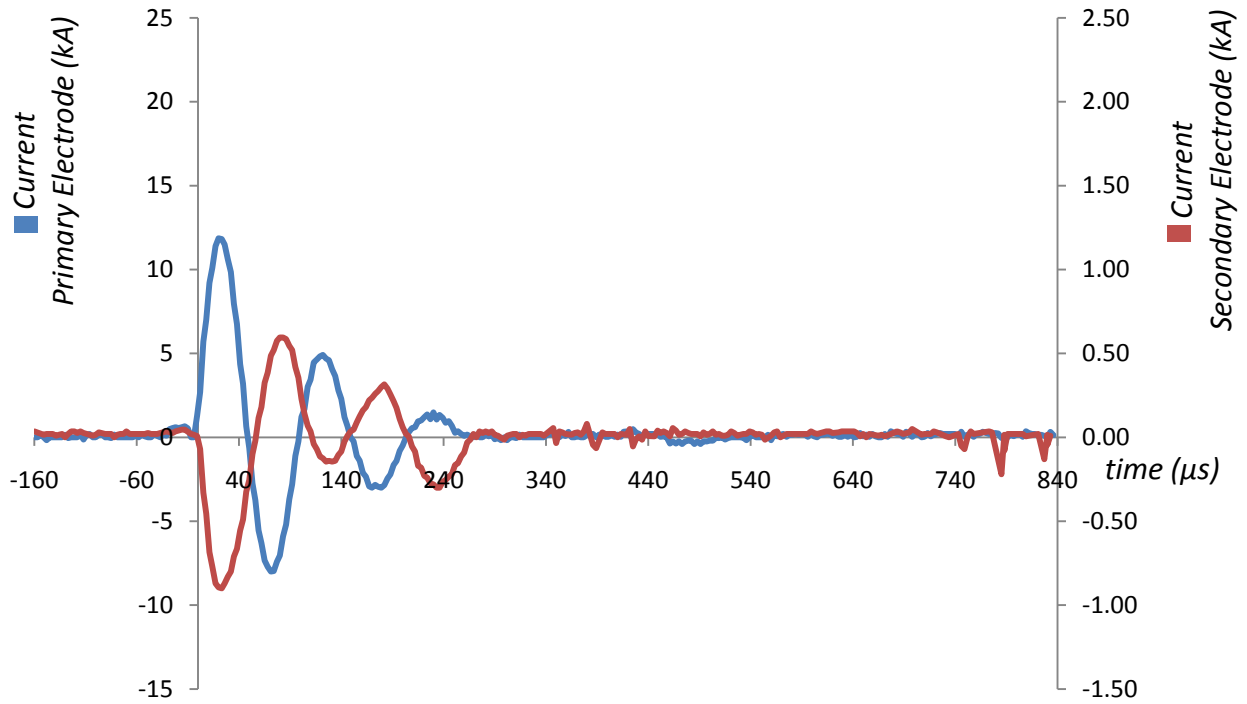
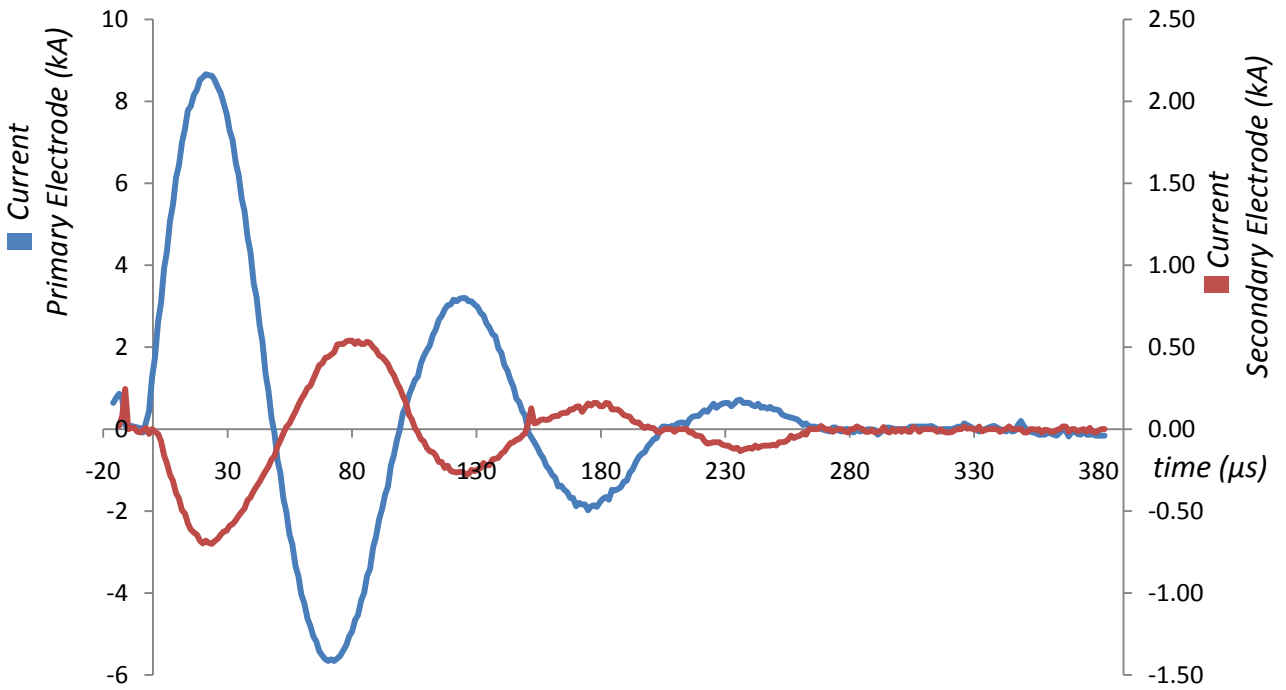**Figure 85: TS-PPT discharge 2kV (220J) Primary Discharge and 3.75V (0.033J) Secondary Discharge.**

118
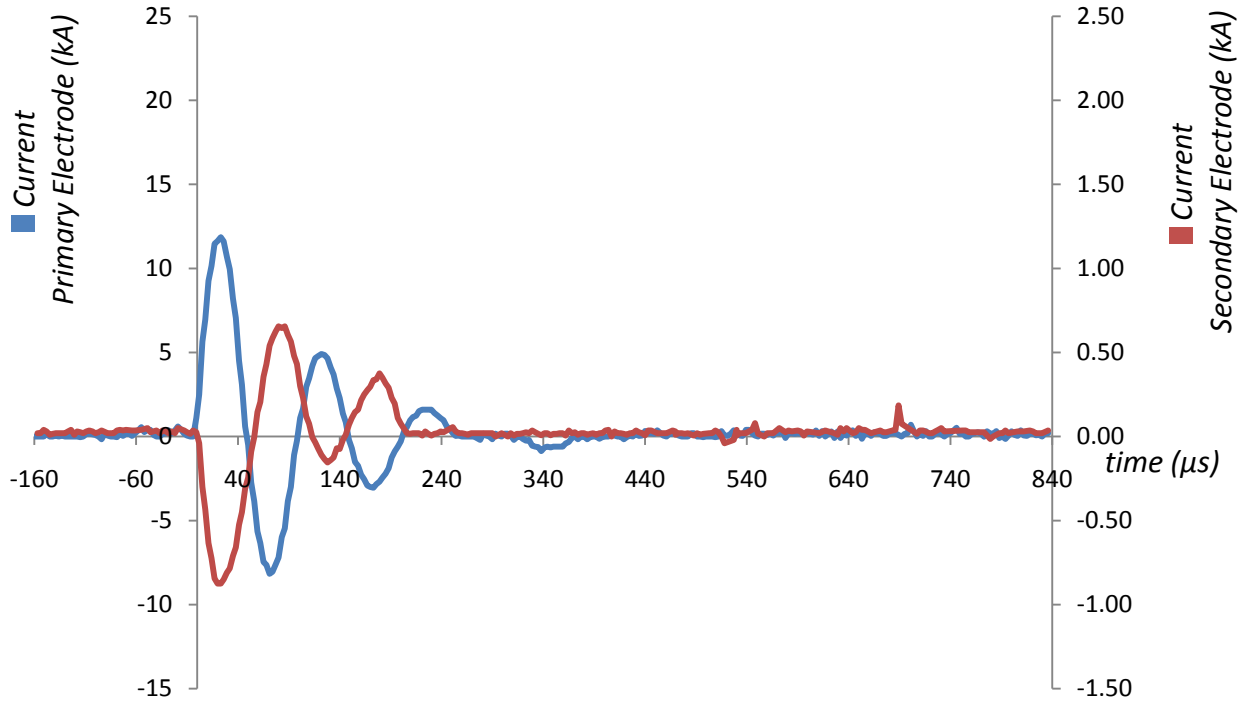
Figure 86: TS-PPT discharge 2kV (220J) Primary Discharge and 7.5V (0.132J) Secondary Discharge.
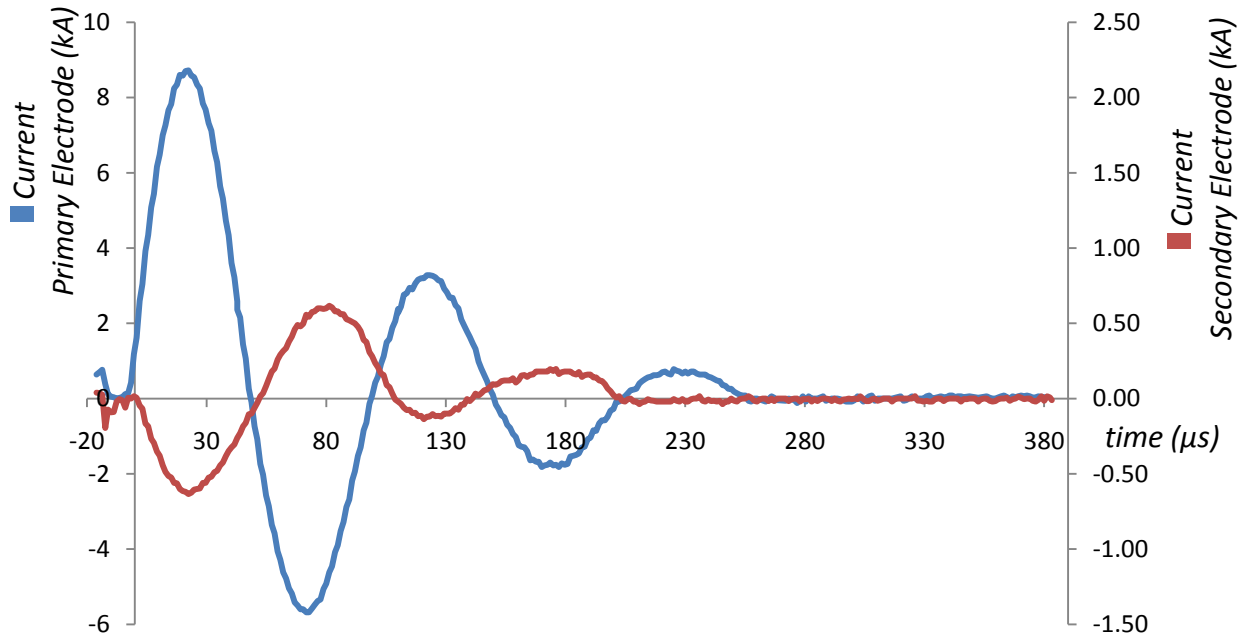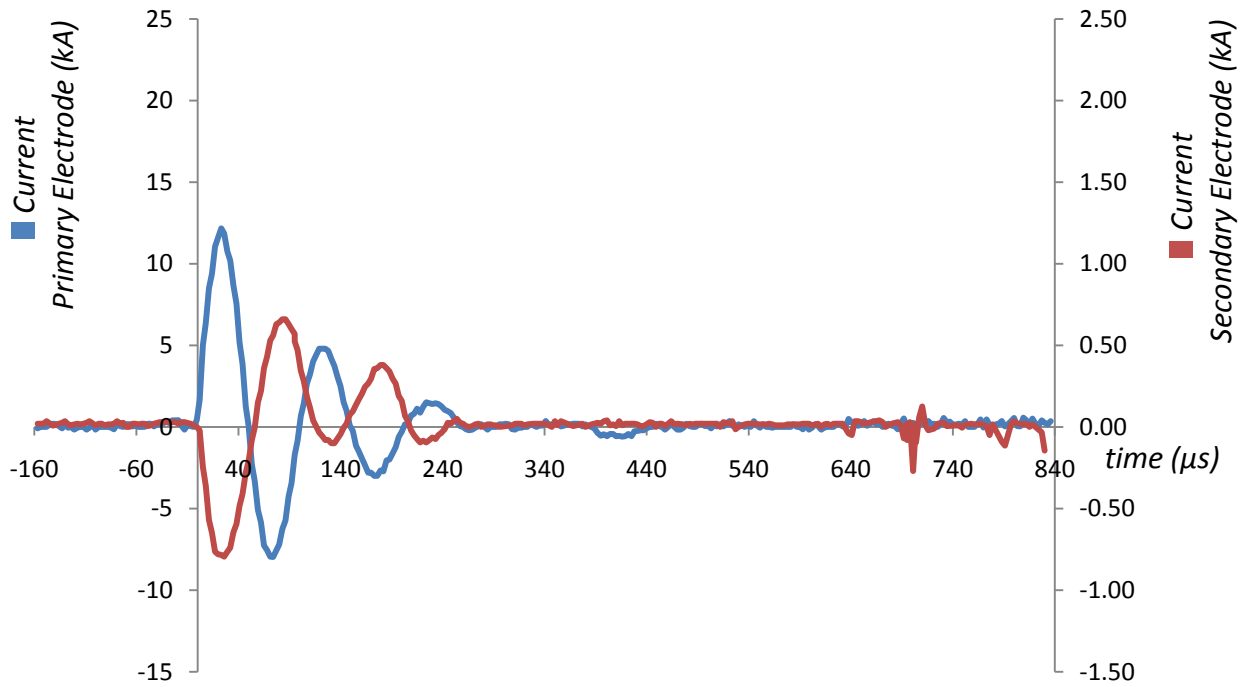

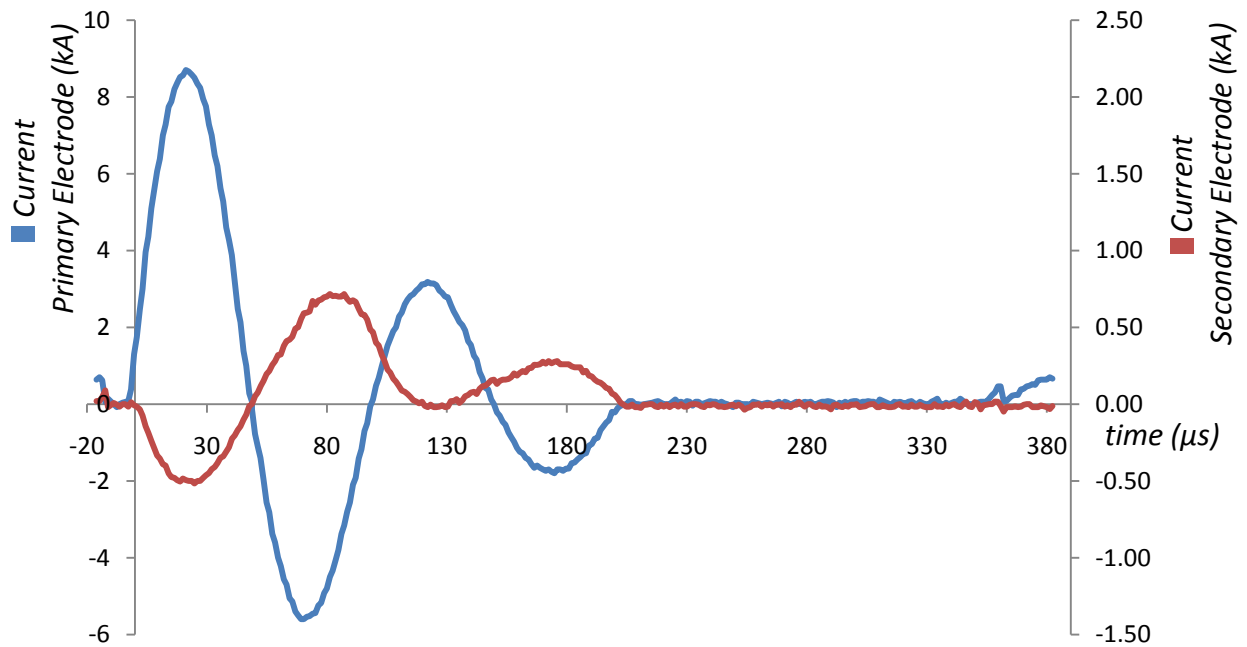**Figure 87: TS-PPT discharge 2kV (220J) Primary Discharge and 15V (0.528J) Secondary Discharge.**

119
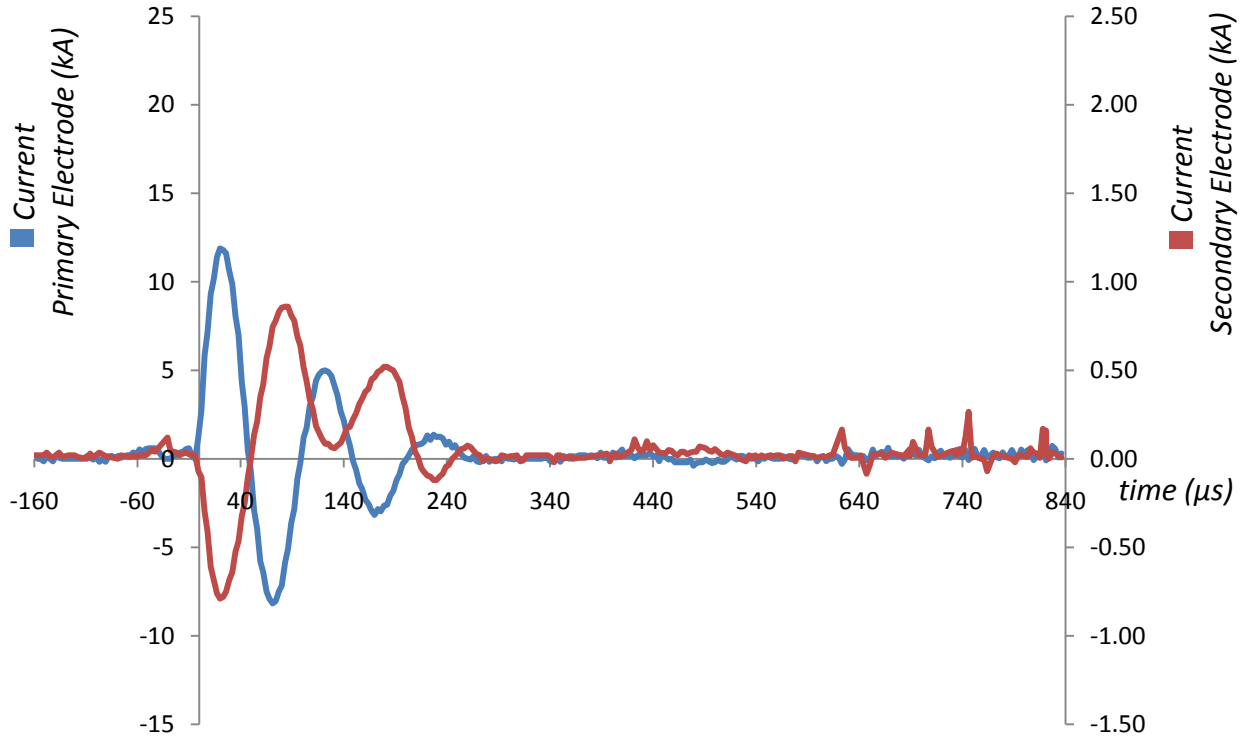
Figure 88: TS-PPT discharge 2kV (220J) Primary Discharge and 30V (2.11J) Secondary Discharge.
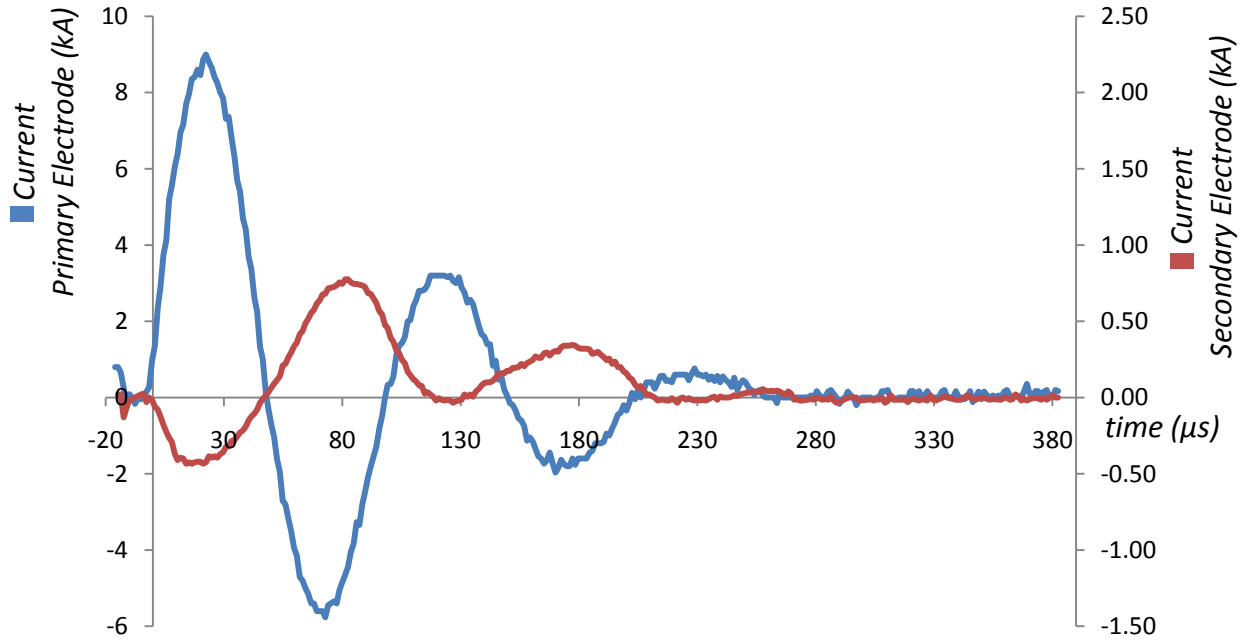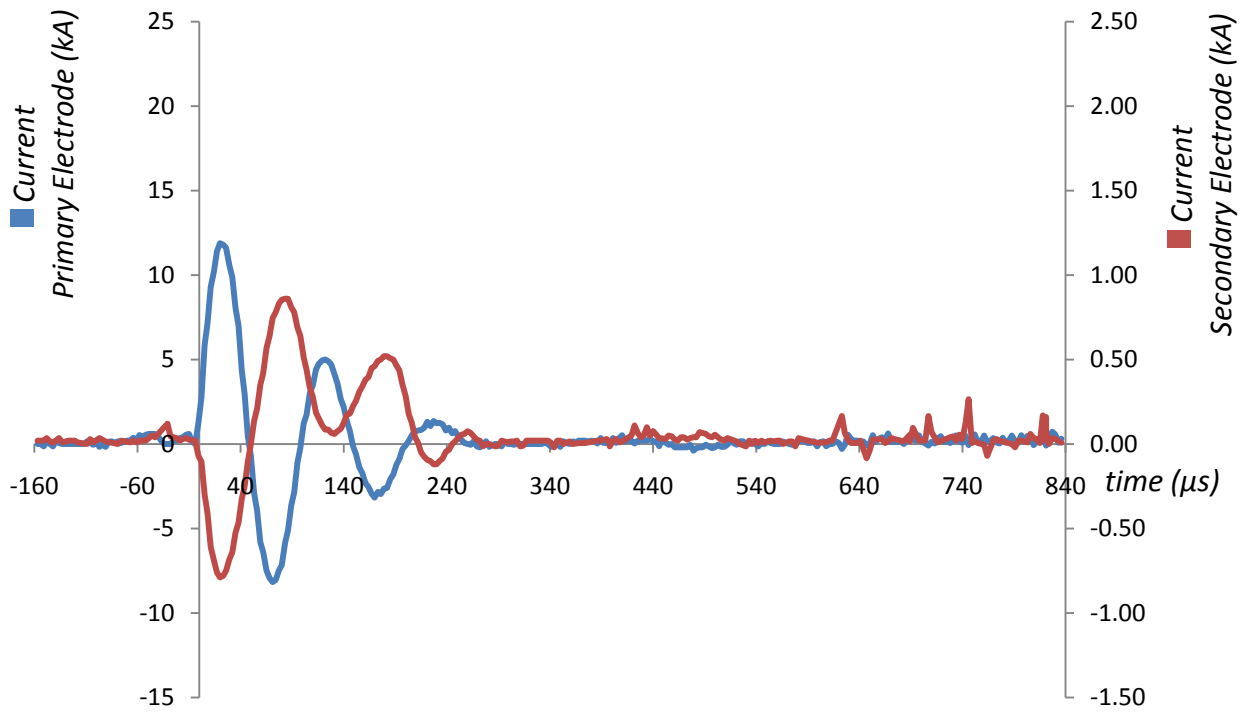

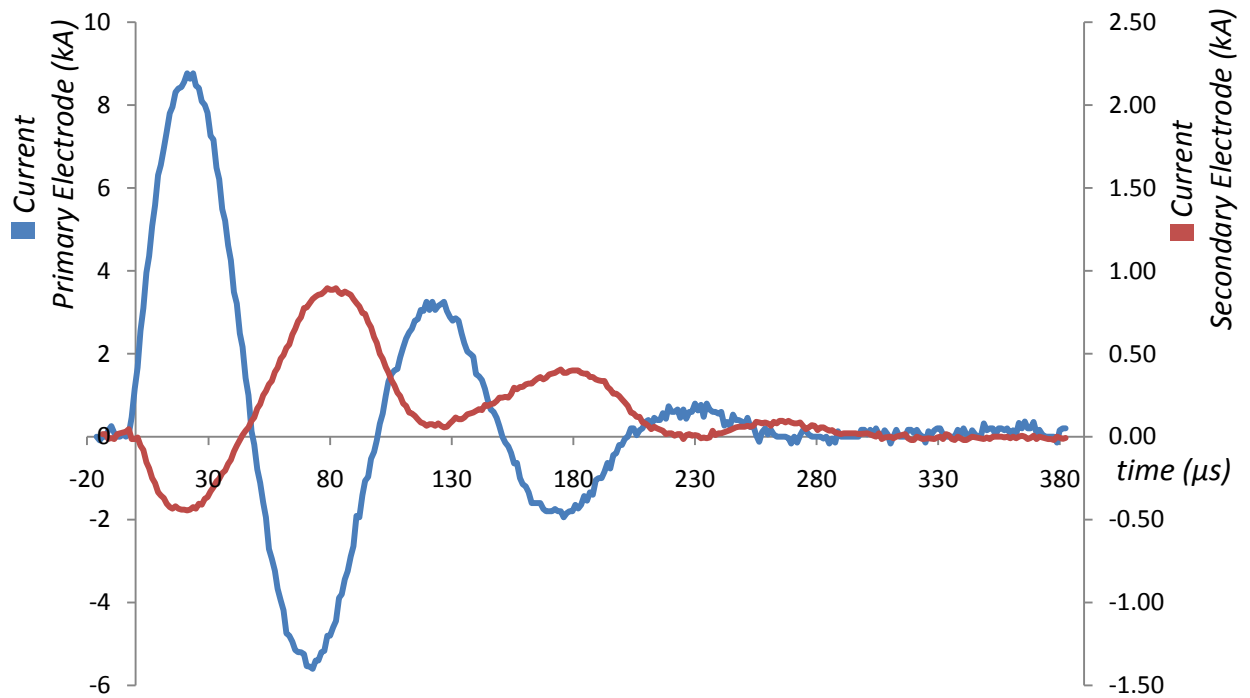**Figure 89: TS-PPT discharge 2kV (220J) Primary Discharge and 35V (2.87J) Secondary Discharge.**
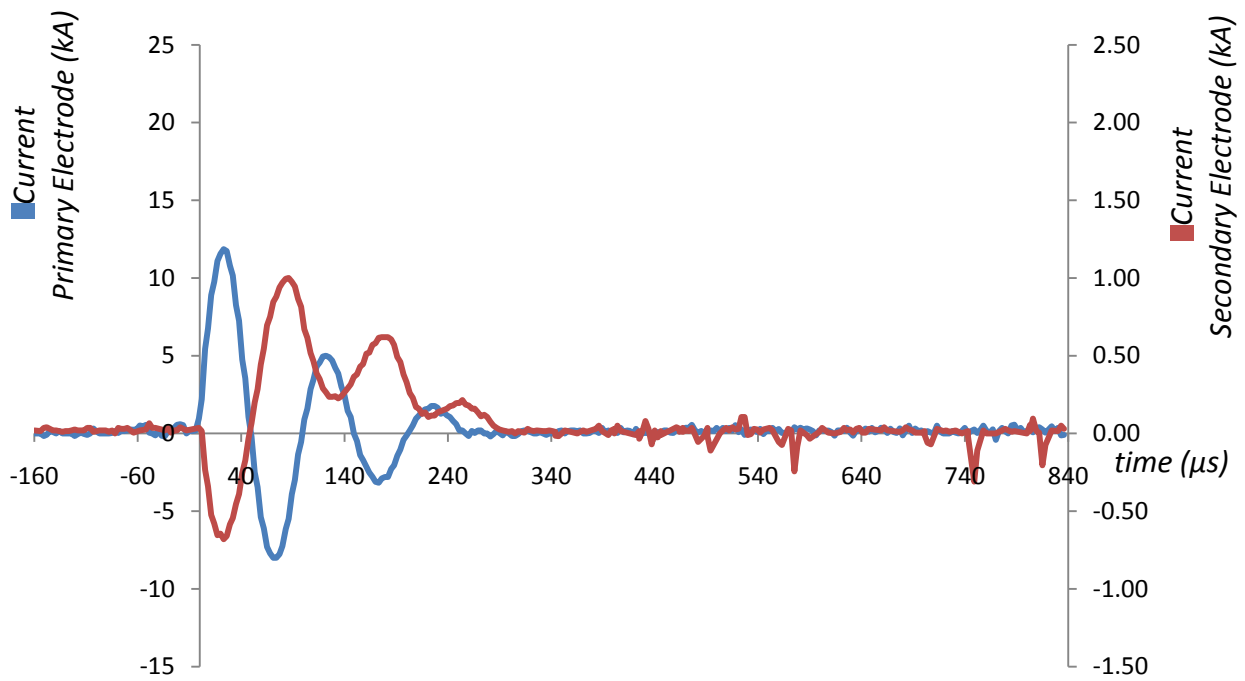
Figure 90: TS-PPT discharge 2kV (220J) Primary Discharge and 50V (5.87J) Secondary Discharge.
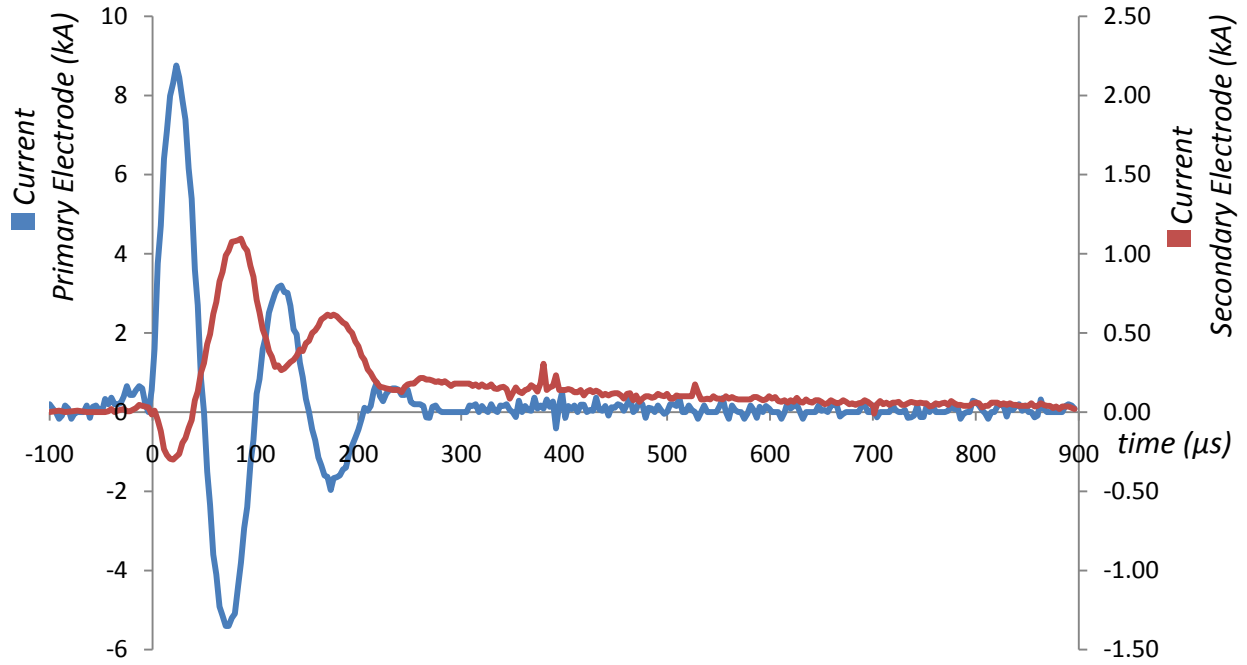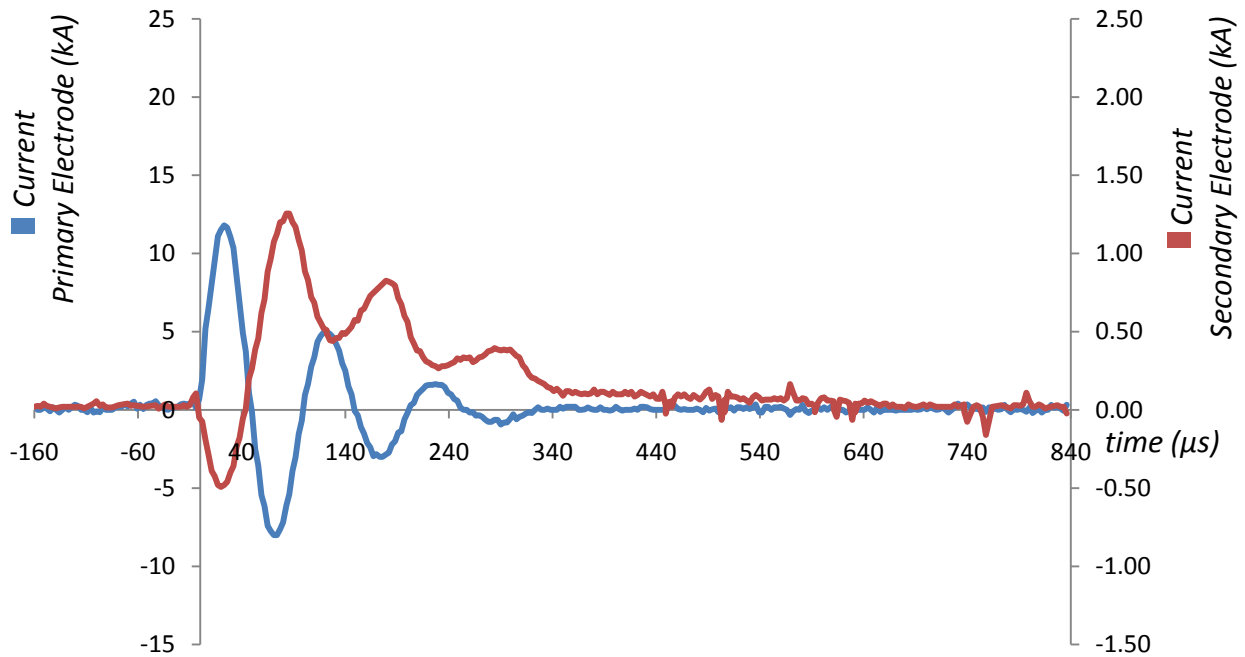

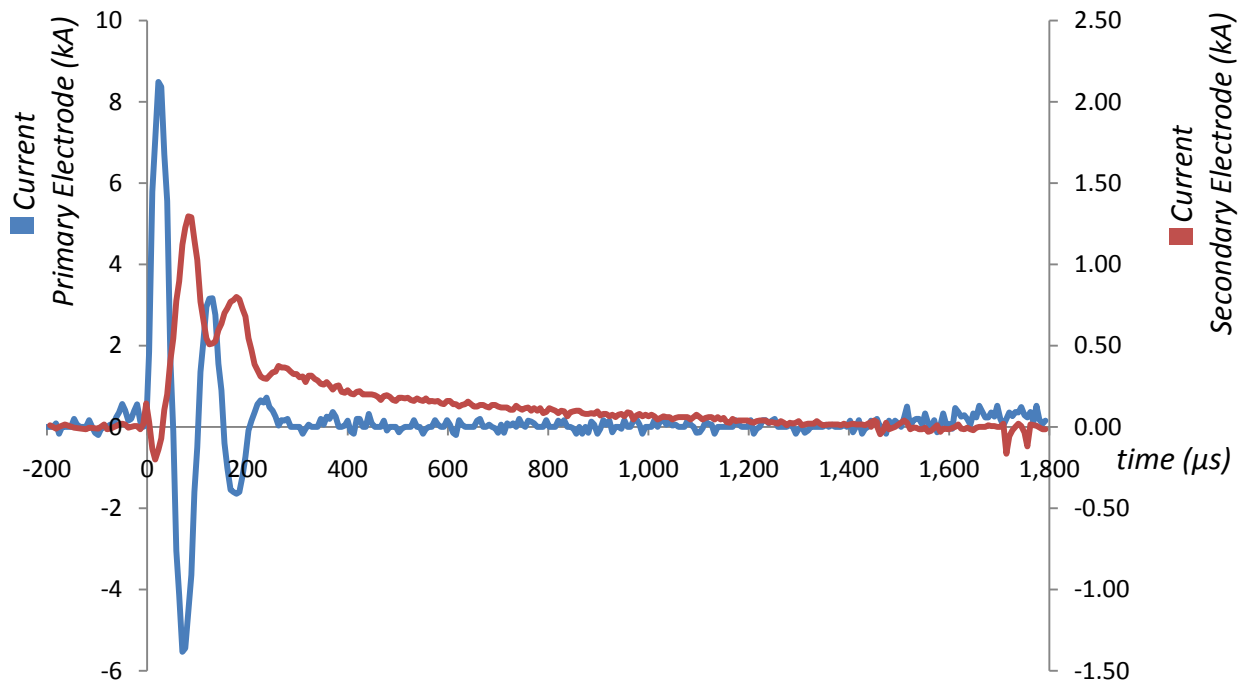**Figure 91: TS-PPT discharge 2kV (220J) Primary Discharge and 75V (13.2J) Secondary Discharge.**

121
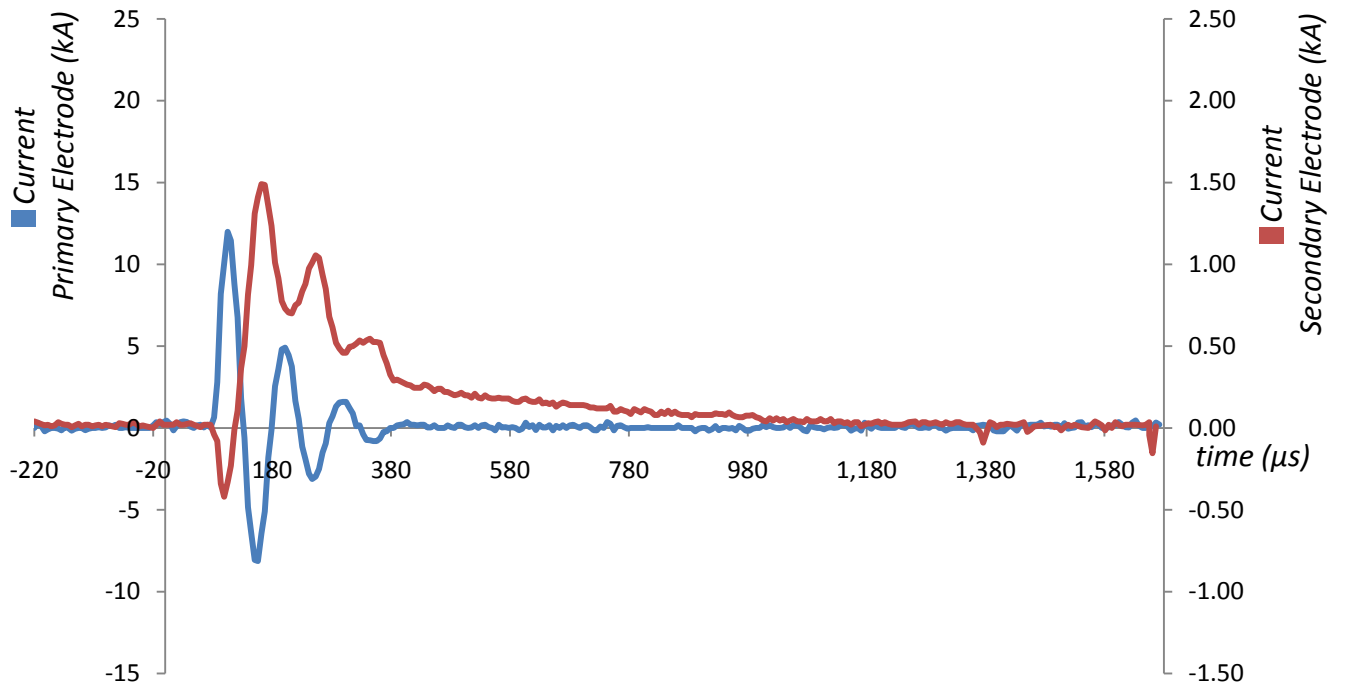
Figure 92: TS-PPT discharge 2kV (220J) Primary Discharge and 100V (23.5J) Secondary Discharge.
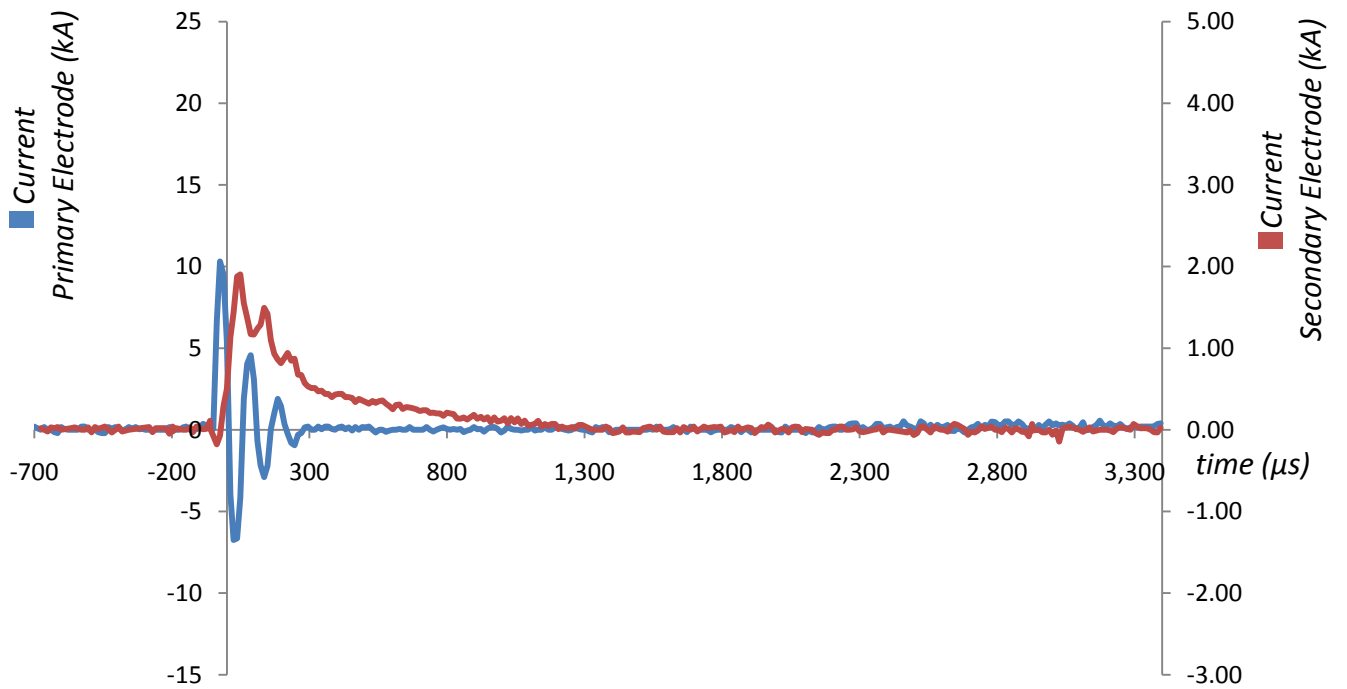
Figure 93: TS-PPT discharge 2kV (220J) Primary Discharge and 150V (52.8J) Secondary Discharge.

122
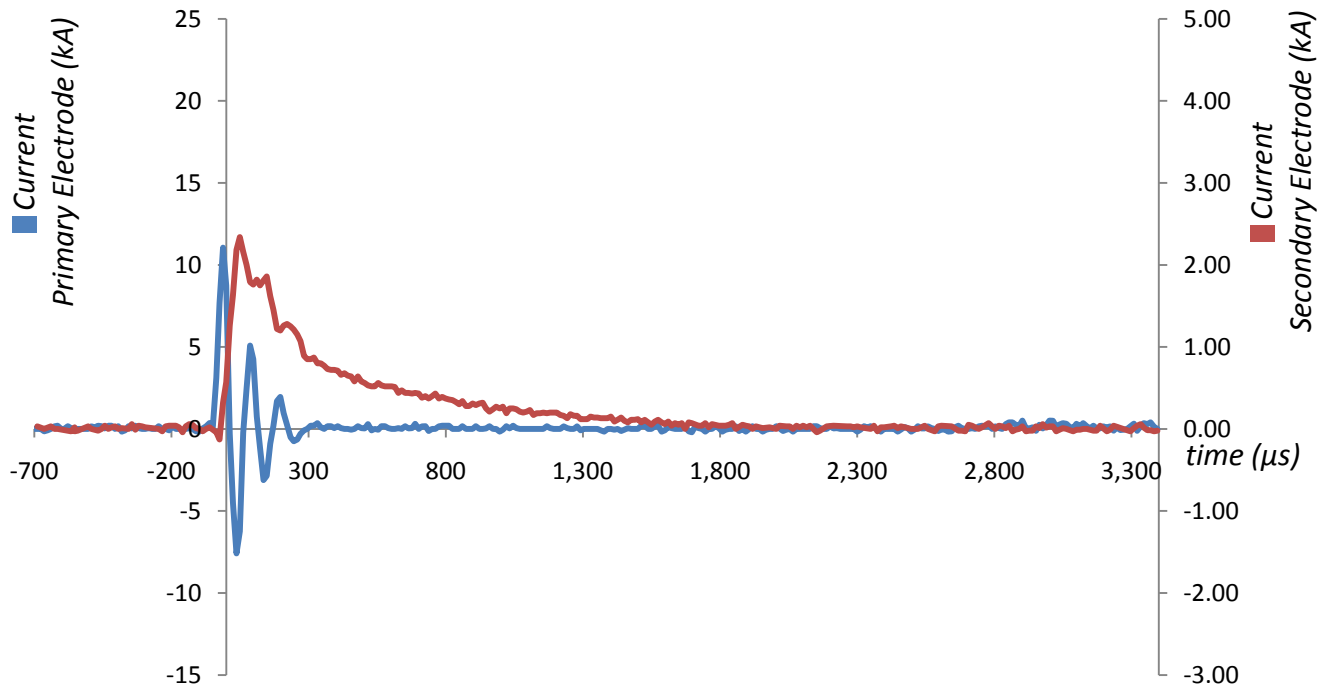
Figure 94: TS-PPT discharge 2kV (220J) Primary Discharge and 200V (94J) Secondary Discharge.
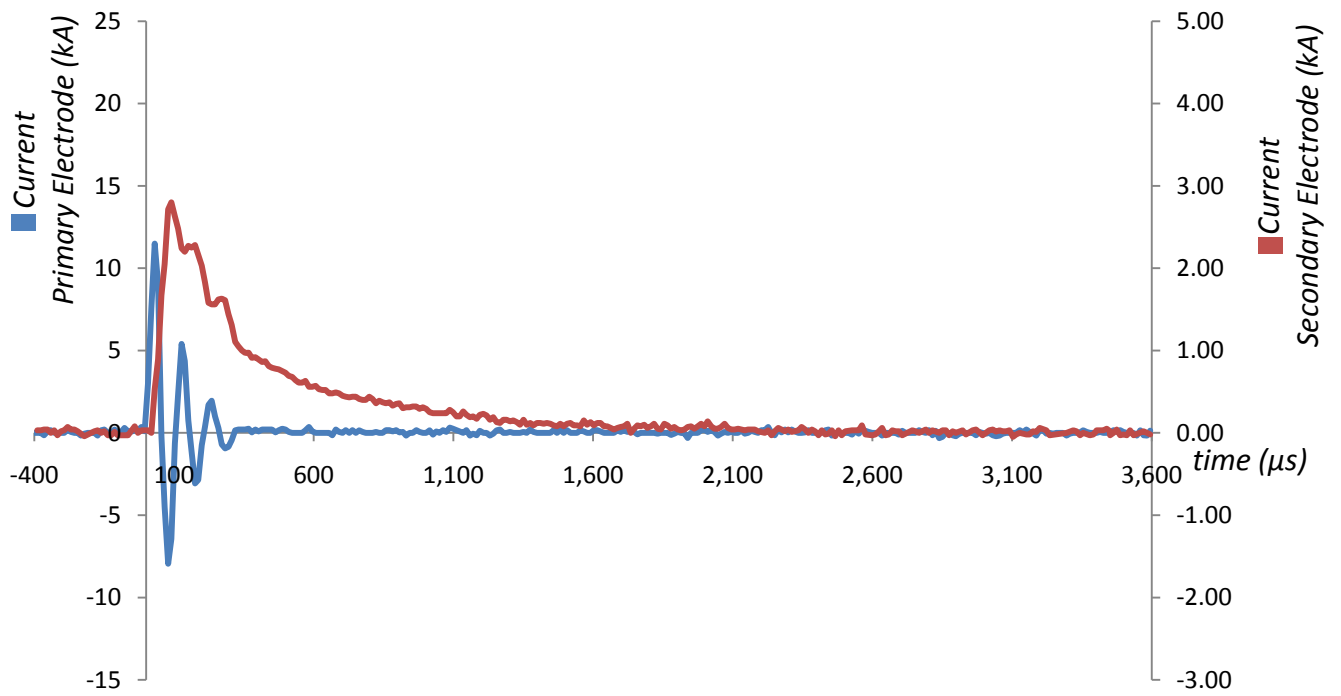
Figure 95: TS-PPT discharge 2kV (220J) Primary Discharge and 250V (146J) Secondary Discharge.
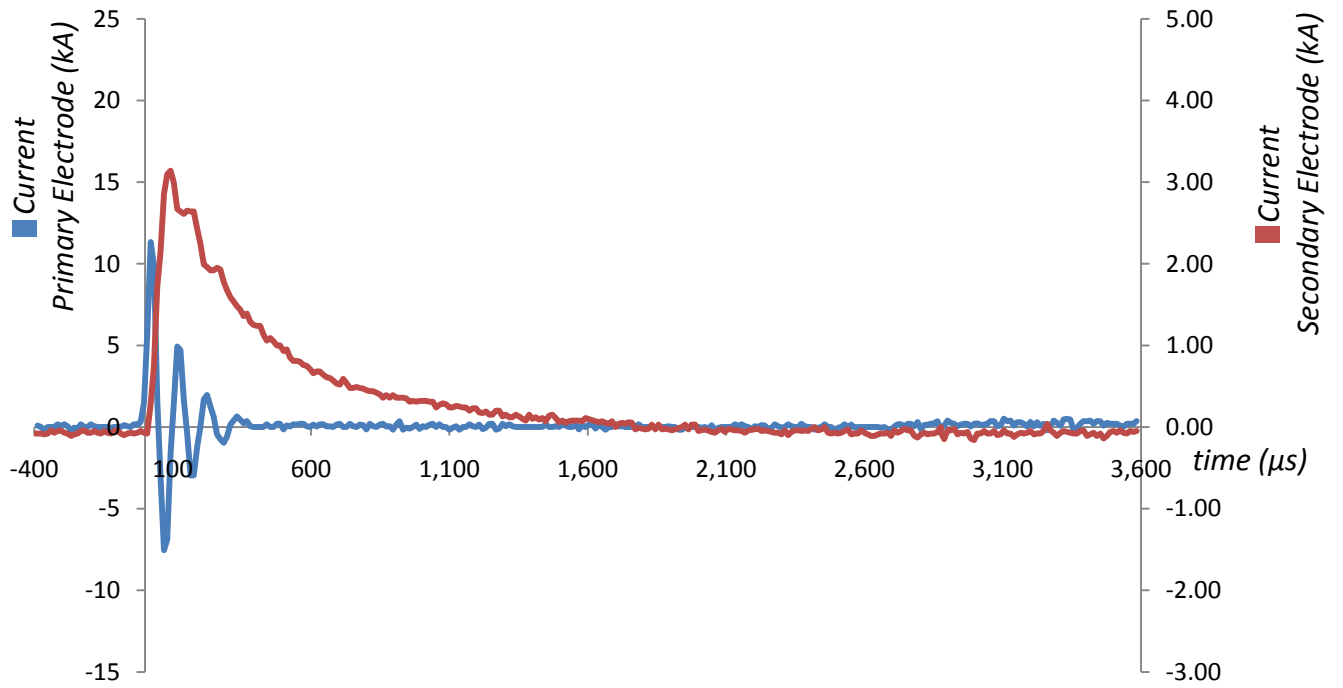
Figure 96: TS-PPT discharge 2kV (220J) Primary Discharge and 300V (211J) Secondary Discharge.
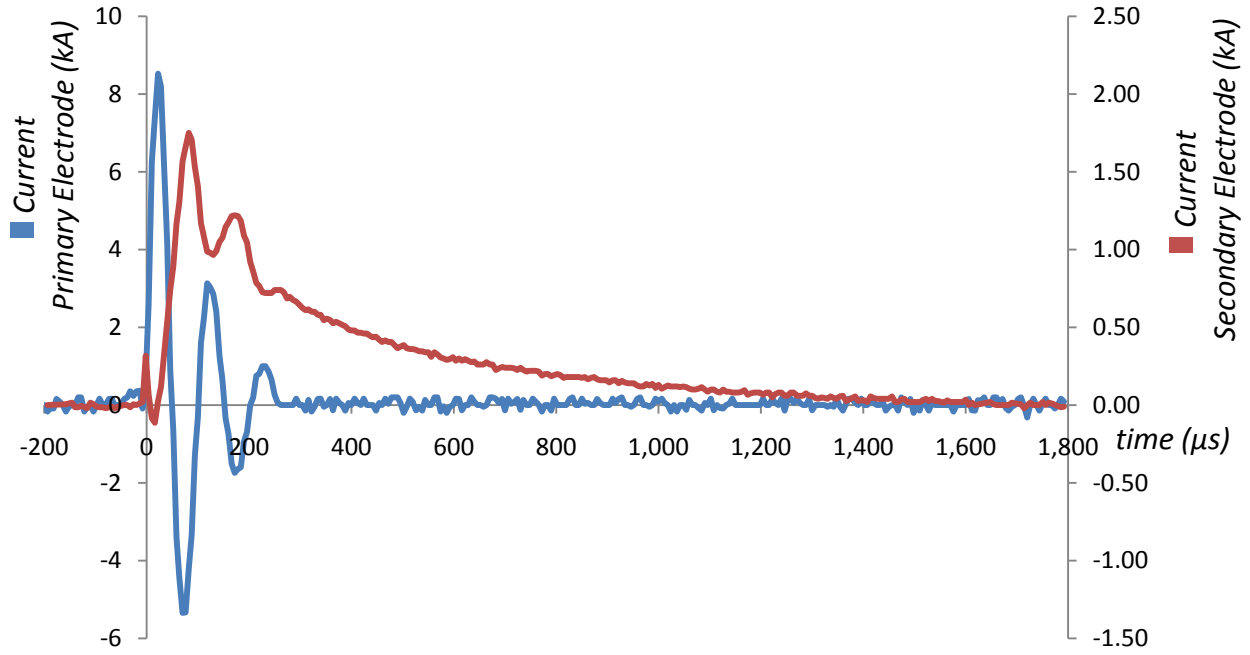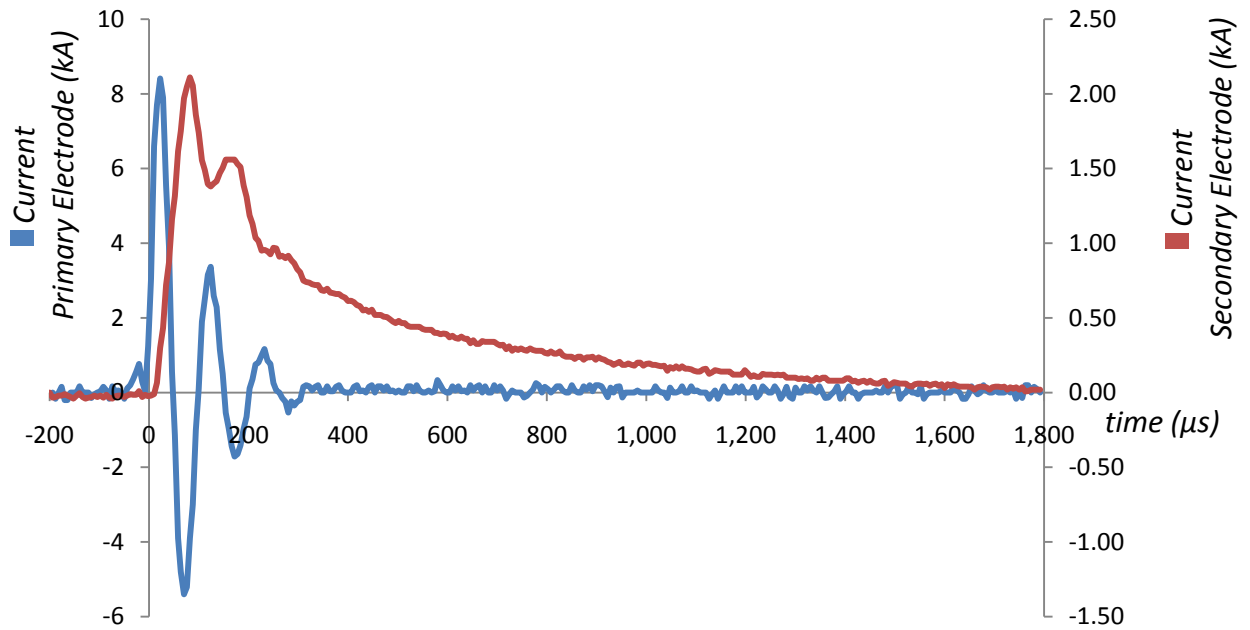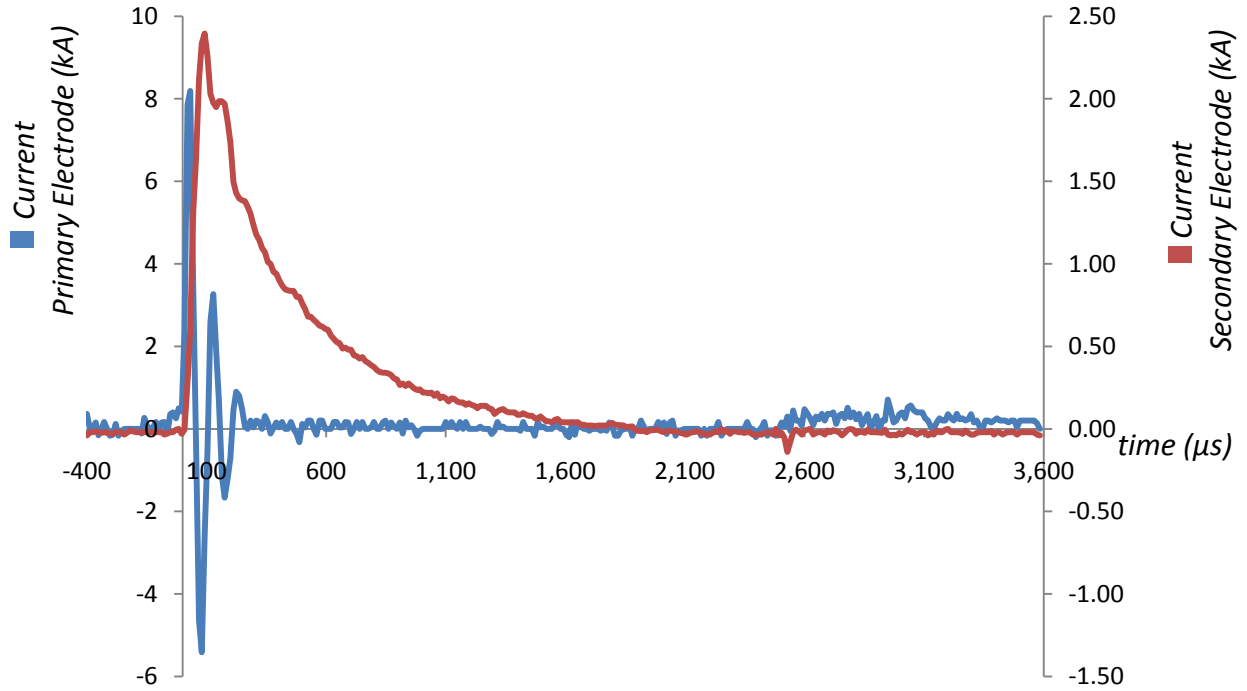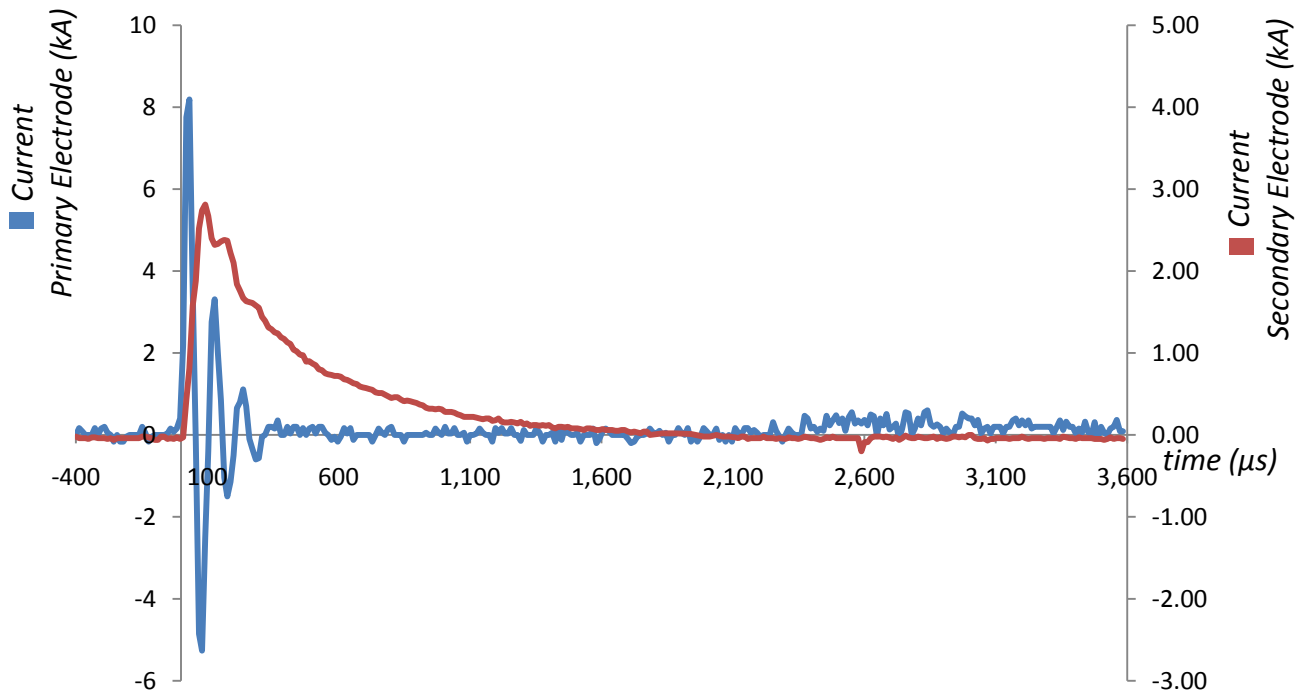
The behaviour of the discharge currents was shown while the primary discharge capacitor was charged at 2kV and the secondary discharge capacitor voltage varied from 0V to 300V.

Chapter 8

8. Analysis of the Results

8.1 Electromagnetic Impulse Analysis

The discharge currents of the TS-PPT give us a great indication on the performance of the thruster. From previous work (40) it known that the impulse bit due to the electromagnetic acceleration of the propellant in a PPT can be estimated as:

$$I_{EM\,1} = \frac{1}{2}L_1' \int I_1{}^2 dt = \frac{1}{2}L_1' \frac{\varepsilon_1}{R_{total\,1}}$$

where $I_{EM\,1}$ is the impulse due to electromagnetic acceleration in the first stage, L_1' is the inductance gradient in the first stage (in μH/m), I_1 is the electric discharge current of the first stage, ε_1 is the total initial energy stored in the primary discharge capacitor and $R_{total\,1}$ is the equivalent total resistance of the primary discharge circuit.

This is valid for the first stage of the TS-PPT, as it works as a regular PPT. As we assumed, conservatively, in the simple analytic model that the thrust efficiency for the second stage would be the same as the first stage, i.e., $\check{\varphi} = \varphi$, we can write:

$$I_{EM\,2} = \frac{1}{2}L_2' \int I_2{}^2 dt = \frac{1}{2}L_2' \frac{\varepsilon_2}{R_{total\,2}}$$

where $I_{EM\,2}$ is the impulse due to electromagnetic acceleration in the second stage, L_2' is the inductance gradient in the second stage (in μH/m), I_2 is the electric discharge current of the

second stage, ε_2 is the total initial energy stored in the secondary capacitor and $R_{total\ 2}$ is the equivalent total resistance of the secondary discharge circuit.

It is necessary to calculate the inductance gradients L_1' and L_2'. For rectangular electrodes, it is possible to calculate these gradients, also using previous works, as (40):

$$L_1' = 0.6 + ln\left(\frac{d_1}{b_1 + c_1}\right)$$

$$L_2' = 0.6 + ln\left(\frac{d_2}{b_2 + c_2}\right)$$

where d_1 is the distance between the electrodes of the primary stage, d_2 is the distance between the electrodes of the secondary stage, b_1 is the width of the electrodes of the primary stage, b_2 is the width of the electrodes of the secondary stage, c_1 is the thickness of the electrodes of the primary stage and c_2 is the thickness of the electrodes of the secondary stage. The resulting inductance gradients will be in µH/m.

Our TS-PPT implementation is such that $d_1 = d_2 = d$, $b_1 = b_2 = b$, $c_1 = c_2 = c$, not considering the curvature[37] of the secondary electrodes. Figure 97 shows a schematic of the front view of the discharge chamber and it is possible to have a clearer idea of these parameters.

---

[37] The TS-PPT studied had a fairly long straight section and a curvature at the end. The curvature was used in an attempt to improve the performance of the gas-dynamically accelerated propellant. For the calculation of the electromagnetic acceleration only straight part was considered.
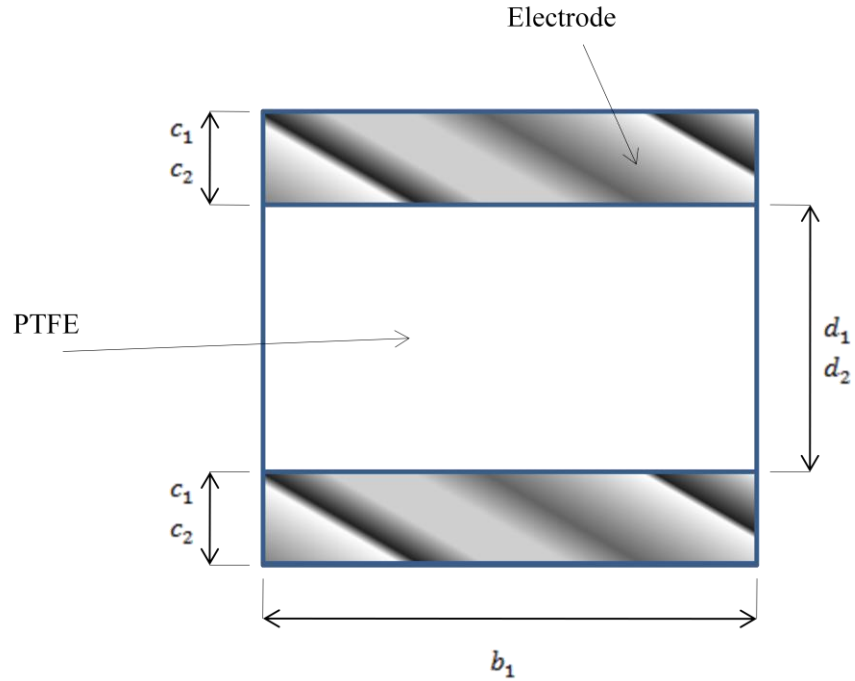
Figure 97: Schematics of the front view of the discharge chamber of the TS-PPT.

The values of the geometric parameters for our TS-PPT are: $d = 21mm, c = 3mm, b = 25mm$.

And the respective inductance gradients are:

$$L_1^{'} = L_2^{'} = L^{'} = 0.485 \frac{\mu H}{m}$$

It is also necessary to calculate $R_{total\ 1}$ and $R_{total\ 2}$. This can be done by analyzing the discharge current behavior, as done in previous work (44). Figure 98 shows a typical primary discharge current graph.
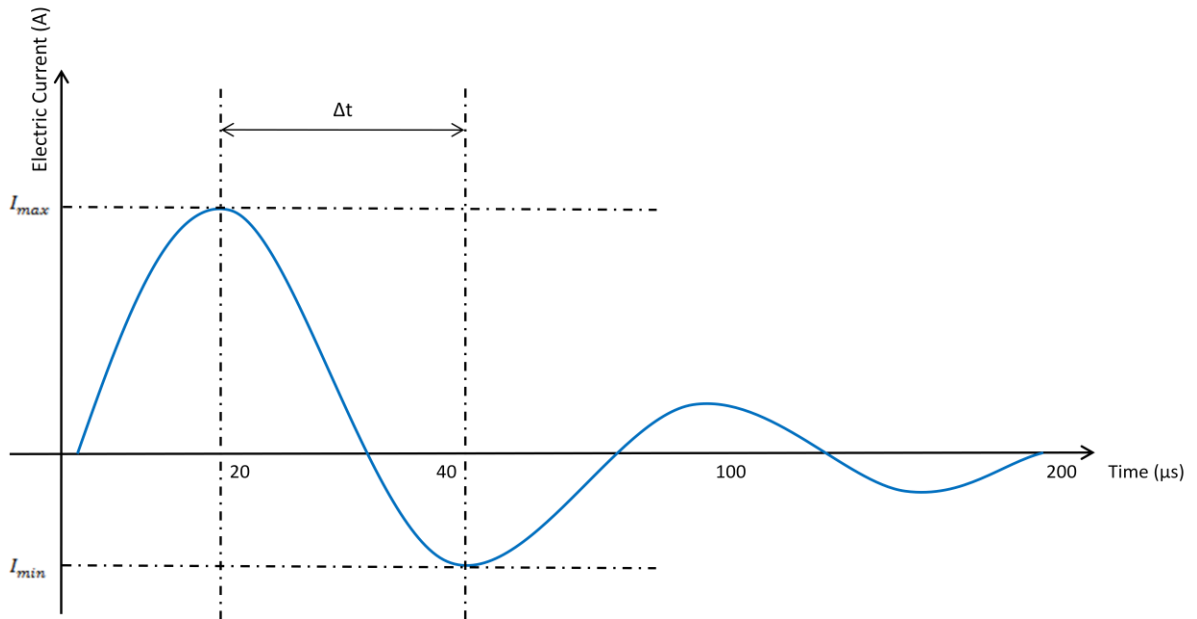
Figure 98: Obtaining circuit parameters from the discharge current.

The relation between the two successive current peaks is:

$$\frac{|I_{max}|}{|I_{min}|} = e^{\frac{R_{total} \cdot \Delta t}{2L_{eq}}}$$

$$R_{total} = \frac{2L_{eq}}{\Delta t} \ln\left(\frac{|I_{max}|}{|I_{min}|}\right)$$

And also the period of the discharge is related to the capacitance and the inductance of the circuit:

$$T = 2\Delta t = 2\pi \sqrt{L_{eq} C_1}$$

And we can then write:

$$L_{eq} = \frac{4\Delta t^2}{4\pi^2} \frac{1}{C_1}$$

128

For performance purposes, at this point, it is convenient to analyse the last discharge currents shown for each of the three primary capacitor voltages, i.e., for primary capacitor voltages of 1 kV, 1.5 kV and 2 kV while the secondary capacitor voltage is kept at 300V. Table 7 summarises the results of electromagnetic impulse bit for the three cases. It should be taken in account the uncertainties mentioned in page 96.

Table 7: Electromagnetic impulse bit for the first stage of TS-PPT.

V_1	V_2	Δt	$|I_{max}|$	$|I_{min}|$	L_{eq}	R_{total}	ε_1	I_{EM_1}	φ_{EM_1}
1kV	300V	59μs	4.92kA	2.9kA	3.27μH	58mΩ	55J	230μNs	4.18μNs/J
1.5kV	300V	48μs	8.19kA	5.27kA	2.12 μH	39mΩ	123J	765μNs	6.22μNs/J
2kV	300V	48μs	11.3kA	7.54kA	2.12 μH	35.8 mΩ	220J	1.49mNs	6.78μNs/J

The impulse bit rises as the primary capacitor energy is increased, as expected. The values of φ_{EM} are below the values of several PPTs – as seen in Figure 9 and Table 4 - but as mentioned, this is a non-optimized design.

As the waveforms of the secondary discharges are mostly underdamped it is not possible to use the same methodology to estimate the electromagnetic thrust. To calculate the electromagnetic impulse bit of the second stage it is necessary to numerically integrate the currents obtained experimentally. As mentioned above, the following relation will be used:

$$I_{EM\,2} = \frac{1}{2} L_2' \int I_2{}^2 dt$$

Similarly to the calculation for the first stage, we are going to analyse the last discharge currents for each of the three primary capacitor voltages, i.e., for primary capacitor voltages of 1kV,

1.5kV and 2kV while the secondary capacitor voltage is kept at 300V and then the primary capacitor voltage is kept at 2kV and the secondary capacitor voltage varies from 300V to 100V. Table 8 summarises the results of electromagnetic impulse bit for the three cases. It should be taken in account the uncertainties mentioned in page 96.

Table 8: Electromagnetic Acceleration for the second stage of the TS-PPT.

V_1	V_2	ε_2	$\int I_2{}^2 dt$	I_{EM2}	φ_{EM2}
1kV	300V	211J	1821 $A^2 s$	441μNs	2μNs/J
1.5kV	300V	211J	1646 $A^2 s$	399μNs	1.89μNs/J
2kV	300V	211J	2023$A^2 s$	490μNs	2.32μNs/J
2kV	250V	146J	1395$A^2 s$	338μNs	2.31μNs/J
2kV	200V	94J	952$A^2 s$	230μNs	2.45μNs/J
2kV	150V	52.8J	480$A^2 s$	116μNs	2.20μNs/J
2kV	100V	23.5J	195$A^2 s$	47μNs	2.01μNs/J

It can be seen that φ_{EM2} is notably smaller than φ_{EM1}. This is attributed to a non optimization of the TS-PPT, to the low voltage applied on the secondary discharges due to power supply and capacitor limitations, and also due to relatively long cabling for the secondary discharge, increasing electrical resistance and inductance. However, it is possible to see that φ_{EM2} does not change significantly when ε_2 changes. This indicates that it should be possible to operate the thruster at various secondary discharge energy levels without significant changes in efficiency.

The total electromagnetic impulse, I_{EM}, for the TS-PPT – first and second stages – with its respective total electromagnetic impulse per total discharge energy ratio can be seen in Table 9. It should be taken in account the uncertainties mentioned in page 96.

Table 9: Summary of the Electromagnetic Acceleration for the TS-PPT

ε_1	ε_2	I_{EM_1}	I_{EM_2}	I_{EM}	φ_{EM}
55J	211J	230µNs	441µNs	671µNs	2.52µNs/J
123J	211J	765µNs	399µNs	1.164mNs	3.48µNs/J
220J	211J	1.49mNs	490µNs	1.98mNs	4.59µNs/J

A relatively low performance was found for both the primary stage and second stage of the TS-PPT. It must be noted, however, that the gas dynamic accelerated portion of the mass was not accounted for. Nevertheless, the mechanism of late ablation acceleration was characterised. It is possible to see that a further impulse can be imparted in the ablating mass – and for this matter in the late ablated mass - with a secondary discharge. This was the main goal of this research.

8.1.1 General Analysis of the Performance

If we calculate the total resistance, total inductance, maximum current, minimum current and electromagnetic impulse bit for the first stage and for the second stage for each of the 39 electric current discharges presented in the previous chapter – with the mathematic models presented on this chapter -, it is possible to have an overview of the TS-PPT with relation to its electromagnetic performance.

Analysis of the behaviour of the total inductance, total resistance of the first stage as a function

of the secondary discharge energy are presented from Figure 99 to Figure 101.
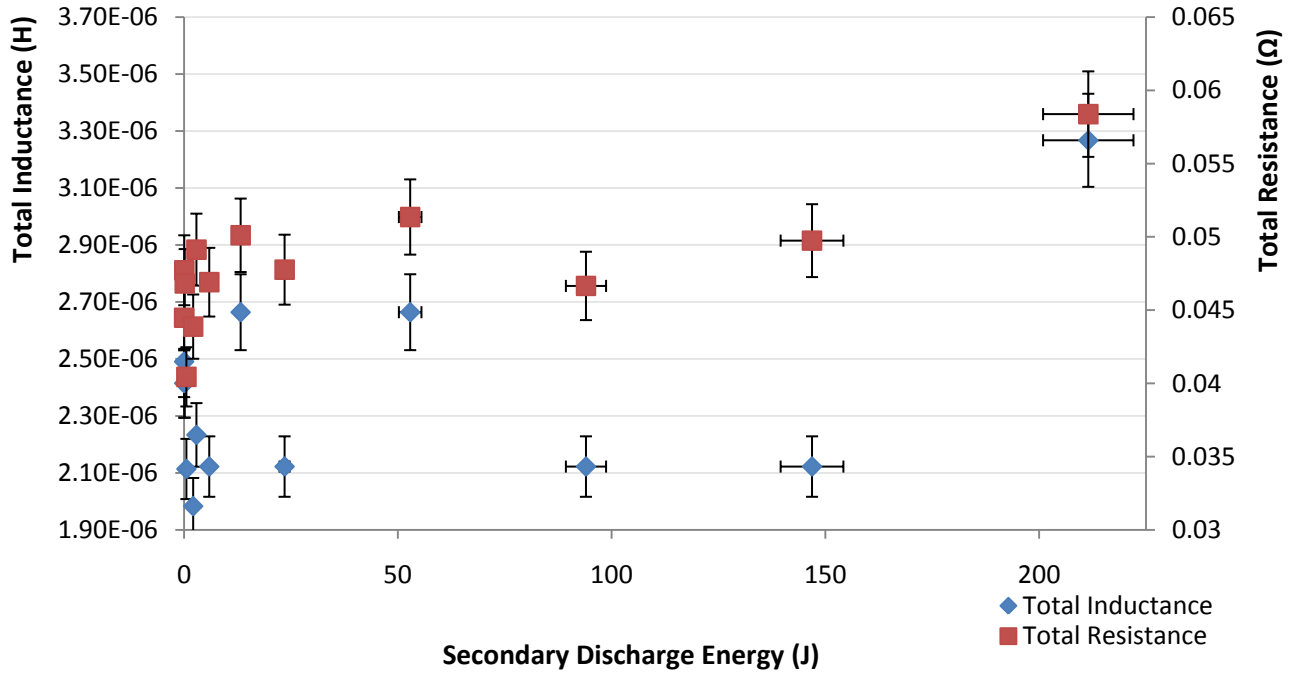
Figure 99: Total inductance and total electric resistance as a function of the secondary discharge energy for 1kV, 55J primary discharge.
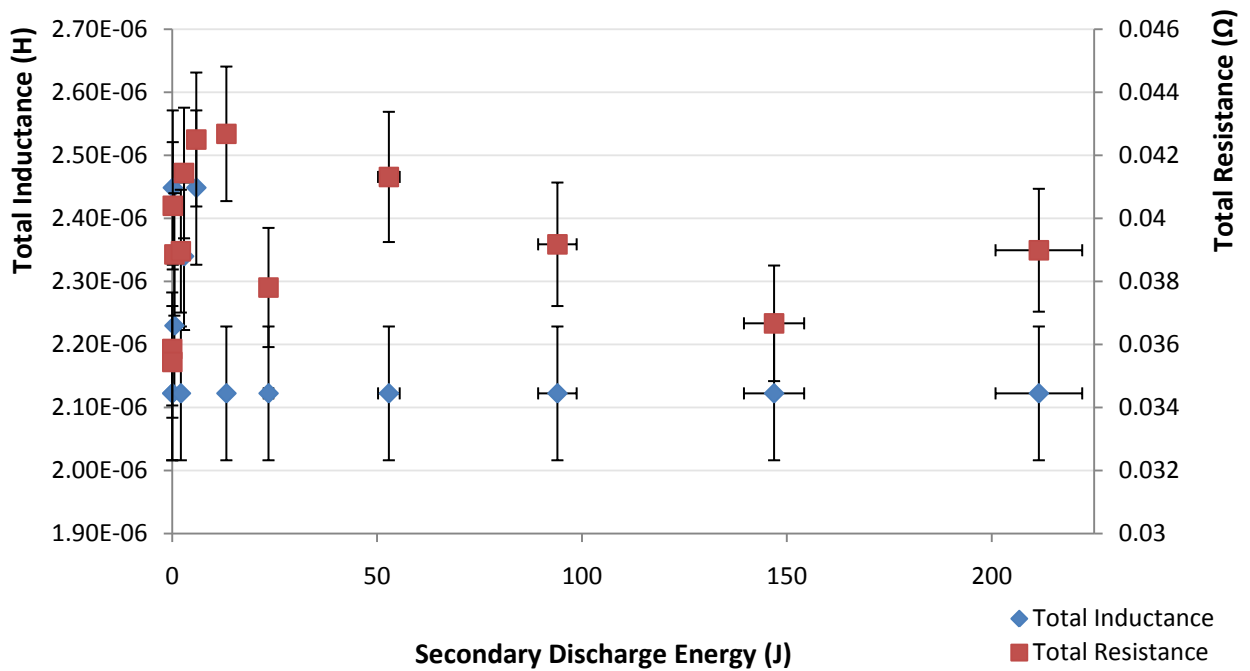
Figure 100: Total inductance and total electric resistance as a function of the secondary discharge energy for 1.5kV, 123J primary Discharge.
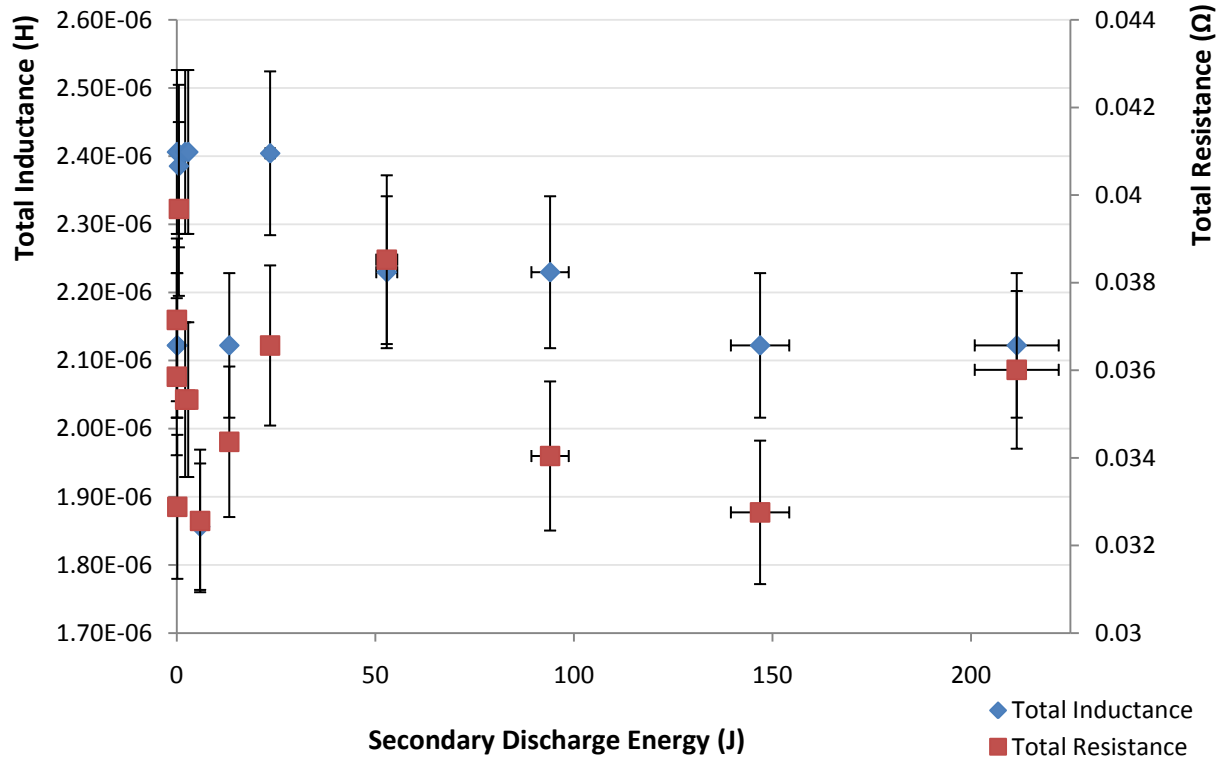
Figure 101: Total inductance and total electric resistance as a function of the secondary discharge energy for 2kV, 220J primary Discharge.

Looking at the scale of the graphs it is possible to see that the total resistance and total inductance do not change significantly. The inductance stays at around 2.1×10^{-6} H. The total resistance oscillates and there is a point of minimum at 150 joules – or 100 joules for the first case. These oscillations are attributed to the inevitable time varying induced magnetic fields from the secondary discharge that affect the primary discharge current.

It is convenient to analyse the electromagnetic impulse bit produced by the TS-PPT with partial contributions from the first and second stages, as shown on Figure 102 to Figure 104.

134
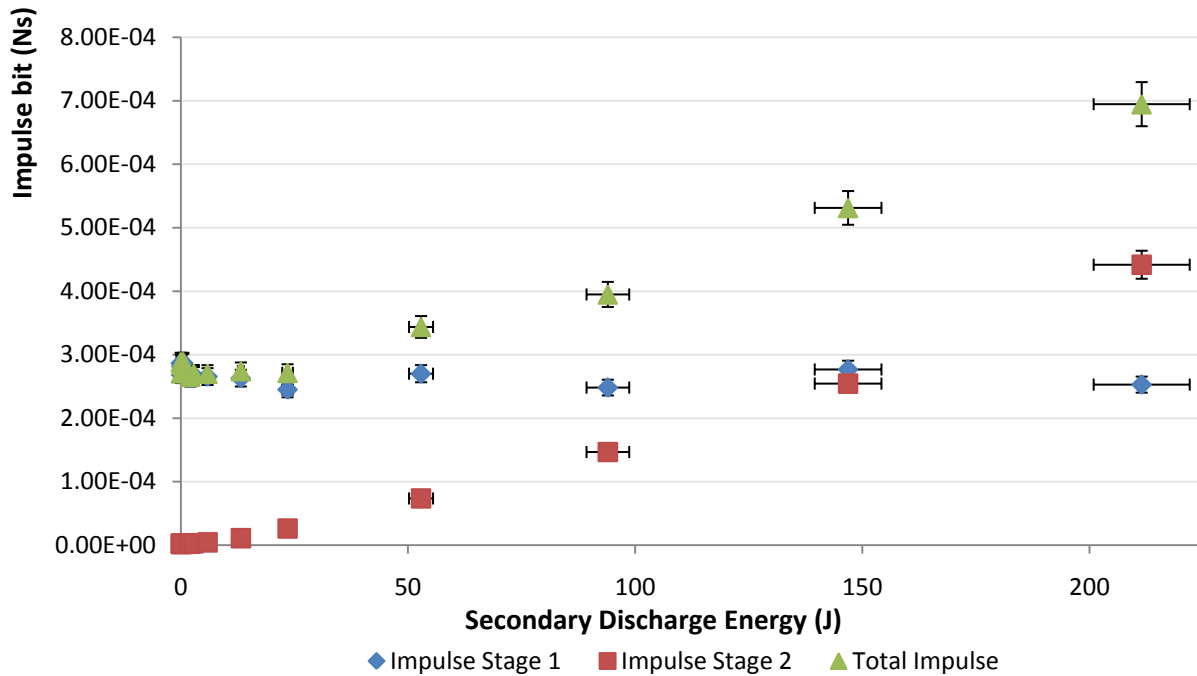
Figure 102: Electromagnetic impulse bit of stage one and the total electromagnetic impulse bit as a function of the secondary discharge energy for 1kV, 55J primary discharge.
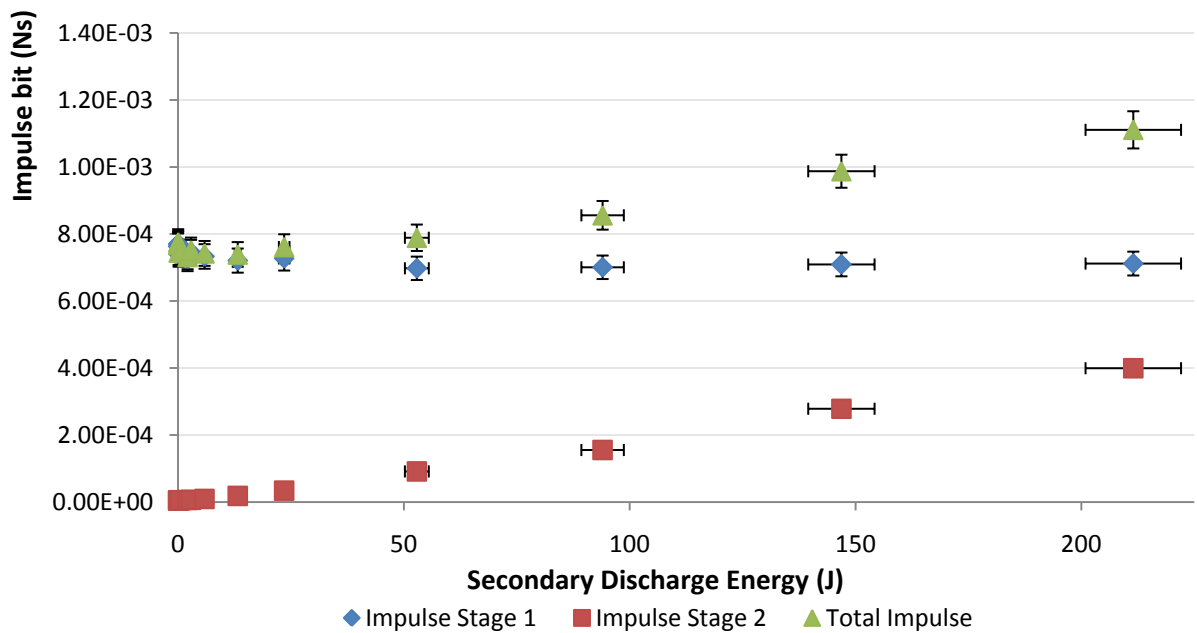
Figure 103: Electromagnetic Impulse Bit of stage one, stage two and the total electromagnetic impulse bit as a function of the secondary discharge energy for 1.5kV, 123J primary discharge.
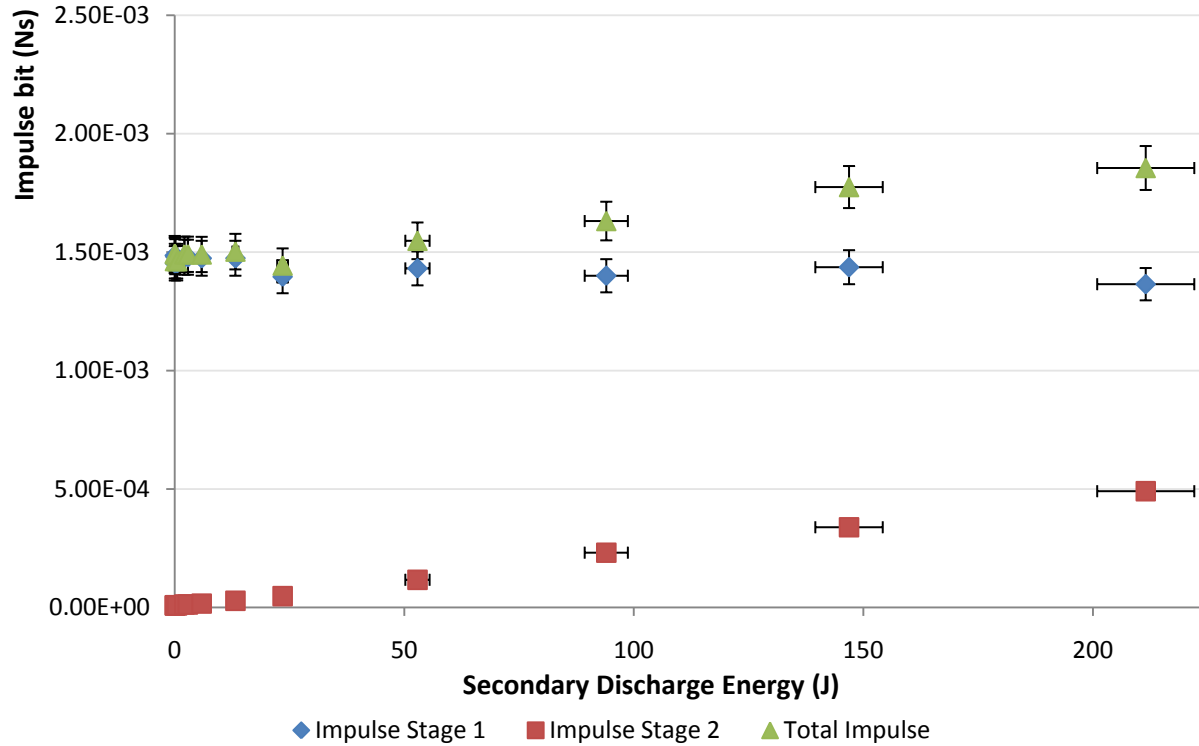
Figure 104: Electromagnetic Impulse Bit of stage one, stage two and the total electromagnetic impulse bit as a function of the secondary discharge energy for 2kV, 220J primary discharge.

As it can be seen, significant contributions to the impulse bit are done with secondary discharge energy level of more than 50 joules. However, the specific impulse bit, in $\frac{Ns}{J}$, of the second stage is low, compared to the first stage. As the electromagnetic thrust is directly proportional to the integral of the square of the discharge current, higher values of specific thrust are expected when the secondary discharge operates at higher voltages, yielding higher currents.

It is also convenient to analyse the electromagnetic specific impulse bit for the first stage, second stage and for both stages for all the 39 cases, as shown from Figure 105 to Figure 107.

136

Figure 105: Electromagnetic specific impulse bit for the first stage, second stage and for both stages as a function of the secondary discharge energy for 1kV 55J primary discharge.
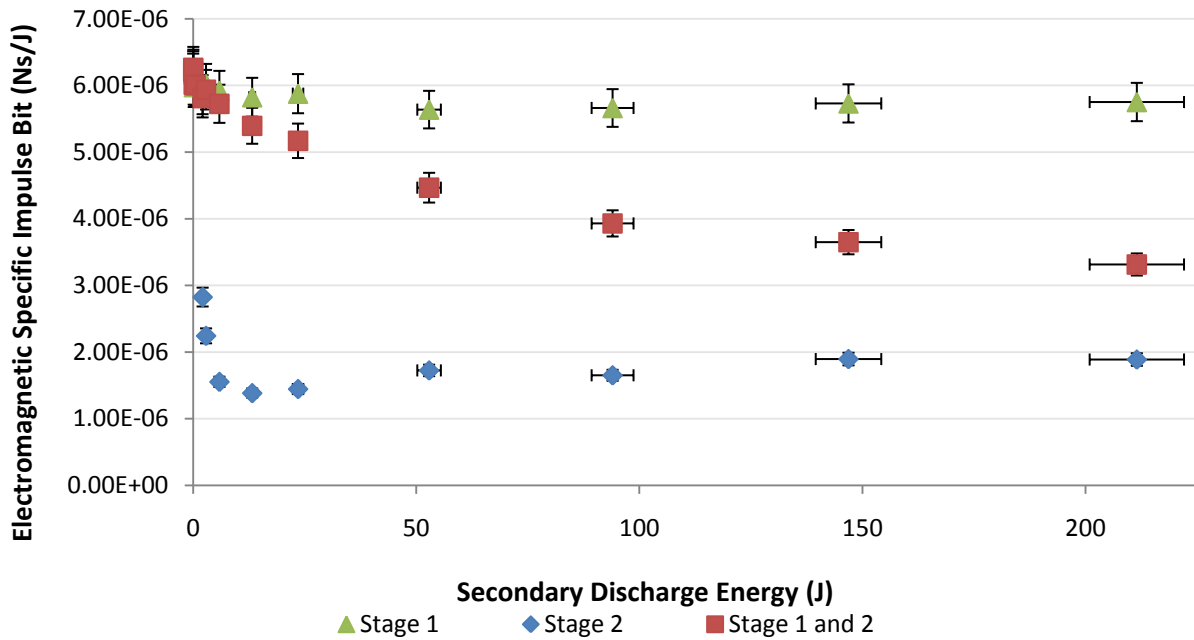
Figure 106: Electromagnetic specific impulse bit for the first stage, second stage and for both stages as a function of the secondary discharge energy for 1.5kV 123J primary discharge.
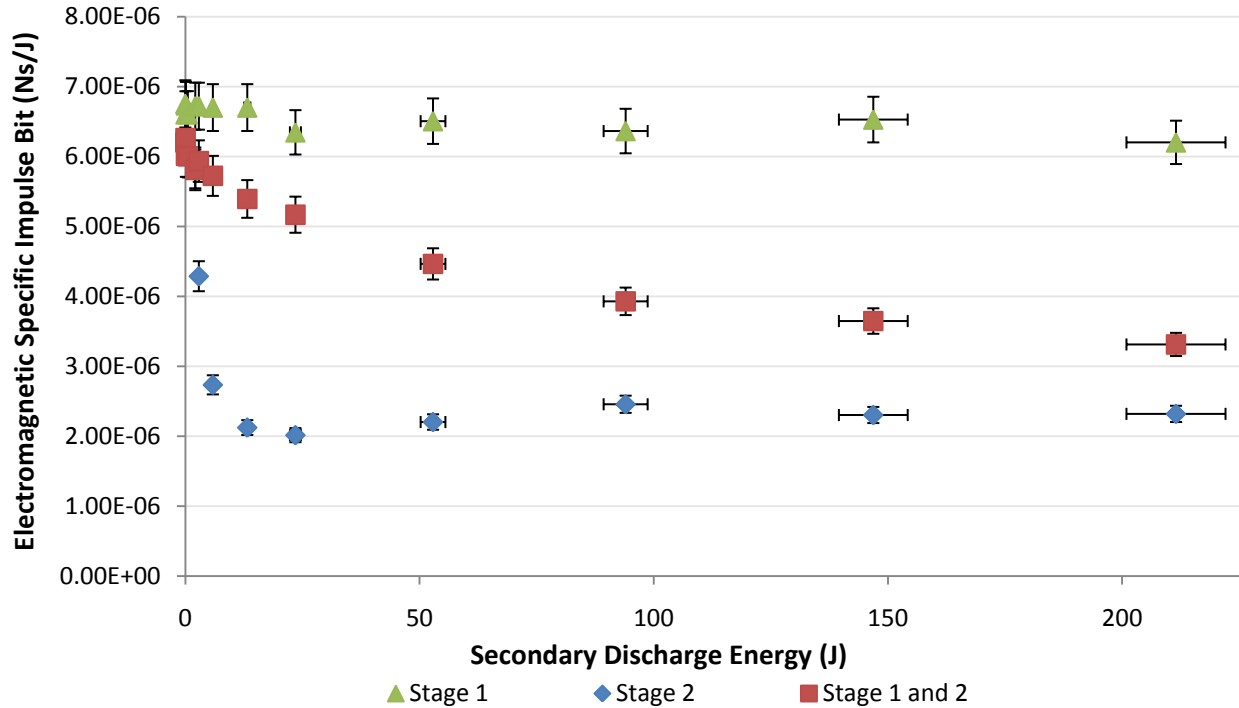
Figure 107: Electromagnetic specific impulse bit for the first stage, second stage and for both stages as a function of the secondary discharge energy for 2kV 220J primary discharge.

The electromagnetic specific impulse bit (*ESIB*) of the first stage remains reasonably constant while varying the secondary discharge energy, for each of the primary discharge energies. This is another indication of the relative independence of the two discharges, in this respect. The *ESIB* of the second stage is high at low energies due to the numerical integration taking in account the current produced by the primary discharge even when the initial energy in the secondary capacitor was zero, which would yield a false infinite *ESIB*. In the first and second cases it can be seen an increase in the *ESIB* of the second stage at higher discharge energies. Due to the lower *ESIB* of the second stage, compared with the first stage, the total *ESIB* is reduced as more energy is spent in the lower efficiency second stage. However, it must be noted that the second discharge does not produce late ablation and therefore no more propellant is consumed. Also, as mentioned before, higher values of *ESIB* are expected for the second stage when it is optimised.

One of the most important conclusions is the increase in the specific impulse and therefore an increase in propellant efficiency, which is the main goal of accelerating the late ablation. Using the $\Delta m / \varepsilon_1$ measured of $0.32 \frac{\mu g}{J}$ it is possible to calculate the specific impulse for all the 39 cases, keeping in mind that only the primary discharge ablates propellant and also that only the electromagnetic impulse bit is being taking in account. Figure 108 to Figure 110 shows the results for the specific impulses.
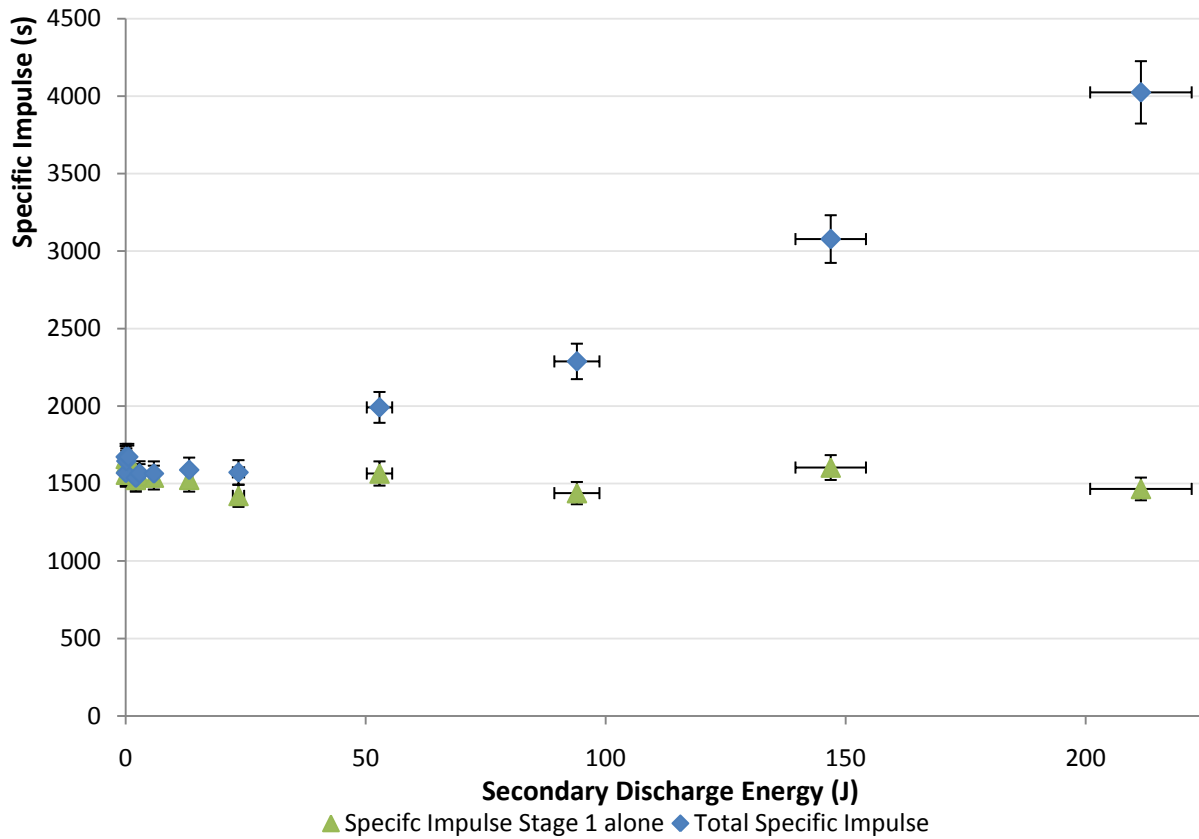
Figure 108: Specific Impulse for the electromagnetic impulse bits of the first stage alone and for both stages as a function of the secondary discharge energy for 1kV 55J primary discharge.
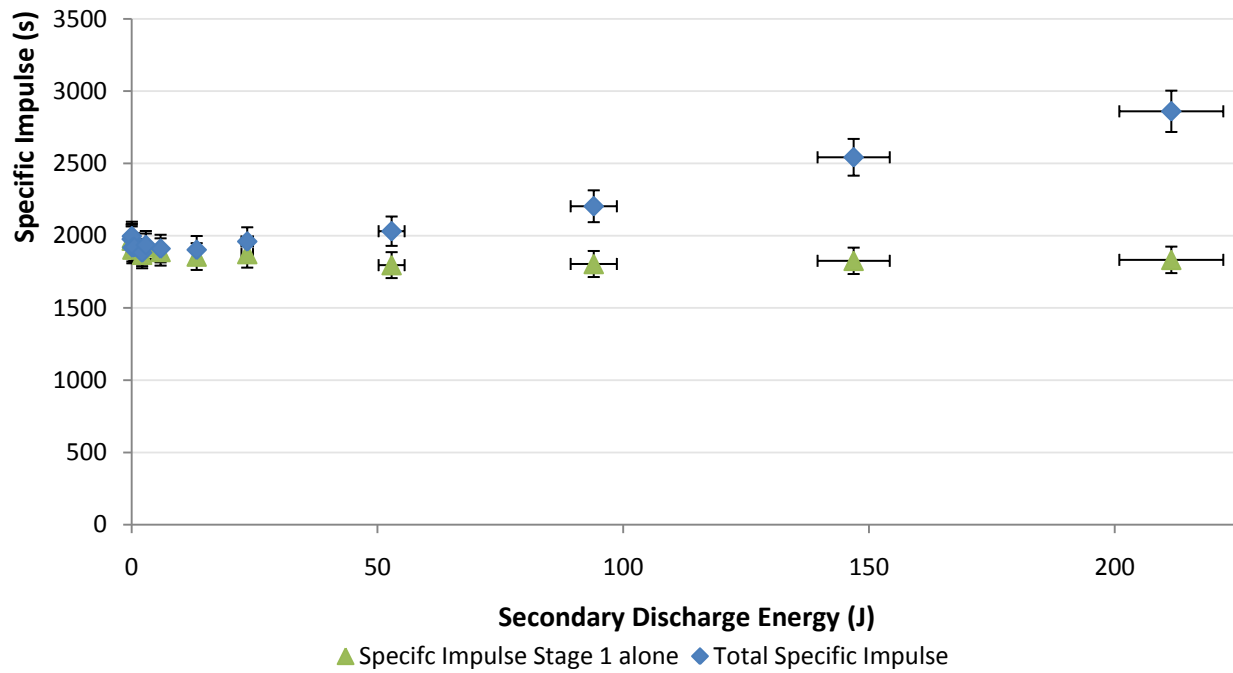
Figure 109: Specific Impulse for the electromagnetic impulse bits of the first stage alone and for both stages as a function of the secondary discharge energy for 1.5kV 123J primary discharge.

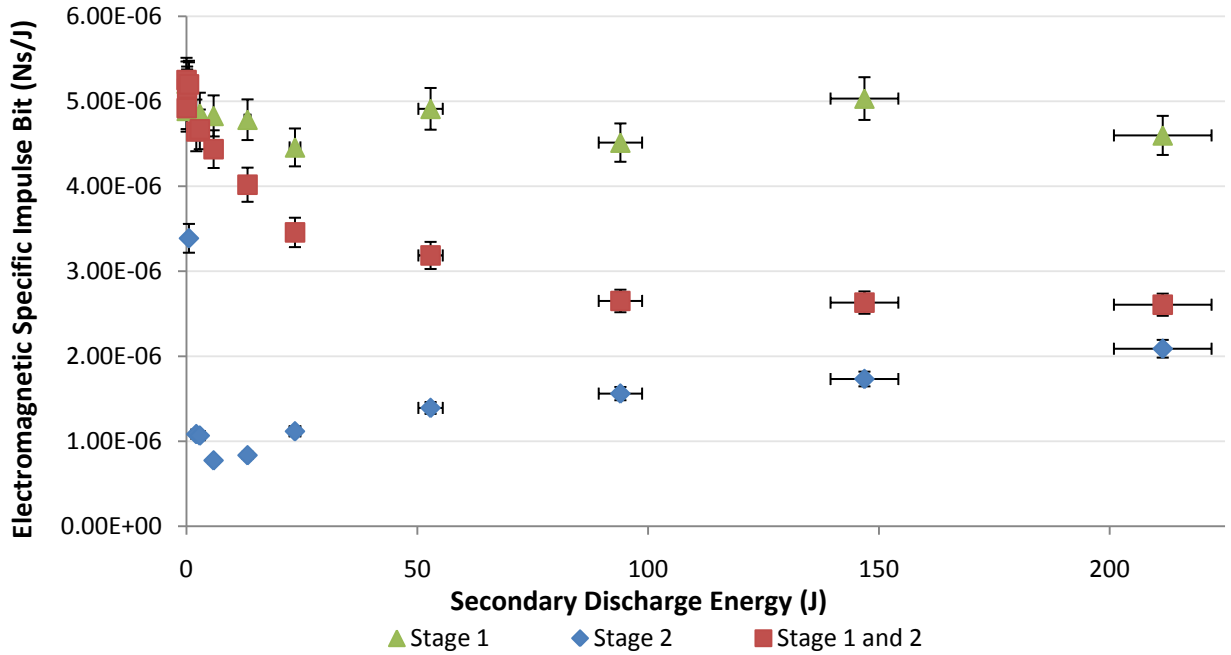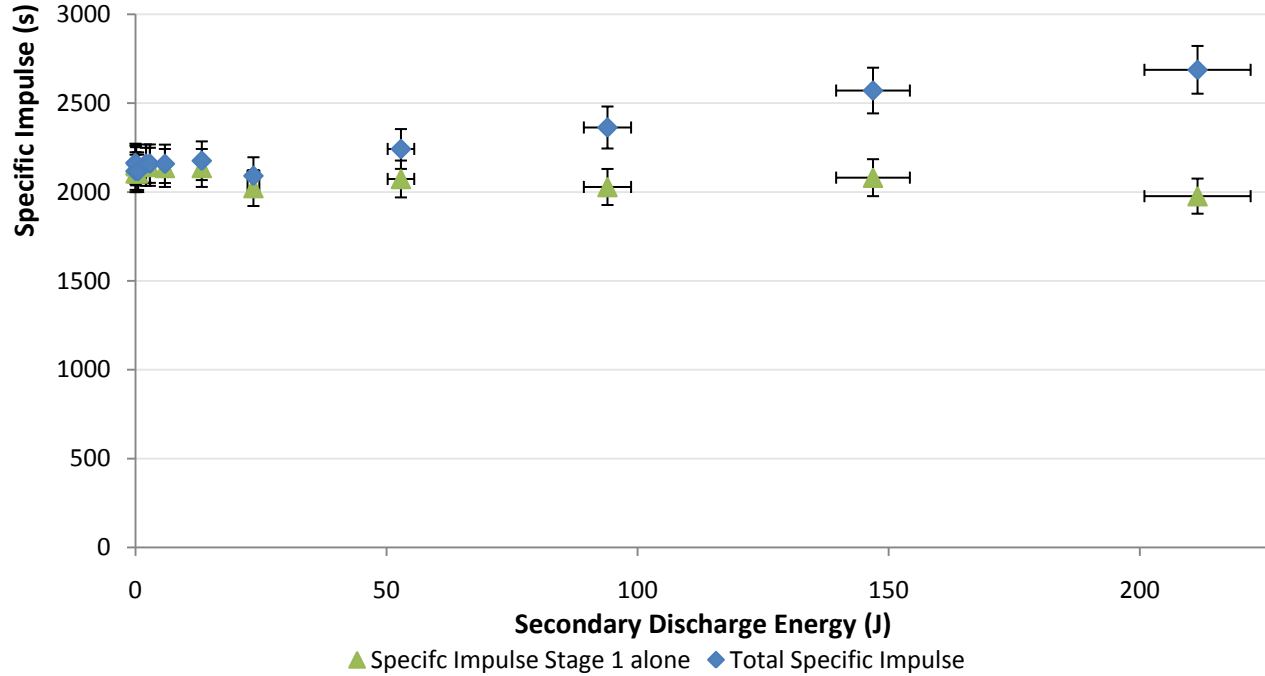**Figure 110: Specific Impulse for the electromagnetic impulse bits of the first stage alone and for both stages as a function of the secondary discharge energy for 2kV 220J primary discharge.**

As seen there is an increase in the specific impulse when the second stage is added, but no more mass is ablated, as the discharge takes place downstream, far from the propellant surface. A higher propellant efficiency is achieved. Higher values of specific impulse were achieved when less mass was ablated which in turn means a smaller ε_1, compared to ε_2, as predicted by the simple analytic model. Higher values of specific impulses are expected for an optimised TS-PPT, and especially for an optimised second stage of the TS-PPT.

Finally, it is convenient to observe the efficiency – in our case taking in account only the electromagnetic impulses -, defined in the simple analytic model in the form of:

$$\eta_{2B} = \frac{1}{2} g_0 I_{s\,TS} \left(\frac{I_{bit\,1}{}^{*} + I_{bit\,2}{}^{*}}{\varepsilon_1 + \varepsilon_2} \right)$$

Figure 111 to Figure 113 shows the efficiency for all 39 cases.
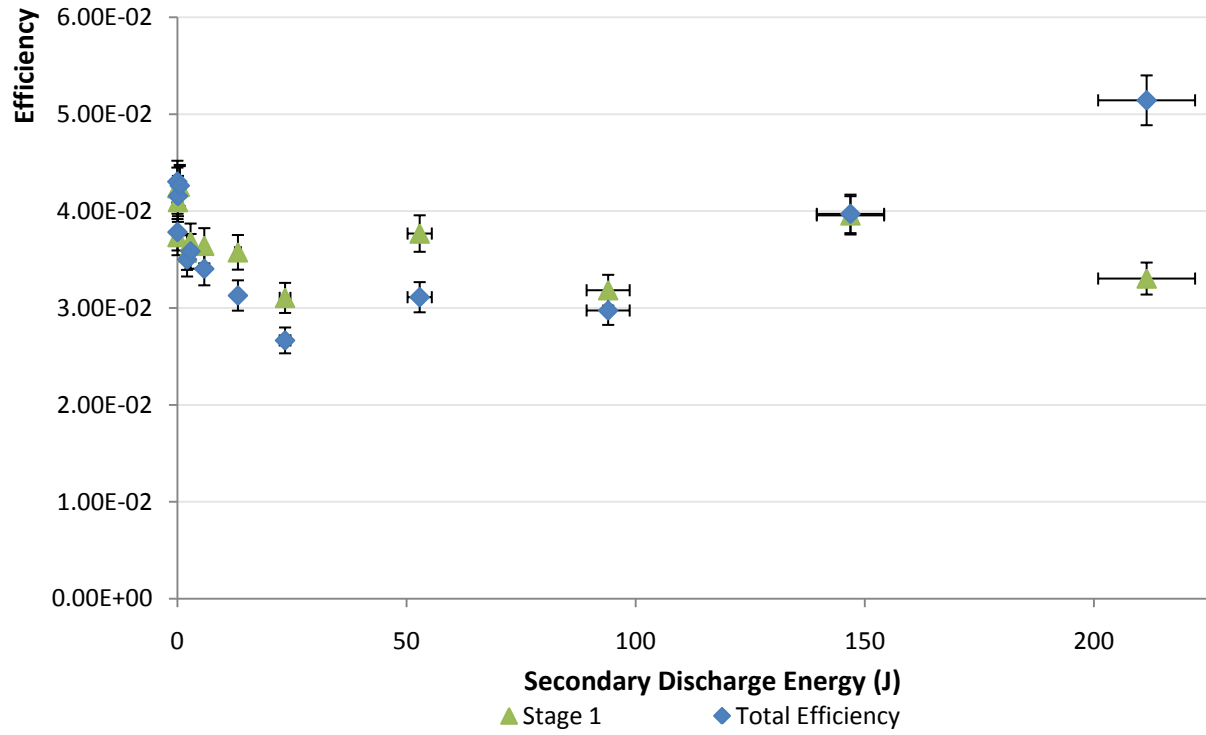
Figure 111: Efficiency of the stage one and the total efficiency as a function of the secondary discharge energy for 1kV 55J primary discharge.
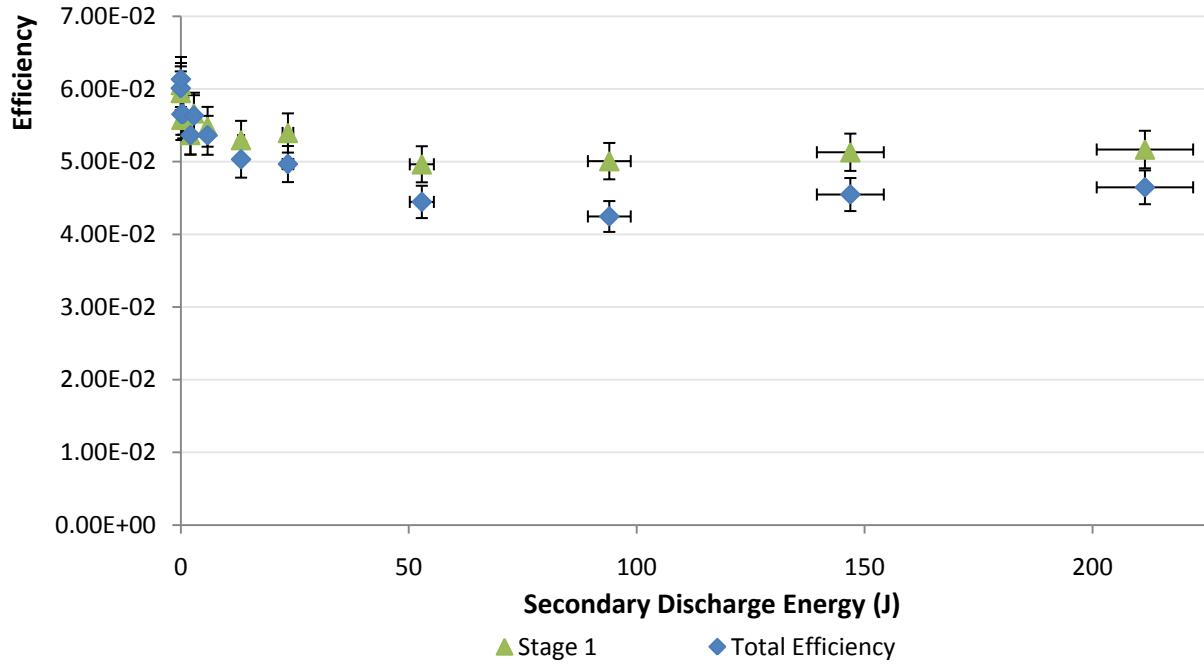
Figure 112: Efficiency of the stage one and the total efficiency as a function of the secondary discharge energy for 1.5kV 123J primary discharge.
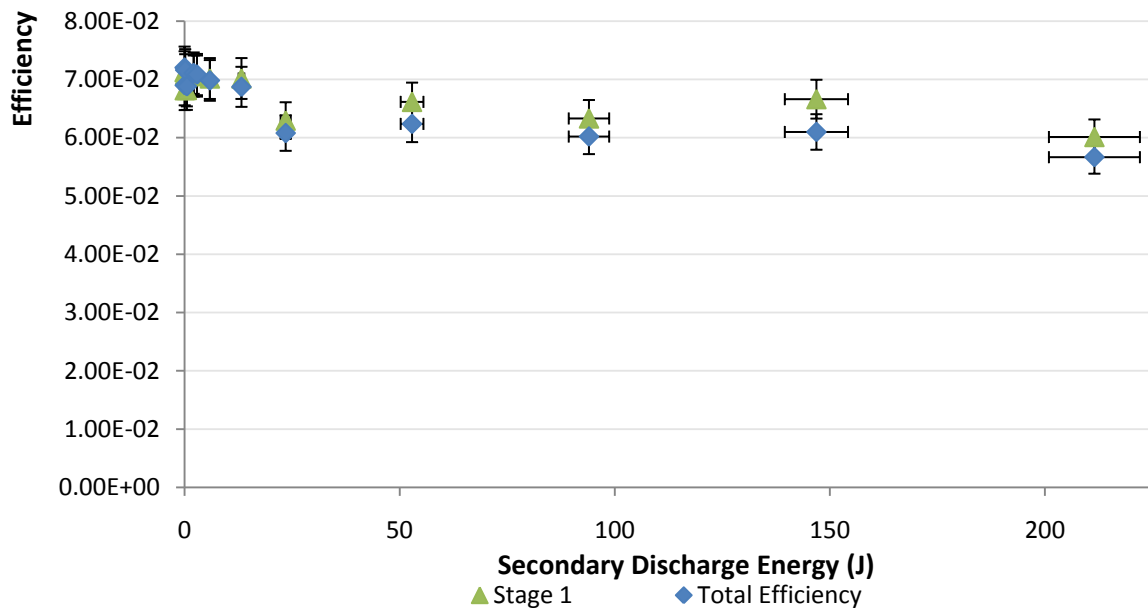
Figure 113: Efficiency of the stage one and the total efficiency as a function of the secondary discharge energy for 2kV 220J primary discharge.

143

It is clear again that, as mentioned in the simple analytic model section, the total efficiency is higher when the total energy of the second stage is higher than the energy of the first stage, i.e., $\varepsilon_2 > \varepsilon_1$, even considering that the actual specific thrust of the second stage was lower than the first stage in this non-optimised design.

These analyses of the experimental results confirm the hypothesis that it is possible to increase the total efficiency of the PPT with a second stage, therefore dividing the ablation and acceleration processes.

8.2 TS-PPT operation regimens analysis

Four distinct regimens were observed during the tests, delimited by increasing the second discharge voltage.

8.2.1 First Regimen

With very low voltages applied to the secondary electrodes, between 0 V and 50V (depending on the primary discharge voltage), yields an oscillatory secondary discharge current approximately 90° out of phase with relation to the primary discharge. The length of the discharge is approximately the same as the primary discharge. A significant current was measured even when the secondary capacitor was initially completely discharged and at the end of the discharge there was a residual voltage in the capacitor, directly proportional to the main discharge voltage.

The current is due to induced currents from the first discharge time varying magnetic field that yields a voltage difference across the secondary electrodes that, in turn, provoke the current. The residual voltage on the secondary capacitor is due the charging from the aforementioned

phenomena. Figure 114 (a) illustrates this regimen. This trend is observed for secondary discharge voltages between 0 and 50V (with primary discharge voltage of 1 kV or 1.5 kV) and between 0 and 15 V (with primary discharge voltage of 2 kV), the secondary discharge capacitor voltage (yellow, 100V/div), secondary discharge current (green, 500 A/div) and primary discharge current (pink, 2000 A/div) at 100 µs/div (horizontally). This figure was obtained with 2 kV primary discharge and 0 V secondary discharge.

8.2.2 Second Regimen

At intermediate voltages, between 30 V and 75V (depending on the main discharge voltage), a mainly positive secondary discharge current is observed, with a reduction on the phase difference with relation to the primary discharge current – although still considerably out of phase compared to the primary discharge. The length of the discharge is considerably longer than the first regimen, with a long tail after the main discharge is over.

The primary discharge still modulates the secondary discharge, but now the primary discharge has an "offset" due to its initial voltage that reduces greatly the negative portion of the discharge. Figure 114 (b) illustrates this regimen. This trend was observed for secondary discharge voltage of 50V (with primary discharge voltage of 1.5 kV) and between 30 and 75 V (with primary discharge voltage of 2 kV) – not observed at 1 kV-, showing the secondary discharge capacitor voltage (yellow, 100V/div), secondary discharge current (green, 500 A/div) and primary discharge current (pink, 5000 A/div) at 100 µs/div (horizontally). This figure was obtained with 2kV primary discharge and 75 V secondary discharge.

8.2.3 Third Regimen (transition regimen)

With the capacitor of the secondary discharge charged between 75 V and 100 V it is observed a transition regimen with two clear phases. The first phase is oscillatory and presents a higher peak, mainly positive current discharge. The second phase is a very distinct long tail that starts after the main discharge, resembling a critically damped RLC circuit discharge. The modulation of the secondary discharge due to the first discharge is less apparent, but still present. Figure 114 (c) illustrates this regimen. This trend was observed for secondary discharge voltages between 75 V and 100V (for all three primary voltages), showing the secondary discharge capacitor voltage (yellow, 100V/div), secondary discharge current (green, 500 A/div) and primary discharge current (pink, 5000 A/div) at 100 µs/div (horizontally). This figure was obtained with 2kV primary discharge and 100 V secondary discharge.

8.2.4 Fourth Regimen

The fourth and last regimen has a completely positive secondary discharge current and resembles the current shape of a critically damped circuit, although it also has a slightly oscillating phase modulated by the primary discharge. The length of the secondary discharge is much longer than the main discharge. Figure 114 (d) illustrates this regimen. This trend was observed for secondary discharge voltages above 150 V (for 1 kV main discharge), 200 V (for 1.5 kV main discharge) or 250 V (for 2 kV main discharge), showing the secondary discharge capacitor voltage (yellow, 100V/div), secondary discharge current (green, 1000 A/div) and primary discharge current (pink, 5000 A/div) at 100 µs/div (horizontally). This figure was obtained with 1.5kV primary discharge and 300 V secondary discharge.

146
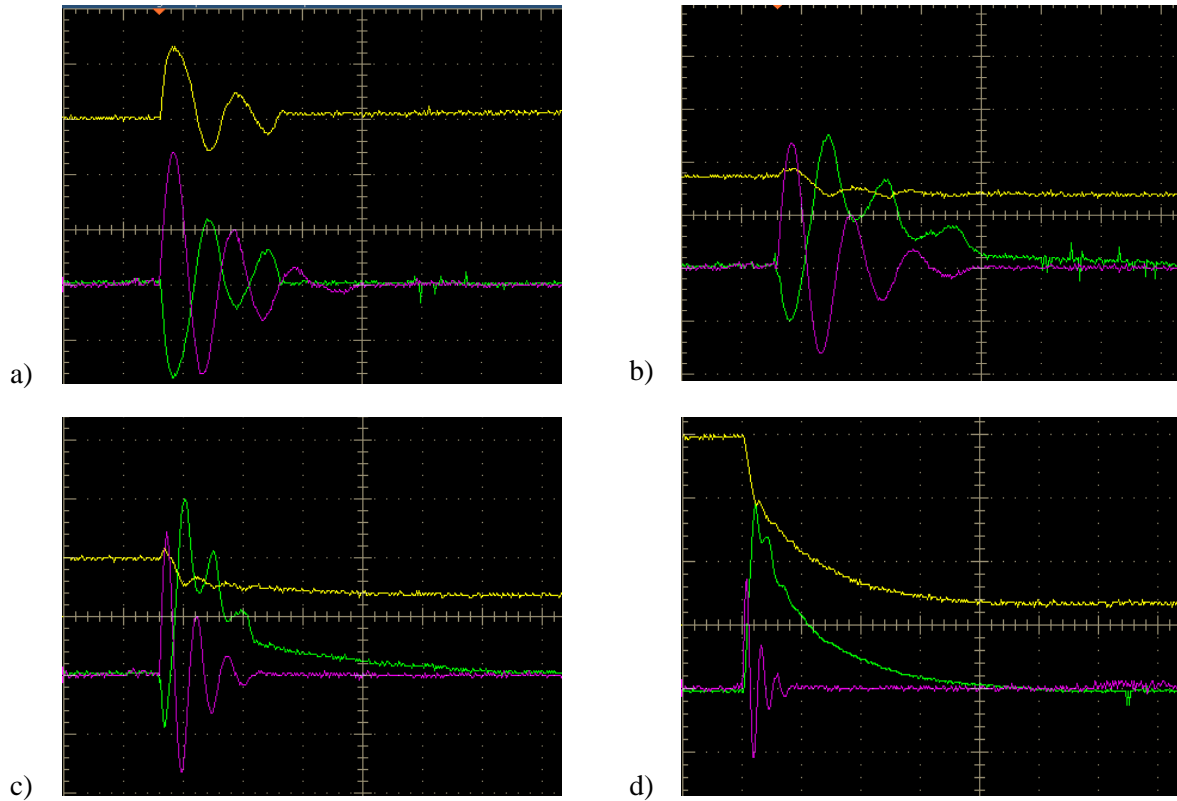
Figure 114: The four regimens. Primary discharge current in pink. Primary discharge capacitor voltage in yellow. Secondary discharge current in green.

8.2.5 Summary of the Regimens Analysis

The first regimen is largely dependent on the primary discharge and considerable current was measured even when the capacitor was initially discharged. The second regimen has an offset, directly proportional to the secondary discharge voltage. The third regimen shows a relatively pronounced discharge tail after the main discharge and the fourth regimen shows a very long discharge tail after the main discharge.

After the main discharge is over, there is no more plasma being produced upstream the secondary electrodes and the propellant starts to produce the LTA. After the last portion of plasma produced by the first electrodes passes through the secondary electrodes, the current

147

flowing in the secondary electrodes, at this point, would supposedly be flowing in the LTA. Tests measuring the length of the discharge showed that, by increasing the secondary discharge voltage, the duration of the secondary discharge was also increased. However, for a given main discharge voltage, there is a maximum length of the secondary discharge. This characteristic supports the hypothesis that the secondary current discharge would be flowing on the LTA, as there is a limited amount of LTA for a given main discharge voltage. In fact, a residual voltage was measured in the secondary capacitor for secondary discharge voltages above 200 V – which can explain in part the relative low efficiency observed for the secondary discharge.

The maximum delay observed at different secondary discharge voltages indicates the transition of the secondary discharge from an oscillatory mode, with the first part negative, to a completely positive discharge. This transition occurs at different voltages, depending on the main discharge voltage. When there is 0V applied on the secondary discharge capacitor, a current on the secondary electrodes is generated by the main discharge with the first negative portion. To overcome this first negative portion and initiate the positive only discharge mode it is necessary to have increasingly higher voltage applied on the secondary discharge capacitor as the primary discharge voltage is increased. The voltages that correspond to the maximum delays can be seen as the voltages above which the discharge is completely positive. Figure 115 shows the secondary discharge delay – with respect to the primary discharge - as a function of the secondary discharge voltage and the peaks indicate the transition to a completely positive regimen.

Figure 116 shows the length of the secondary and primary discharges as a function of the primary discharge voltage and secondary discharge voltage. It can be seen that after a certain

point the length of the secondary discharge does not increase for a fixed primary discharge voltage.

The secondary discharge maximum current was also analysed and it was found a linear relation with respect to the secondary discharge initial voltage, as expected. Figure 117 shows the results of this analysis.

Figure 118 shows an integrated image of one full cycle of the TS-PPT operating in two-stage mode.
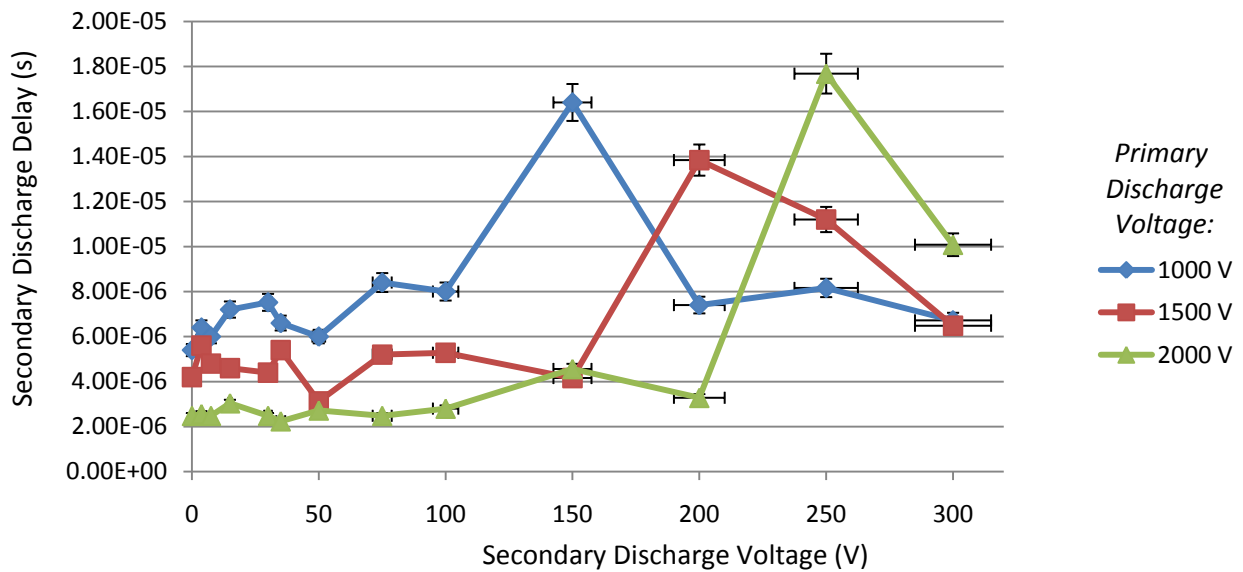
Figure 115: Delay between the first discharge and the second discharge as a function of the voltage applied on the secondary electrodes for three different primary discharge voltages.
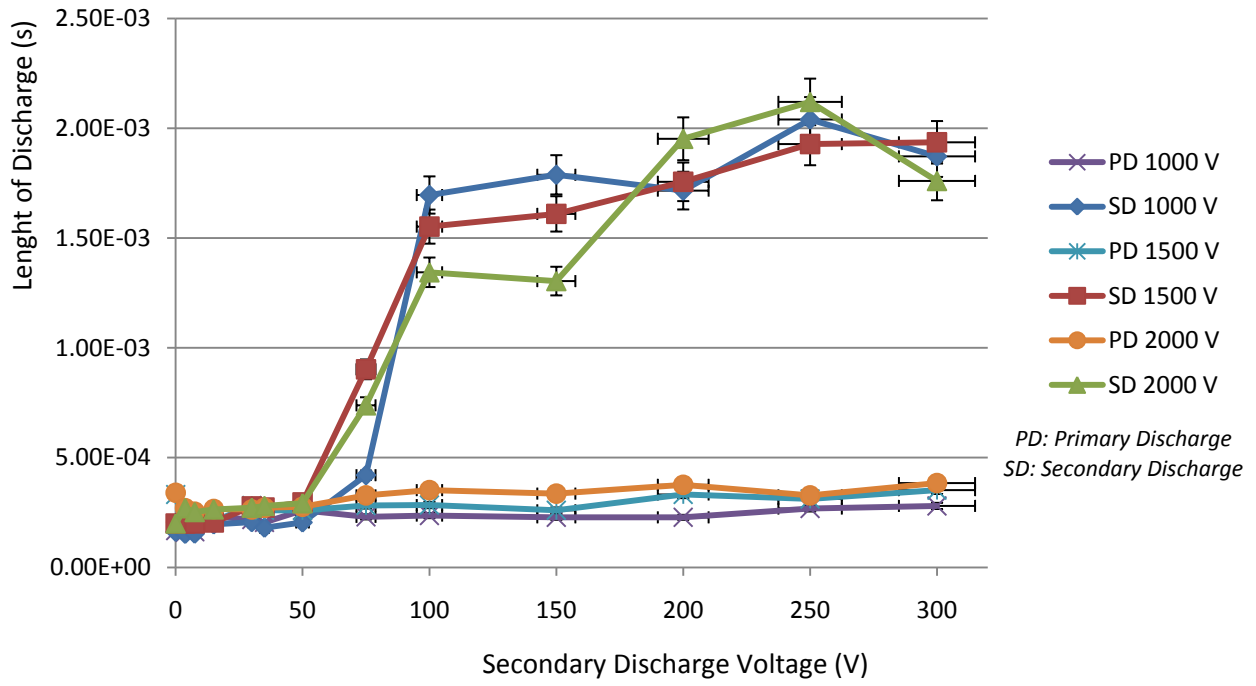
Figure 116: Length of the secondary discharge as a function of the voltage applied in the secondary electrodes for three different primary discharge voltages.
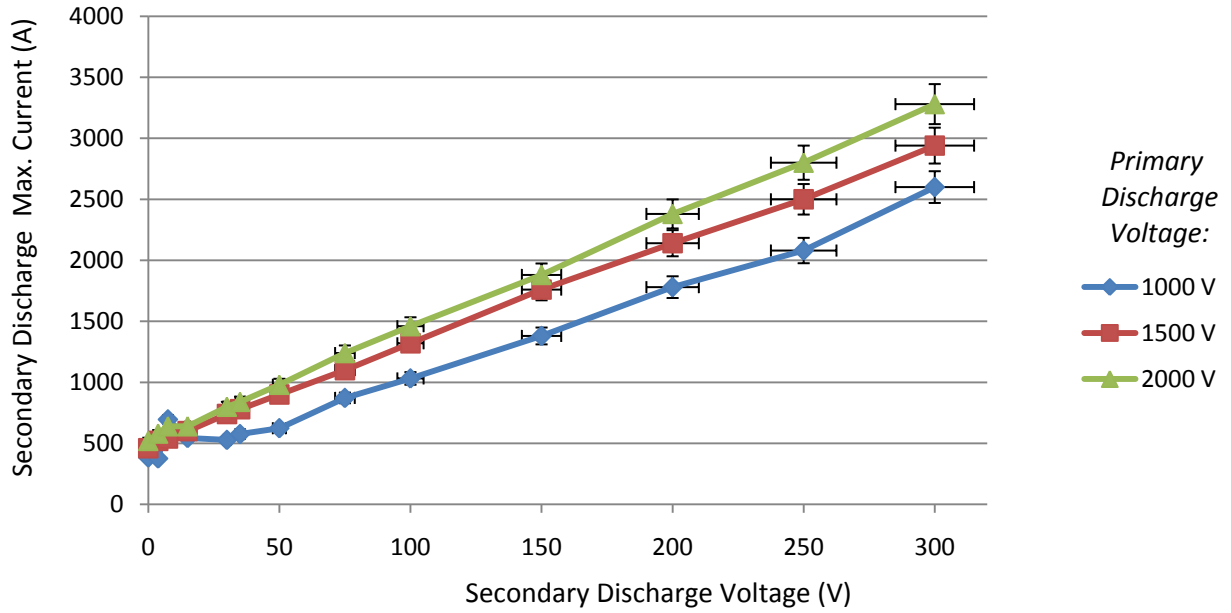
Figure 117: Relationship between secondary discharge voltage and secondary discharge maximum current.
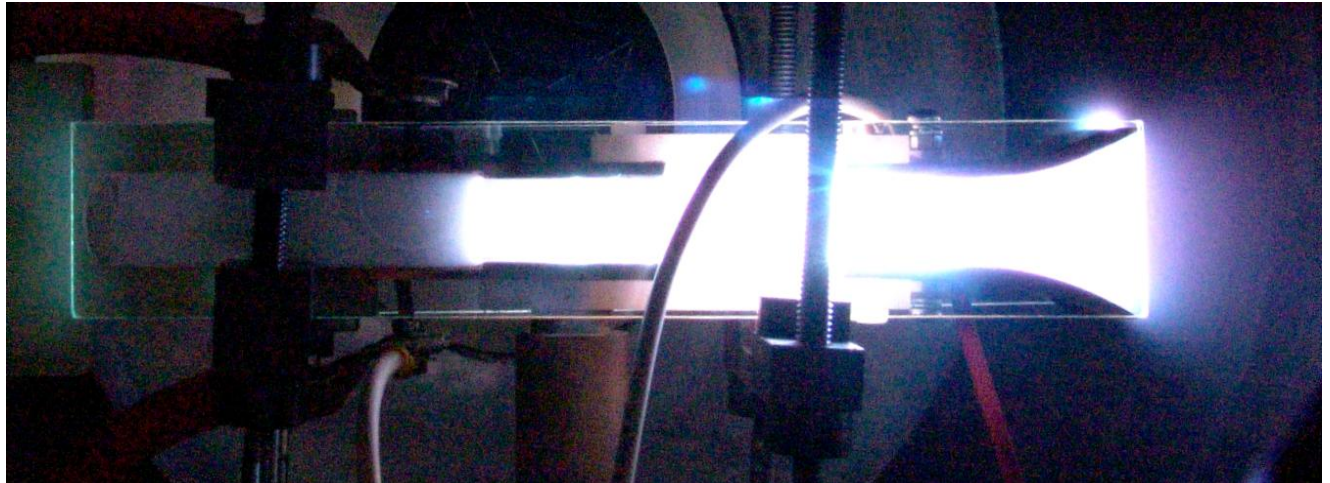
Figure 118: The TS-PPT discharge chamber during a two-stage test.

8.3 Discharge Chamber Geometry Analysis

While the long rectangular geometry with glass walls tested provided a convenient way of observing the discharges, after long tests, significant amount of carbon deposits were found on

151

the inner surface of the glass walls. After a certain number of discharges, these carbon deposits were preventing the current from flowing on the (dielectric) propellant surface, due to its much higher conductivity and tests had to be stopped for cleaning. This factor may also have contributed to an observed low efficiency.

This section provides an insight into the analysis of suitability of a prospective ideal discharge chamber. To achieve this, other geometries were studied providing a useful input in future implementations of the TS-PPT.

The main goals of the analysis of prospective improved discharge chambers are to shorten its length and reduce friction of the exhaust products with the walls, while providing for the four electrode design of the TS-PPT.

A coaxial geometry and a much shortened rectangular geometries were analyzed.

8.3.1 Coaxial Geometry

In this design the electrodes are concentric and a spark plug is at the centre of the discharge chamber. To allow for the second set of electrodes the coaxial design needed a conical section, where the secondary electrodes would be mounted. To minimise the occurrence of carbon deposits, the conical section had an angle of 45° with its main axis. Above this angle the plume densities are very low (51) and the deposits would also be minimised.

Figure 119 shows a two-dimensional view of the TS-PPT coaxial discharge chamber. In this figure, from the centre of the thruster outwards, there are five numbered electrodes. The first is the anode of the spark plug, the second is the cathode of the spark plug. Between these two electrodes there is a PTFE hollow cylinder, shown in white, which makes the spark plug essentially a coaxial PPT, similar to the rectangular geometry used earlier. The third electrode is

152

the anode 1. In this design the cathode 1 is not a separate electrode; instead the cathode of the spark plug is used. Between the electrodes two and three is the propellant, also shown in white, a conical shaped spring-fed PTFE. The fourth electrode is the anode 2, placed in the conical section of the TS-PPT discharge chamber. The fifth electrode is the cathode 2, a rod placed on the axis of the thruster, suspended by three other rods and aligned with the anode 2.
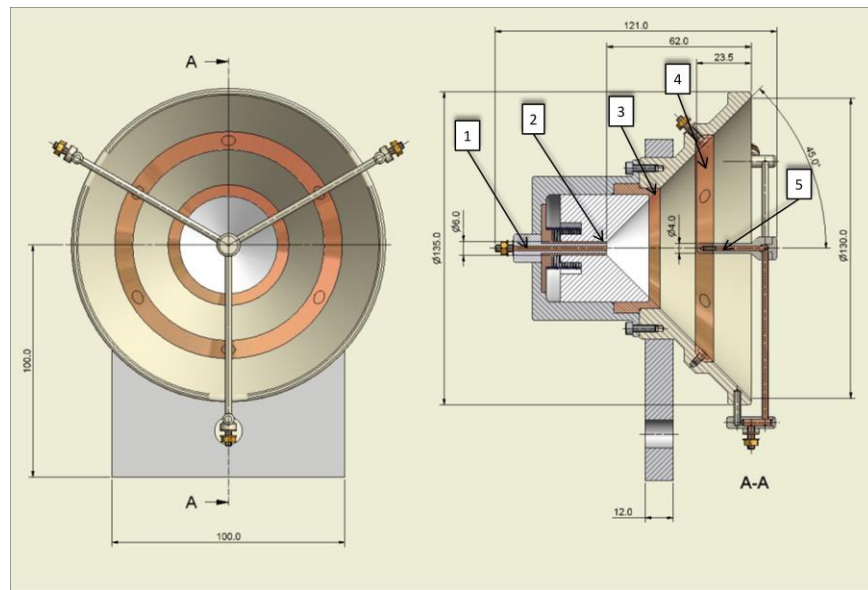
Figure 119: Prospective Coaxial Discharge Chamber for the TS-PPT. Electrode 1: Spark plug anode. Electrode 2: Spark plug cathode and cathode 1. Electrode 3: Anode 1. Electrode 4: Anode 2. Electrode 5: Cathode 2.

Figure 120 shows a perspective view and two cut views of the coaxial discharge chamber. In this concept the spark plug discharge triggers the main discharge. The cathode 2 (electrode 5) and anode 2 (electrode 4) are responsible for generating additional discharges to accelerate the LTA.
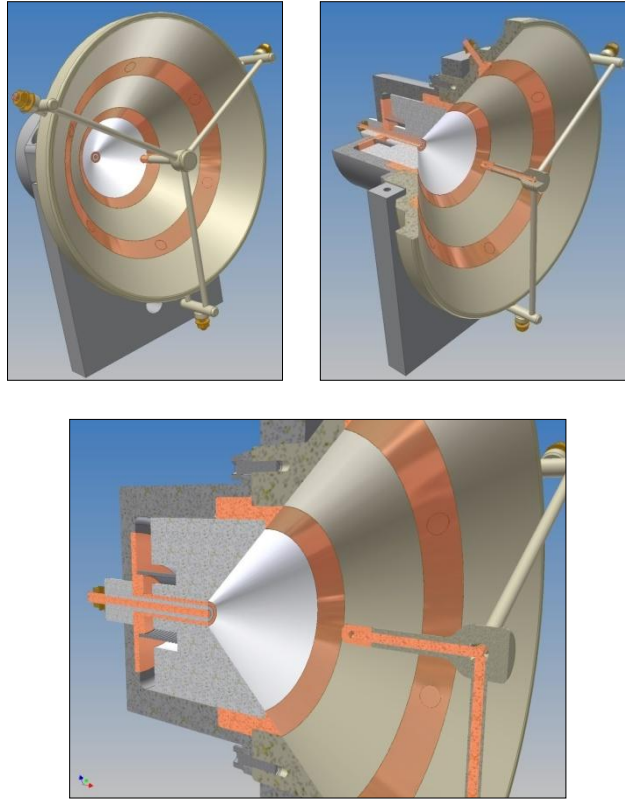
Figure 120: Details of the coaxial TS-PPT discharge chamber.

8.3.2 Shortened Divergent almost-rectangular geometry

The motivation for this geometry analysis came during the course of this research, when I was asked to design and build a version of the TS-PPT for a small satellite called UniSat-5 from the University of Rome. This new TS-PPT had a power limitation of 10 W and a maximum total mass of 1 kg. A rectangular geometry was studied and a prototype built at the University of Southampton with cooperation of the Brazilian National Institute for Space Research (INPE). This TS-PPT (UniSat-5 TS-PPT) implementation comprises a rectangular discharge chamber with a 20mm x 5 mm x 45 mm PTFE propellant bar and a 45° angled nozzle where the secondary electrodes are assembled. The spark plug is mounted on the cathode 1. In this design

three separate capacitors will be used for the spark plug, main discharge and secondary discharge. The primary and secondary capacitors are charged in parallel from a single power supply. The discharge initiation is triggered by voltage breakdown on a spark plug gap, that consists of a PTFE driven spark plug, similar to a coaxial PPT. This geometry is much shorter that the presented rectangular geometry. The basic concept of this new revised rectangular discharge chamber is shown in Figure 121. The angle of the divergent is 45 degrees to reduce carbon deposition. Figure 122 shows the computer design model of the concept.
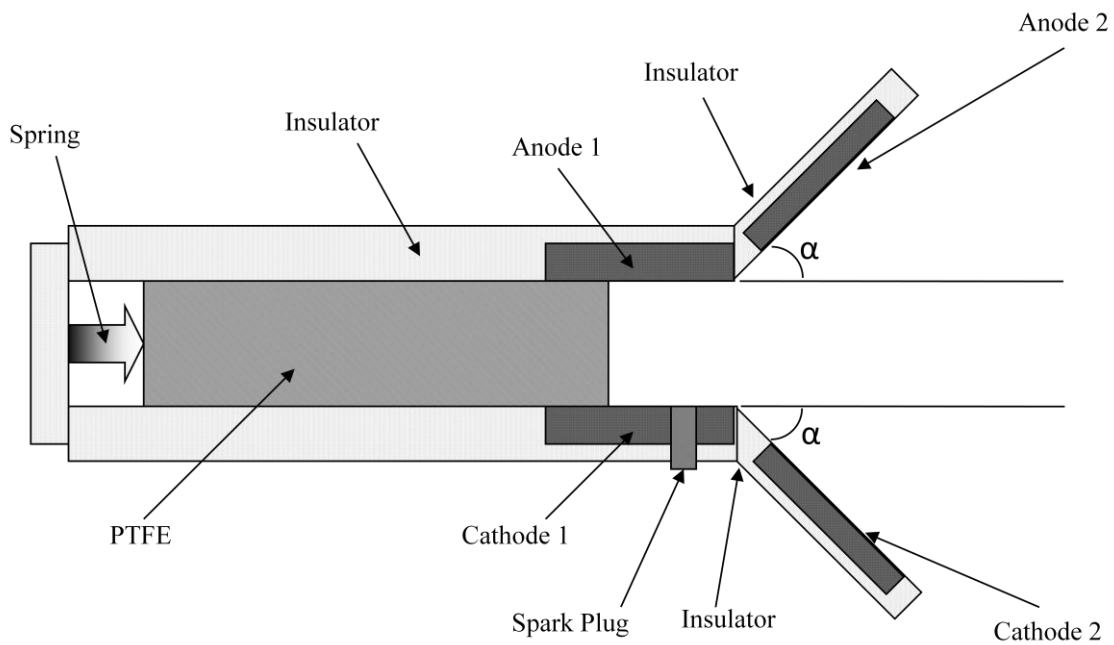
Figure 121: Revised rectangular discharge chamber.
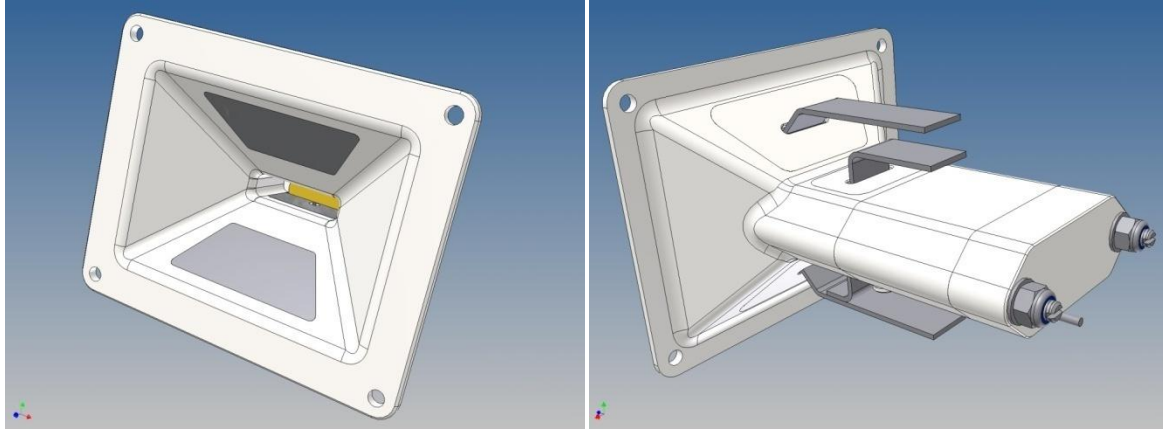
Figure 122: Computer Design Model of the improved rectangular design.

The discharge circuit of the UniSat-5 TS-PPT is shown schematically in Figure 123. It is extremely similar to the TS-PPT tested, but has a protection diode due to the utilisation of only one power supply for both primary and secondary capacitors. Also, to reduce weight there is no autotransformer and a high voltage power supply (up to 15kV) was used. Table 10 summarises the data for the UniSat-5 TS-PPT. Figure 124 shows the computer design of the finished project with details of the capacitors, spark plug, discharge chamber, power supplies, structure and electrodes. Figure 125 shows the thruster built.
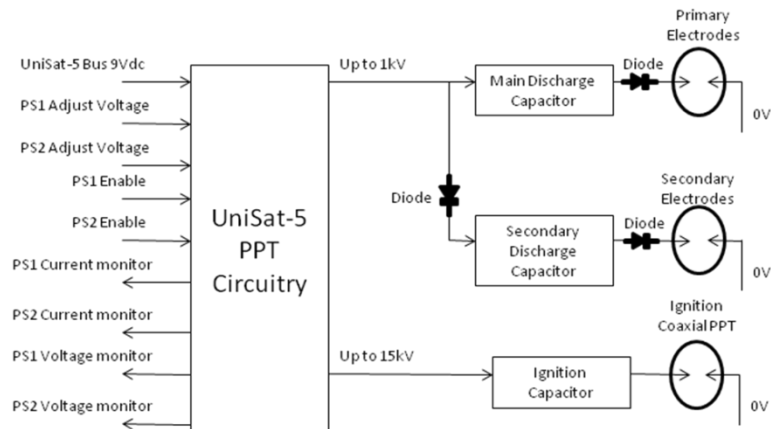
Figure 123: Schematic of the UniSat-5 TS-PPT circuit.

	Target	Achieved
Total System Mass	1.000 kg	1.381 kg
Total System Volume	$152.0 \times 106.0 \times 128.0$ (mm)	$152.5 \times 113.0 \times 128.0$ (mm)
Maximum Power	5W	4W
Discharge Energy (Primary + Secondary)	5 J + 5J	5J + 5J
Primary Discharge Energy per Propellant Discharge Area	5 J / cm^2	~4.46 J / cm^2
Operating Frequency	0.5 Hz	0.4 Hz
Total Impulse (estimated)	20 Ns	-
Impulse Bit (estimated)	140 μNs	-
Propellant Mass	0.007 kg	0.007 kg
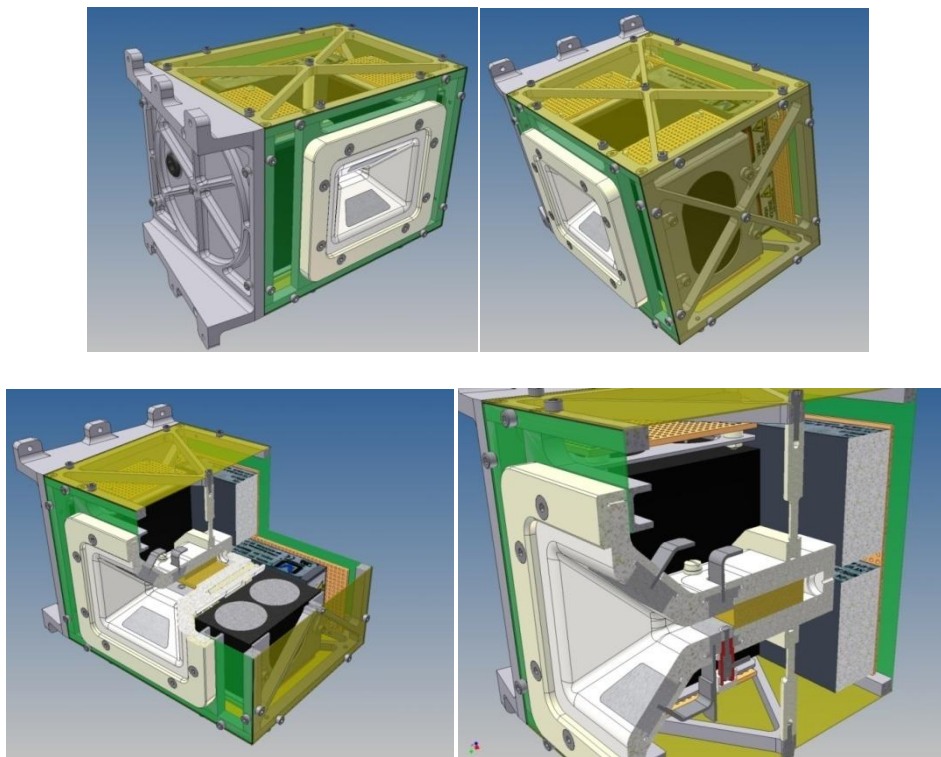
Figure 124: UniSat-5 TS-PPT computer design.

Figure 125: UniSat-5 TS-PPT.

Chapter 9

9. Conclusion and Future Work

9.1 Conclusion

Practically since its inception the Pulsed Plasma Thruster has been widely known for three main characteristics: simplicity, robustness and low efficiency. After numerous studies on how to increase the efficiency of the PPT, many of them identified the late ablation as a main contributor to the low efficiency and several subsequent works studied ways to minimise the production of the late ablation.

In this work a new approach to the PPT thrust production was carried out. The production of the thrust in the PPT was divided in two phases: i) ablation and ii) acceleration. Each of these phases is carried out by two physical stages: first and second. The first stage is mainly responsible to dosing the total amount of propellant that will participate in the pulse cycle. The second stage is responsible for accelerating the propellant. Both stages' main role are non-exclusive, as the first stage also accelerates the propellant and radiation from the second stage could contribute to a very small increase in ablation. This new thruster was given the name of two-stage pulsed plasma thruster –TS-PPT.

A simple analytic model was developed to show the advantages of adding a second stage to the conventional PPT. It was shown analytically that by using two stages it was possible to have higher values of specific impulse and efficiency and that it was possible to decouple the ablation and acceleration phases of the thrust production in the PPT.

Two methods of implementing the TS-PPT were shown, high frequency burst and double discharge. The high frequency burst looked very interesting and promising, but was relatively complex to implement due to its high frequency switching operation. Without prejudice to the principle of the HFB method, the double discharge method was much simpler and more in accordance with the philosophy of the PPT and was selected as the implementation method.

A prototype of a TS-PPT was designed and built. Also the vacuum facility had to be assembled and many parts designed and built. The laboratory where the tests were carried out also had to be completely adapted and refurbished to allow the tests. The TS-PPT prototype built had a rectangular geometry and four electrodes and a spark plug. The first two electrodes were placed in contact with the propellant surface and were mainly responsible for the ablation process. To allow the discharge initiation, a spark plug was placed in the cathode. The second two electrodes were placed downstream to avoid generating more late ablation. Glass walls ware used to enable visualization of the discharges. The TS-PPT was controlled by a computer attached to a power system that used Insulated Gate bipolar Transistors (IGBT) as a high voltage, high current, high speed switch. The TS-PPT had a $110\mu F$ capacitor for the primary discharge and a $4700\mu F$ capacitor for the secondary discharge, operating at a maximum of 2kV and 300V, respectively.

The average mass ablated in one pulse, Δm, was measured and found to be $0.32\frac{\mu g}{J}$, a relatively low value when compared to other PPTs, and attributed to an unexpectedly higher propellant area discharge due to discharges on the side of the propellant and also to the long duration of the primary discharge. However, for the goals of this research this was not considered a problem.

Simple time-of-flight measurements for the first stage, using the second stage as probe, indicated that the fastest portion of the plasma that was able to break down the secondary discharge was

160

travelling at approximately $14.28 \frac{km}{s} \pm 4.65 \frac{km}{s}$. This value was within the range of speed of the species of the PPT exhaust found in the literature.

Several measurements of current were taken for both the first and the second stage, while the primary discharge energy and the secondary discharge energy was varying. These measurements allowed insights on the electromagnetic impulse of the TS-PPT for both the first stage and the second stage. Based on the current discharges it was possible to calculate the equivalent total resistance and total inductance of the primary and secondary circuits for all cases measured.

It was not observed a significant change in the total resistance and in the total inductance of the primary discharge when the secondary discharge energy was increased, indicating a good decoupling of the two stages. This relative decoupling, at this point, is seen as a positive aspect, as the first stage can be treated as an isolated regular PPT.

Analysis of the impulse bit indicated that it is possible to increase the total impulse bit when adding the second stage, as expected.

The electromagnetic specific impulse bit of the second stage was rather lower than expected, and this low performance was attributed to a non-optimised design and to the utilisation of low voltages for the second discharge - due to limitations of our power supplies – yielding lower currents that yield lower impulse bits. For the demonstration of the mechanism this was not considered a problem, but a good indicator for future implementations.

One of the main objectives was to increase the specific impulse of the PPT. Based on the results the specific impulse was greatly improved by adding the second stage, especially when the energy of the second stage was higher than the energy of the first stage. At 55J primary discharge and 50J secondary discharge (total 105J) a specific impulse of around 2000s was calculated based on the current discharges, while the first stage alone had a specific impulse of around

1500s. Specific impulses as high as 4000s were obtained. This findings indicates that the simple analytic model was correct in its prediction of higher performance for $\varepsilon_2 > \varepsilon_1$.

Calculations of the efficiency were also carried out and indicated that it was possible to increase the efficiency of the PPT by adding the second stage. Increases of efficiency as high as 60% over the single stage were obtained, but even higher values are expected when the second stage operates at higher voltages and with an optimised design. Similar to findings of the specific impulse, higher efficiencies were found for $\varepsilon_2 > \varepsilon_1$.

During the operation of the TS-PPT with the two stages, four regimens of operation were observed, related to the secondary discharge. In the first regimen the secondary current was basically modulated by the first discharge. In the second regimen the secondary discharge current was also modulated by the first discharge but had a tail after the primary discharge, indicating that current was flowing in the secondary electrodes after the main discharge was over. In the third regimen (or transition regimen) a very distinct long tail after the primary discharge was over was observed in the secondary discharge and the secondary current was mainly positive. The fourth regimen had a completely positive secondary discharge that resembled a critically damped circuit with very little modulation from the first discharge and the longest tail observed, indicating that a reasonable portion of the current was flowing in the late ablation, after the primary discharge was over. The length of the secondary discharge was limited by the primary discharge energy, as expected, due to the total mass bit, Δm, being proportional to ε_1, which is another indication that the current is indeed flowing in the late ablation.

The discharge chamber of the prototype presented problems and charring was observed in the propellant bar. While this did not present itself as a problem for this research, other possible discharge chamber geometries were analysed with the intention to reduce the total length of the

discharge chamber and wall interactions. A novel coaxial conical geometry was presented. Also a novel rectangular geometry that was designed and built, but unfortunately not in time for its tests to be included in this work, but nevertheless it used the exact same principles of the TS-PPT as was considered relevant to the work presented. This novel rectangular TS-PPT is going to be used in the UniSat-5 satellite of the University of Rome and is due to be launched in space in 2010. Both novel geometries present a more unimpeded approach and were much shorter, with a divergent at 45°.

With the results presented it was shown that it is possible to accelerate the late ablation, increase the specific impulse and potentially increase the efficiency of the PPT for the first time.

9.2 Future Work

This work opens a new door to investigations on the improvement of the PPT by using two stages. Future work should investigate the performance of the second stage operating at higher voltages. Shorter electric conductors from the capacitor to the discharge chamber and faster capacitors for the primary discharge are also to be considered, as improving the efficiency of the first stage will improve the overall efficiency of the TS-PPT. New geometries that suit the TS-PPT operation need to be investigated, such as those shown.

The electromagnetic coupling of the second discharge current and the first discharge current may be beneficial if properly implemented. This may lead to an improved electromagnetic acceleration. In this case the current direction needs to be judiciously chosen.

An assessment of the high frequency burst method is also desirable, when suitable technology makes it simpler to implement.

Measurements of the impulse bit of any implemented TS-PPT with a thrust balance is also desirable and will provide a total efficiency measurement, accounting also for the gas dynamic generated thrust.

Ultra high speed photography will help to visualise the discharges and aid optimisation of the discharge timing. A time resolved spectrometry will help analyse the species coming out of the thruster as well as their speed and also the ionization level. Langmuir probes could be used for determining the speed of the plasma. Also a capacitor - probe - as described in this work - could be used for a simple time of flight measurement of the fastest portion able to achieve a certain break down voltage on a set of electrodes connected to a capacitor placed after the secondary discharge.

10. References

1. *Electric propulsion: An evolutionary technology.* **Curran, F.M., Sovey, J.S., and Myers, R.M.** Montreal : 42nd Congress of the International Astronautical Federation, October 5-11, 1991. IAF-91-241.

2. *An experimental investigation of a high-voltage electron-bombardment ion thruster.* **Byers, D. C.** 1, s.l. : Journal of Electrochemical Society, 1969, Vol. 116. pp. 9-17.

3. **Sutton, G. P. and Biblarz, O.** *Rocket propulsion elements.* New York : John Wiley & Sons, 2001.

4. *Pulsed Plasma Microthruster for Synchronous Meteorological Satellite (SMS).* **Guman, W. J., and Williams, T. E.** s.l. : AIAA Paper, 1974. 73-1066.

5. *Solid propellant electrical thrustors for attitude control and dift correction of space vehicles.* **LaRocca, A. V. (General Electric Co., Philadelphia. PA.).** San Diego : AIAA, 5th Electric Propulsion Conference, March 7-9, 1966. Paper 66-229.

6. *Analysis of PPT Potentialities in Solving the Satellite Orbit Control Tasks.* **Akimov, V., Nagel, I., Ogloblina, I., Antropov, N., Pokryshkin, A., Popov, G., Rudikov, A.** s.l. : 25th International Electric Propulsion Conference, 1997. IEPC 97-146.

7. *Operational Noval Spacecraft Teflon Pulsed Plasma Thruster System.* **Ebert, W. L., Kowal, S. J., Sloan, R. F.** s.l. : AIAA, July 1989. Paper 89-2497.

8. *The On-Orbit Role of Electric Propulsion.* **Janson, S. W.** s.l. : AIAA, 1993. Paper 93-2220.

9. *Investigation of Pulsed Plasma Thrusters for Spacecraft Attitude Control.* **Meckel, N. J., et al.** Cleveland, OH : IEPC, 1997. Paper 97-128.

10. *Propulsion requirements and options for the New Millennium Interferometer (DS-3) Mission.* **Blandino, J. J. (JPL Pasadena, CA) and Cassady, R. J. (PRIMEX Aerospace Co., Redmond, WA).** Cleveland, OH : AIAA - 34th Joint Propulsion Conference and Exhibit, 1998. 1998-3331.

11. *Design and fabrication of a flight model 2.3 kW ion thruster for the Deep Space Mission.* **Christenses, J. A., et al.** Cleveland, OH : AIAA - 34th Joint Propulsion Conference, 1998. 1998-3327.

12. **Jahn, R. G.** *Physics of electric propulsion.* New York : McGraw-Hill, 1968.

13. **Jahn, Robert G. and Choueiri, Edgar Y.** Electric Propulsion. *Encyclopedia of Physical Science and Technology.* 3rd Edition. s.l. : Academic Press, 2002, Vol. 5.

14. *Pulsed Plasma Thruster.* **Burton, R. L. and Turchi, P. J.** 5, s.l. : Journal of Propulsion and Power, 1998, Vol. 14.

15. *Micro Pulsed Plasma Thruster Development.* **Pottinger, S.J. and Schalermann, C.A.** Florence, Italy : 30th IEPC - International Electric Propulsion Conference, 2007.

16. *Ablative Z-Pinch Pulsed Plasma Thruster.* **Markusic, T. E., et al.** Huntsville, AL : AIAA - 36th Joint Propulsion Conference, 2000.

17. *Effect of Propellant Temperature on Efficiency in the Pulsed Plasma Thruster.* **Spanjers, Gregory G., et al.** 4, s.l. : Journal of Propulsion and Power, 1998, Vol. 14.

18. *Propellant Losses Because of Particulate Emission in a Pulsed Plasma Thruster.* **Spanjers, G. G., et al.** 4, s.l. : Journal of Propulsion and Power, 1998, Vol. 14.

19. *Continuing Develoment of the Short-Pulsed Ablative Space Propulsion System.* **Palumbo, D. J. and Guman, W. J.** s.l. : AIAA-Paper 72-1154, 1972.

20. *Micropropulsion System Selection for Precision Formation Flying Satellites.* **Reichbach, Jeffrey, Sedwick, Raymond J. and Martinez-Sanchez, Manuel.** s.l. : M.Sc. Thesis - Massachusetts Institute of Technology, 2001.

21. *Solid Propellant Pulsed Plasma Microthruster Studies.* **Guman, William J. and Peko, Paul E.** New York : AIAA 6th Aerps[ace Sciences Meeting, 1968.

22. *Performance Improvements in Solid Fuel Microthrusters.* **Vondra, Robert J. and Thomassen, Keith I.** San Diego, CA : AIAA 10th Aerospace Sciences Meeting, 1972.

23. *Performance Study of a Solid Fuel-Pulsed Electric Microthruster.* **Solbes, Albert and Vondra, Robert J.** Bethesda, MD : AIAA 9th Electric Propulsion Conference, 1973.

24. *Effect of Propellant and Electrode Geometry on Pulsed Ablative Plasma Thruster Performance.* **Palumbo, D. J. and Guman, W. J.** New Orleans, Louisiana : AIAA 11th Electric Propulsion Conference, 1976.

25. *Micropropulsion Research at AFRL.* **Gulczinski III, F. S., et al.** Huntsville, AL : AIAA - 38th Joint Propulsion Conference & Exhibit, 2000.

26. *Pulsed Plasma Microthruster Propulsion System for Synchronous Orbit Satellite.* **Guman, William J. and Nathanson, David M.** 4, s.l. : Journal of Spacecraft, 1970, Vol. 7.

27. *A Pulsed Electric Thruster for Satellite Control.* **Vondra, Robert, Thomassen, Keith and Solbes, Albert.** 2, s.l. : IEEE, 1971, Vol. 59.

28. *Flight Qualified Pulsed Electric Thruster for Satellite Control.* **Vondra, R. J. and Thomassen, K. I.** Lake Tahoe, Nevada : Journal of Spacecraft, 1974.

29. *Pulsed Plasma Thruster of the Erosion Type for a Geostationary Artificial Earth Satellite.* **Rudikov, A. I., Antropov, N. N. and Popov, G. A.** 9-11, s.l. : Acta Astronautica, 1995, Vol. 35.

30. *A Micro Pulsed Plasma Thruster (PPT) for the "Dawgstar" Spacecraft.* **Cassady, R. Joseph, et al.** s.l. : IEEE Aerospace Conference, 2000.

31. *Exhaust Velocity Studies of a Solid Teflon Pulsed Plasma Thruster.* **Thomassen, Keith I. and Vondra, Robert J.** New York : AIAA - 9th Aerospace Sciences Meeting, 1972.

32. *Interferometric Density Measurements in the Arc of a Pulsed Plasma Thruster.* **Thomassen, K. I. and Tong, D.** s.l. : AIAA - 9th Electric Propulsion Conference, 1973.

33. *Pulsed Plasma Thruster Plume Investigation Using a Current-Mode Quadruple Probe Method.* **Gatsonis, Nikolaos A., et al.** Indianapolis, IN : AIAA 38th Joint Propulsion Conference, 2002.

34. *Investigation of propellant inefficiencies in a pulsed plasma thruster.* **Spanjers, G. G., et al.** Lake Buena Vista, FL : AIAA, ASME, SAE and ASEE, 32nd Joint Propulsion Conference and Exhibit, 1996. AIAA Paper96-2723.

35. *Modeling of late-time ablation in Teflon pulsed plasma thrusters.* **Mikellides, P.G. and Turchi, P.J.** Lake Buena Vista, FL : 32nd ASME/SAE/ASEE Joint Propulsion Conference and Exhibit, 1996. AIAA-1996-2733.

36. *Experimental and theoretical investigation of an inverse-pinch coaxial pulsed plasma thruster.* **Kamhawi, H., et al.** Huntsville, AL : 36th AIAA/ASME/SAE/ASEE Joint Propulsion Conference and Exhibit, 2000. AIAA-2000-3261.

37. *Analyses of Teflon surface charring and near field plume of a Micro-Pulsed Plasma Thruster.* **Keidar, Michael and Boyd, Ian D.** Pasadena, CA : International Electric Propulsion Conference, 2001.

38. *Effects of Postpulse Surface Temperature on Micropulsed Plasma Thruster Operation.* **Antonsen, Erik L, et al.** 5, s.l. : Journal of Propulsion and Power, 2005, Vol. 21.

39. *On the model of Teflon ablation in an ablation-controlled discharge.* **Keidar, Michael, Boyd, Iain D and Beilis, Isak I.** 1675-1677, s.l. : Journal of Physics D: Applied Physics, 2001, Vol. 34.

40. *Energy Balance and Efficiency of the Pulsed Plasma Thruster.* **Burton, R.L., Wilson, M.J. and Bushman, S.S.** Cleveland, OH : 34th AIAA/ASME/SAE/ASEE Joint Propulsion Conference and Exhibit, 1998. AIAA-1998-3808.

41. **Anonymous.** Pulse-width modulation. *Wikipedia.* [Online] 23 May 2009. [Cited: 24 May 2009.] http://en.wikipedia.org/wiki/Pulse-width_modulation.

42. **Kernighan, Brian W. and Ritchie, Dennis M.** *The C Programming Language.* s.l. : Prentice-Hall, 1988. 0-13-110370-9.

43. *Propulsion System Optimisation for Satellite Formation Flying.* **Gessini, Paolo, et al.** Sao Jose dos Campos - SP - Brazil : International Workshop on Satellite Constellations and Formation Flying, 2005.

44. **Schalermann, C.A.** *Investigation of Thrust Mechanisms in a Water Fed Pulsed Plasma Thruster.* s.l. : The Ohio State University, 2003. PhD Thesis.

45. *Energy Measurements in a Coaxial Electromagnetic Pulsed Plasma Thruster.* **Antonsen, E.L., Burton, R.L. and Rysanek, F.** Los Angeles, CA : 35th AIAA/ASME/SAE/ASEE Joint Propulsion Conference and Exhibit, 1999. June 20-23.

46. *Effects of Geometry and Energy on a Coaxial Teflon Pulsed Plasma Thruster.* **Rysanek, F. and Buron, R.L.** Huntsville, Al : 36th AIAA/ASME/SAE/ASEE Joint Propulsion Conference and Exhibit, 2000. July 16-19.

47. *Zero-Dimensional Model for Preliminary Design of Ablative Pulsed Plasma Teflon Thrusters.* **Brito, C.M., et al.** No. 6, s.l. : Journal of Propulsion and Power, 2004, Vol. 20.

48. *Experimental Assessment of a Benchmark Ablation-Fed Pulsed Plasma Thruster.*

Henrikson, E.M. and Mikellides, P.G. Cincinnati, OH : 43rd AIAA/ASME/SAE/ASEE Joint

Propulsion Conference and Exhibit, 2007. AIAA-2007-5221.

49. *Optimization of Performance and Efficiency of a Coaxial Pulsed Plasma Thruster.* **Jaeger,**

S.C., et al. Indianapolis : 38th AIAA/ASME/SAE/ASEE Joint Propulsion Conference and

Exhibit, 2002. AIAA2002-3977.

50. *Design and performance of liquid propellant pulsed plasma thruster.* **Kakami, A., et al.** 419-

425, s.l. : Elsevier - Vacuum Surface Engineering, Surface Instrumentation and Vacuum

Technology, 2004, Vol. 73 (2004).

51. *Experimental Investigations and Numerical Modeling of Pulsed Plasma Thruster Plumes.*

Gatsonis, N.A., Eckman, R., Yin, X., Pencil E.J., Myers, R.M. 3, pp. 454-464, s.l. : Journal of

Spacecraft and Rockets, 2001, Vol. 38.

52. *Langmuir Probe Measurements in the Plume of a Pulsed Plasma Thruster.* **Eckman, Robert**

Francis. s.l. : M.Sc. Thesis Worcester Polytechnic Institute, 1999.

53. **Wentink, T. Jr.** *High Temperature Behavior of Teflon.* Everett, MA : AVCO-Everett

Research Laboratory, 1959. AF04(647)-278.

54. *Directions for Improving PPT Performance.* **Turchi, P. J.** Worthington, OH : 25th

International Electric Propulsion Conference, 1998.

55. **Guman, W. J.** *Pulsed Plasma Techonology in Microthrusters.* Farmingdale, NY : Fairchild

Hiller Corp, 1968. AFAPL-TR-68-132.

56. *Alternate Propellant Evaluation for 100-joule-class Pulsed Plasma Thrusters.* **Eric, J.P. and**

Kamhawi, H. Huntsville, AL : 39th AIAA/ASME/SAE/ASEE Joint Propulsion Conference and

Exhibit, 2003. AIAA-2003-5171.

57. *Model of an Electrothermal Pulsed Plasma Thruster.* **Keidar, M., Boyd, I. D. and Beilis, I.I.** 3, s.l. : Journal of Propulsion and Power, May-June, 2003, Vol. 19.

58. *Optimization Issues for a Micropulsed Plasma Thruster.* **Keidar, M., et al.** 1, s.l. : Journal of Propulsion and Power, January-February 2006, Vol. 22.

59. *Performance Evaluation of a High Energy Pulsed Plasma Thruster.* **Kamhawi, H., et al.** Tucson, AZ : 41st AIAA/ASME/SAE/ASEE Joint Propulsion Conference and Exhibit, 2005. AIAA-2005-3695.

60. *Study on Plasma Acceleration in an Ablative Pulsed Plasma Thruster.* **Koizumi, H., et al.** Cincinnati : 43rd AIAA/ASME/SAE/ASEE Joint Propulsion Conference and Exhibit, 2007. AIAA-2007-5226.

61. *Preliminary Results of a High Frequency Burst Pulsed Plasma Thruster.* **Marques, R. I., Gabriel, S.B. and Costa, F. S.** Cincinnati : AIAA, 2007. 43rd Joint Propulsion Conference and Exhibit.

62. *Pulsed Plasma Thruster Development.* **Marques, R. I. and Costa, F. S.** Sao Paulo : ABCM, 2003. 17th International Congress of Thermal Sciences and Engineering, COBEM 2003.

63. *Propulsores de Plasma Pulsado: Configurações. Histórico e Estudo da Variação de Massa (in Portuguese).* **Marques, R. I. and Costa, F. S.** Rio de Janeiro : ABCM, 2004. 10th Brazilian Congress of Thermal Sciences and Engineering (ENCIT 2004).

64. **Marques, R. I.** *Desenvolvimento de um Propulsor de Plasma Pulsado.* São José dos Campos : INPE - Instituto Nacional de Pesquisas Espaciais, 2004. M.Sc. Thesis (in Portuguese).